NATIONAL AND KAPODISTRIAN UNIVERSITY OF ATHENS

SCHOOL OF SCIENCE

DEPARTMENT OF PHYSICS

SECTION OF ENVIRONMENTAL PHYSICS AND METEOROLOGY

Study of the climatic changes in the North Aegean Sea and their effects on the ecosystem dynamics

PhD Thesis

Gkanasos Athanasios

R.N.: 2015509

ATHENS 2021

ΕΘΝΙΚΟ ΚΑΙ ΚΑΠΟΔΙΣΤΡΙΑΚΟ ΠΑΝΕΠΙΣΤΗΜΙΟ ΑΘΗΝΩΝ

ΣΧΟΛΗ ΘΕΤΙΚΩΝ ΕΠΙΣΤΗΜΩΝ

ΤΜΗΜΑ ΦΥΣΙΚΗΣ

ΤΟΜΕΑΣ ΦΥΣΙΚΗΣ ΠΕΡΙΒΑΛΛΟΝΤΟΣ - ΜΕΤΕΩΡΟΛΟΓΙΑΣ

Μελέτη των κλιματικών αλλαγών στο Βόρειο Αιγαίο και επιπτώσεις στη δυναμική του οικοσυστήματος

Διδακτορική διατριβή

Γκανάσος Αθανάσιος

Α.Μ.: 2015509

ΑΘΗΝΑ 2021

Three-member Advisory Committee

Sofianos Sarantis (Supervisor), Associate Professor, National and Kapodistrian University of Athens Department of Physics

Triantafyllou George, Research Director, Hellenic Centre for Marine Research (HCMR), Institute of Oceanography

Petihakis George, Research Director, Hellenic Centre for Marine Research (HCMR), Institute of Oceanography

Seven-member Board of Examiners

Sofianos Sarantis (Supervisor), Associate Professor, National and Kapodistrian University of Athens Department of Physics

Triantafyllou George, Research Director, Hellenic Centre for Marine Research (HCMR), Institute of Oceanography

Petihakis George, Research Director, Hellenic Centre for Marine Research (HCMR), Institute of Oceanography

Somarakis Stylianos, Research Director, Hellenic Centre for Marine Research (HCMR), Institute of Marine Biological Resources

Flocas Helena, Professor, National and Kapodistrian University of Athens Department of Physics

Tombrou-Tzella Maria, Professor, National and Kapodistrian University of Athens Department of Physics

Raitsos Dionysios E., Assistant Professor, National and Kapodistrian University of Athens Department of Biology

ACKNOWLEDGMENTS

The current study was prepared in the Hellenic Center of Marine Research, Institute of Oceanography and the University of Athens, Ocean Physics and Modelling Group. Initially I would like to thank my supervisor, Associate Professor Dr. Sarantis Sofianos, for the opportunity to conduct the PhD in the UOA Physics Department and the overall support. I would also like to thank Dr. George Triantafyllou, Research Director at the HCMR for generously offering me all the theoretical and technical background required for the conduction of the study, as well as the financial support during the entire process.

I sincerely appreciate the contribution from Dr. Stelios Somarakis, HCMR Research Director, who was always present and willing to advise me in all biological related issues. I would also like to thank Dr. Evi Schismenou HCMR for the excellent cooperation during the CLIMAFISH project, which funded a significant part of my PhD. Mrs. Annika Pollani, technical scientist at the HCMR, always assisted me when technical obstacles needed to be addressed. I also appreciate the feedback on my Thesis from Dr. George Petihakis, Research Director at the HCMR.

I appreciate the willingness of the other three members of the seven-member board of examiners Professor Helena Flokas, Professor Maria Tombrou-Tzella and Assistant Professor Dionysios E. Raitsos, to participate in my Thesis evaluation.

But most of all, I would like to thank Mr. Kostas Tsiaras, technical scientist at the HCMR for his enormous contribution. He supported me scientifically and guided me in the whole effort. Without his assistance, this project would not be feasible.

Last I would like to express my gratitude to my wife Despoina for all the patience she showed during the conduction of this PhD.

ΠΕΡΙΛΗΨΗ

Η κλιματική αλλαγή έχει γίνει πιο αισθητή από ποτέ και ήδη επηρεάζει το θαλάσσιο οικοσύστημα σε παγκόσμια κλίμακα. Για τη μελέτη των μεταβαλλόμενων κλιματικών συνθηκών, εστιάσαμε στο Βόρειο Αιγαίο και στα πιο διαδεδομένα είδη μικρών πελαγικών ψαριών, τον γαύρο και τη σαρδέλα. Μελετήσαμε τις συνέπειες στα είδη από τις αλλαγές στη θερμοκρασία, την αλατότητα, την εισροή νερών από τη Μαύρη Θάλασσα και μεταβολή της εισροής θρεπτικών από τα γειτονικά ποτάμια. Για τις ανάγκες της μελέτης αναπτύχθηκε ένα πολυειδικό (γαύρος/σαρδέλα), πλήρους κύκλου ζωής μοντέλο για το Βόρειο Αιγαίο, αμφίδρομα συζευγμένο με υδροδυναμικό βιογεωχημικό μοντέλο. Η αρχική μονοδιάστατη εκδοχή του μοντέλου, προσομοίωσε επιτυχώς την ανάπτυξη, τις βιομάζες και τις περιόδους αναπαραγωγής και των δύο ειδών, ενώ επιπρόσθετα διαφάνηκε μία ξεκάθαρη εξάρτηση ανάμεσα στην αλίευση των ειδών και τη συγκέντρωση ζωοπλαγκτού. Το επόμενο βήμα στην ανάπτυξη του μοντέλου, απέδωσε την τρισδιάστατη εκδοχή αυτού. Τα κυριότερα χαρακτηριστικά και η χωρική κατανομή των βιομαζών των ειδών, ήταν για άλλη μια φορά σε συμφωνία με τα δεδομένα. Επιπρόσθετες προσομοιώσεις έδειξαν πως τοπικά τα είδη ανταγωνίζονται για την τροφή. Προσομοιώσεις με χρήση κλιματικών σεναρίων IPCC έδειξαν πως μια μελλοντική αύξηση της θερμοκρασίας θα οδηγήσει σε υποβάθμιση του οικοσυστήματος μέσω της μείωσης των πλαγκτονικών συγκεντρώσεων, επηρεάζοντας αρνητικά τον γαύρο και οδηγώντας σε επικράτηση της σαρδέλας. Τέλος, μεταβολές στα εισερχόμενα από τα ποτάμια θρεπτικά και στην εισροή υδάτων από τη Μαύρη Θάλασσα, επίσης υποβαθμίζουν τους πληθυσμούς των ειδών.

ΛΕΞΕΙΣ-ΚΛΕΙΔΙΑ

ΒΟΡΕΙΟ ΑΙΓΑΙΟ, ΒΙΟΕΝΕΡΓΗΤΙΚΟ ΜΟΝΤΕΛΟ, ΓΕΝΕΤΙΚΟΣ ΑΛΓΟΡΙΘΜΟΣ, ΚΛΙΜΑΤΙΚΗ ΑΛΛΑΓΗ

ABSTRACT

Climate change is more than ever observed and is affecting the marine ecosystem in global scale. For the study of changing climate conditions, we focused in the North Aegean Sea and the most common species of small pelagic fish, anchovy and sardine. We studied the effects on species from changes in temperature, salinity, Black Sea Water input and nutrients load from the surrounding rivers. For the needs of the study, a multispecies anchovy and sardine, full-life-cycle model was developed for the North Aegean Sea and was two-way coupled to the hydrodynamic/biogeochemical model. The initial one-dimensional version of the model successfully simulated both species growth, biomasses and spawning periods. A clear dependence between species exploitation and zooplanktonic concentration was derived.

The next step in the model development yielded a three dimensional version. The species main attributes and the spatial distribution of biomasses, was once again in agreement with data. Additional simulations showed that locally, species compete for resources. Sensitivity experiments presented a negative reaction of both species to a temperature increase, especially that of anchovy. Simulations using IPCC climatic scenarios showed that a future temperature increase will result to an ecosystem degradation through a reduction in planktonic concentrations, negatively affecting anchovy and resulting to a prevalence of sardine. Last, variations of river nutrient inputs, as well as Black Sea Water inflow, also significantly downgrade species populations.

KEYWORDS

NORTH AEGEAN SEA, BIOENERGETICS MODEL, GENETIC ALGORITHM, CLIMATE CHANGE

Contents

1. Introduction

Climate change in the Mediterranean Sea is an already documented process (Skliris *et al.,* [2011, 2012]) and may have significant effects in the ecosystem. Long-term changes of the environmental conditions may introduce ecosystem shifts, which can potentially lead to limited resources, prompting an increasing inter and intra species competition (Katara *et al.,* 2011). In this study, the two most common species of small pelagic fish, anchovy and sardine are being used as a proxy for the study of the consequences of the climatic change on the ecosystem.

Small pelagic fish (SPF), like anchovies and sardines, are short-lived, highly fecund, planktivorous fishes that play a key role in marine food webs and are very important for marine food web, fisheries and human communities worldwide (Checkley *et al.,* 2009). They are very sensitive to environmental changes and extremely variable in their abundance at both inter-annual and inter-decadal scales (Alheit *et al.,* 2009; Checkley *et al.,* 2017).

An effective management system for these resources would require better understanding of the mechanisms controlling rapid variations in abundance and productivity of populations, and the consequences that these variations may have for ecological interactions (Bakun *et al.,* 2010; Pikitch *et al.,* 2012).

For European anchovy, coupled bioenergetics or bioenergetics-IBMs have been successfully implemented in the Black Sea (Oguz *et al.,* 2008), the Bay of Biscay (Pecquerie *et al.,* 2009; Gatti *et al.,* 2017), the North Aegean Sea (Politikos*,* [2011, 2015]) and the Gulf of Lions (Pethybridge *et al.,* 2013). A European sardine model has also been developed in the Bay of Biscay (Gatti *et al.,* 2017). These models were based on either the 'Wisconsin' (Kitchell

et al., 1977) or the Dynamic Energy Budget (DEB) (Kooijman, 2010) framework, and they were offline or, occasionally, online coupled with regional hydrodynamic-biogeochemical models.

There are two categories, the 1-D models that lack the horizontal dimension, i.e. a movement/migration module, yet they comprise an initial step useful for calibrating growth, egg production and/or population biomass to the average thermal and trophic conditions of the ecosystem (e.g. Ito *et al.,* 2007, Megrey *et al.,* 2007). They have also been used effectively in basin-scale or latitudinal comparisons between stocks (e.g. Ito *et al.,* 2015, Huret *et al.,* 2019). Finally, 1-D IBMs provide a means to test straightforwardly the outcomes of management measures (e.g. temporal fishing bans, reductions of fishing mortality), especially in the Mediterranean Sea where the collection of spatially explicit fisheries data has only recently been started and the utility of the collected information has often been questioned (Damalas, 2017).

An evolution of the above are the end-to-end models that were introduced for the study of complex ecosystem dynamics (Travers *et al.,* 2007), in order to dynamically integrate physical and biological processes of different trophic levels in the marine environment, from nutrients to primary production and from zooplankton to pelagic fish. Such models have being successfully implemented for anchovy and sardine in the California Current (Rose *et al.,* 2015) and for the Canary Current ecosystem (Sánchez-Garrido *et al.,* 2019). Politikos (2015) developed an end to end, 3-D IBM, describing the full-life cycle of anchovy in the N. Aegean.

In the present study, the existing anchovy model was extended by developing a 1-D and then a 3-D,end to end model, for both anchovy and sardine stocks in the N. Aegean. To this aim, a 3-D hydrodynamic/biogeochemical model was online coupled with a full-life cycle Individual Based Model (IBM), describing the dynamics and spatial distribution of both anchovy and sardine stocks in the area. The 1-D model implementation was particularly useful

in setting up the main attributes of the two species dynamics, despite its limitation in resolving horizontal processes, while with the use of a 3-D spatially explicit model, a more realistic description of the two species dynamics is provided, including the spatial variability induced by fish movement and eggs/larvae advection by ocean currents.

2. North Aegean Sea

2.1 North Aegean sea state and ecosystem status

The physical setting of the North Aegean Sea is unique due to a combination of topographic particularities including islands, straits, peninsulas and a combination of very shallow and very deep areas like the North Aegean Trough. The latter consists of three depressions (Sporades, Athos and Lemnos basins), with a maximum depth of 1300m. These separate the shallow shelf areas in the North, from the generally deeper central Aegean Sea.

Lateral exchange with adjacent basins includes the modified Black Sea Waters (BSW) and the Levantine Intermediate Waters (LIW). This process contributes to the seasonal and interannual variability of dense water formation in the open-sea areas, especially over the deep basins of the North Aegean Sea.

The shallow shelf areas are characterized by coastal currents influenced from the surrounding rivers inflows. But compared to all the rivers combined, the inflow of Black Sea Water (BSW) from the Dardanelles strait is larger in terms of volume and contributes the most to the general circulation of the area. Topographic features that determine the BSW pathways are the neighboring islands and the shallow Lemnos plateau (Fig 1).

The surface circulation patterns in the North Aegean are determined by this water mass, displaying a split in two branches, mainly north and south of the island of Lemnos, forming various gyres and thermohaline fronts (Zervakis and Georgopoulos, 2002). In general the BSW follows a northwestern route, passing through the strait between the Lemnos and

Imvros islands and contributing to the creation of the semi-permanent Samothraki gyre (Zervakis and Georgopoulos, 2002).

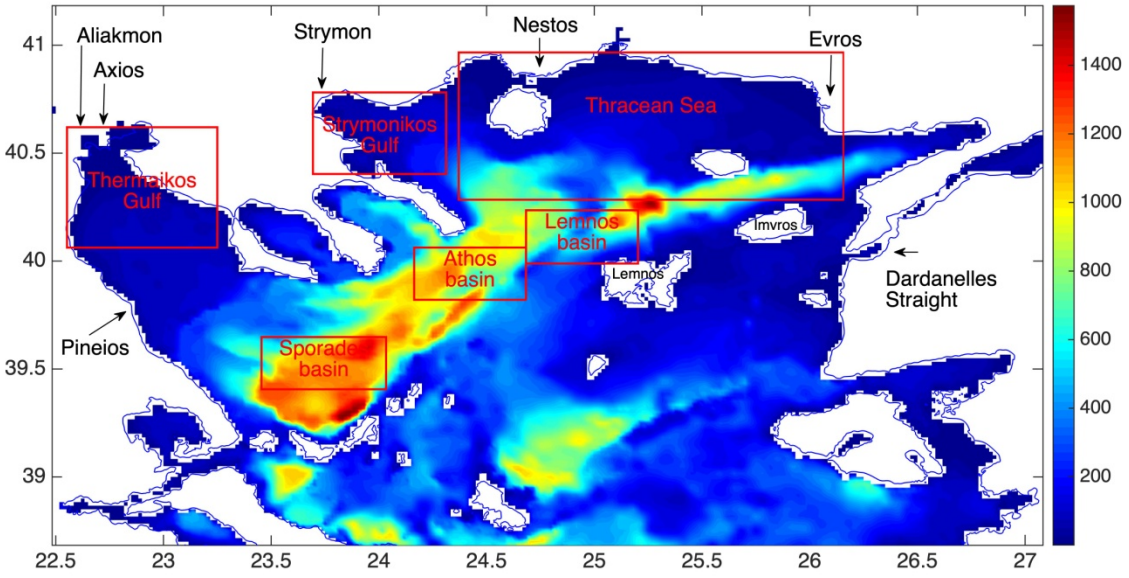

Figure 1. Map of the North Aegean Sea showing the model domain.

BSW is rich in particulate and dissolved organic matter (Polat and Tugrul, 1996; Sempere *et al.,* 2002), while in terms of dissolved inorganic nutrients is less important than the inputs from the N. Aegean rivers (Krom *et al.,* 2004; Polat and Tugrul, 1996; Tsiaras *et al.,* 2012). The importance of the rivers in the area, is more apparent when comparing their total nutrients load that amounts to about 50% of that from the Adriatic Sea rivers (Ludwig *et al.,* 2009), which is a significantly larger area.

In general, river inputs in the global ocean of nitrogen and phosphorus have presented a 3-fold and 5-flod increase between 1970 and 1990 in the global ocean and the Mediterranean Sea respectively (Smith *et al.,* 2003; Ludwig *et al.,* 2009), due to anthropogenic activities, like the use of fertilizer in the agriculture. Although this trend declined in the 90s,

thanks to the establishment of urban waste treatment and the banishment of phosphorus containing detergents, their contribution to the increased nutrients concentrations, is still crucial.

Summing up, this combination of the nutrient rich waters coming from the surrounding rivers and low salinity BSW, trigger an increased primary and secondary production (Frangoulis *et al.,* 2010; Siokou - Frangou *et al.,* 2002) in an overall oligotrophic Aegean Sea, thus sustaining one of the most important fish stocks in the Mediterranean Sea.

The combination of natural climate variability (Atlantic Multidecadal Oscillation) and climate change (Macias, Garcia-Gorriz and Stips, 2013) results to warming of the Mediterranean sea (from the early 1990s), especially in the Eastern Basin (Skliris *et al.,* 2012). Future (2070 to 2099) surface temperature increase may range from +1.73^{o}C to +2.97^{o}C (Adloff *et al.,* 2015), while surface salinity is projected to increase between +0.48 to 0.89 over the same period. Moreover, the Atlantic waters entering the Mediterranean are projected to be less dense (Adloff *et al.,* 2015), thus changing the structure and formation of stationary fronts and of mesoscale structures, with implications on pelagic fish (Alvarez-Berastegui et al., 2016). The aforementioned changes in stratification, combined with decreases in the strength of upwelling events and precipitation, will result to a degradation of the primary production in the basin, resulting to a decline of species richness (Benedetti *et al.,* 2017).

2.2 North Aegean Sea anchovy and sardine status

The N. Aegean is considered to be one of the main habitats of the most predominant small pelagic fish in the Mediterranean Sea, anchovy (*Engraulis Engrasicolus*) and sardine (*Sardina Pilchardus*). Other important habitats of these species include the Gulf of Lions, the Straits of Sicily/Tunisian Coast and the Alboran, Catalan and Adriatic Seas. Considering that the Mediterranean is a generally oligotrophic Sea, these regions provide the few suitable habitats, characterized by local capacity for food provision and increased larval retention, where spawning and nursery grounds are largely overlapping (Somarakis *et al*., 2019).

In most cases in the Mediterranean, the nutrient rich waters that contribute to an enhanced primary production, originate from river freshwater discharge or are related with upwelling and circulation patterns. When combined with a highly stable upper layer, together with strong fronts and weak wind induced turbulent mixing, they constitute the ocean triads theory (Agostini & Bakun, 2002). These features that are common in areas supporting the main anchovy and sardine stocks in the Mediterranean contribute to relatively high concentrations of food and create preferable conditions for larval feeding and retention of eggs. Other patterns, related with a variability of global origin, such as the effects of NAO index in the Canary Current ecosystem (Sanchez - Garrido *et al.,* 2017), may also contribute to favorable food conditions.

But even in these areas, some of the physical conditions that are favorable for sardine may be adverse for anchovy and vice versa, since food and temperature are environmental factors that oscillate in opposite phase and this may be related to the fact that for example in the North Aegean Sea, spawning takes place during autumn and winter for sardine and during spring and summer for anchovy (Gkanasos *et al.,* 2019). Findings in the western North Pacific

(Takasuka *et al.,* 2018) point out the role of adverse environmental conditions on food availability, through a connection between the anchovy intra-specific density dependence and the anchovy and sardine (inter) specific density dependence. Also, a previous study (Katara *et al.,* 2011) analyzing catch data in the Aegean and Ionian Seas, showed that both species show a negative relationship with increasing temperature that is stronger for sardine.

The long-term variability of the two species is often characterized by environmentally driven out-of-phase oscillations that have been well documented in various areas of the global ocean, such as in the East and West Atlantic and Pacific Oceans (Checkley *et al.,* 2017), although their understanding is still incomplete. Similar fluctuations, also connected with environmental factors, have also been observed in the Mediterranean anchovy and sardine landings long-term variability (Voulgaridou and Stergiou, 2003), while an opposite relation of anchovy (positive) and sardine (negative) with temperature in the Mediterranean Sea has been identified in other studies (Stergiou *et al.,* 2016; Tzanatos *et al.,* 2014).

In the Mediterranean Sea, most anchovy and sardine stocks have been declining in recent years (e.g. Tsikliras *et al.,* 2015; Vasilakopoulos *et al.,* 2014; Vilibic *et al.,* 2016), showing also decreasing trends in maximum size and somatic condition (Brosset, [2015, 2017]). For example, in the Gulf of Lions, where fishing pressure on anchovy and sardine stocks is very low, the reductions in biomass, body condition and maximum size/age have been attributed to increasing temperature and reduced water mixing, affecting planktonic productivity (Brosset*,* [2015, 2017]; Saraux *et al.,* 2019).

An in between species comparison yields the main biological differences between anchovy and sardine in the N. Aegean Sea and these include their reproductive traits (winter spawning, low daily fecundity in sardine – summer spawning, high daily fecundity in anchovy (Ganias *et al.,* 2014; Somarakis *et al.,* 2019) and the generally longer life span and maximum

size of sardine (Somarakis *et al.,* 2006). On the other hand, the two stocks have many similarities, e.g., closely correlated diel feeding patterns/food consumption rates (Nikolioudakis*,* [2011, 2012, 2014]), similar diel vertical migration behavior (Giannoulaki *et al.,* 1999; Tsagarakis *et al.,* 2012) and high diet overlap.

For both species, food availability is a requirement very early at larval stage after yolk-sac exhaustion. So difference in diets and prey size selectivity between anchovy and sardine appears rapidly (Morote *et al.,* 2010). Early larvae of anchovy are first feeding on microzoopankton in the size range 50 to 100 μm (Garcia & Palomera, 1996), with a large part of copepod eggs, nauplii and copepodites (Regner, 1996). Generally, prey size range increase with larval size (Tudela *et al.,* 2002; Catalan *et al.,* 2010). Similarly to anchovy larvae, prey size range of sardine increases with larval size.

Adult anchovy mainly feed on copepods during daytime, as observed in the Bay of Biscay and the Mediterranean Sea (Tudela & Palomera 1995; Plounevez & Champalbert 2000), while sardine, was also noticed (Bode *et al.,* 2004) to follow a zooplanktivorous diet.

Also, the Mediterranean sardine is considered to be primarily a capital breeder, i.e. it stores energy and uses it later for egg production (Ganias *et al.,* 2007; McBride *et al.,* 2015; Somarakis *et al.,* 2019). In contrast, the Mediterranean anchovy is thought to be more closer to the income breeding pattern, i.e. egg production is mainly fueled by direct food intake during the spawning period (Somarakis, 2005)

Last, temperature optima for growth are almost identical for the two species, at least during the juvenile stage (Schismenou, [2013, 2016]; Somarakis *et al.,* 2019).

3. Models

3.1 Low trophic level (LTL) model

The coupled biophysical model used for the simulations conducted in this study, consists of the hydrodynamical Princeton Ocean model (POM; Blumberg and Mellor, 1983) and the European Regional Seas Ecosystem Model (ERSEM, Baretta *et al.,* 1995). Together they form the Lower Trophic Model (LTL) that is online two way coupled with the fish model (Fig. 2).The coupled model has been implemented in the Cretan Sea (Petihakis *et al.,* 2002), the North Aegean Sea (Tsiaras*,* [2012; 2014]; Petihakis et al., 2014; Politikos *et al.,* 2015; Chust *et al.,* 2014) and is currently operational on Mediterranean basin-scale (Kalaroni *et al.,* 2020), as part of the POSEIDON forecast system (www.poseidon.hcmr.gr).

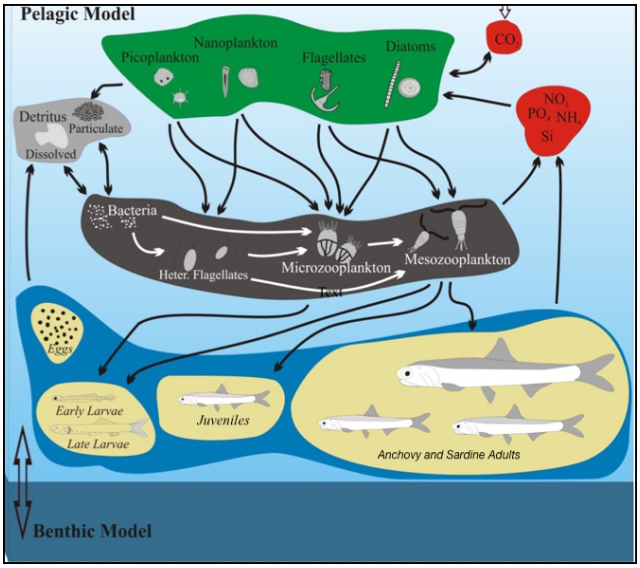

Figure 2. Representation of the anchovy and sardine model coupled with the lower trophic level (LTL) model.

3.1.1 Hydrodynamic model (POM)

The numerical model used for the simulation of the hydrodynamic characteristics of the North Aegean Sea (i.e temperature, salinity, vertical mixing, diffusion, circulation), is a three-dimensional, primitive equation, free surface, sigma coordinate model. A 2.5 turbulence closure submodel (Mellor and Yamada, 1982) calculates the vertical eddy viscosity/diffusivity taking into account the wind stirring and the stratification of the water column. The model simulates and produces fields of baroclinic and barotropic current velocities, the sea surface height as well as fields of temperature, salinity and turbulence (or vertical diffusion).

The model grid is a curvilinear orthogonal coordinates system and the variables are displaced using an Arakawa – C grid (Arakawa, 1972). It uses vertical sigma coordinates in the vertical and has a free sea surface. The time step used is variable for computing cost reduction, based in a time split technique (Courant-Friedrichs-Levy, 1928), where a small time step is used for the barotropic (External Mode) equations and a larger time step for the baroclinic (Internal Mode) equations. The external mode solves the sea surface height and the vertically integrated velocities, while in the internal mode the *U, V, W* velocities, the temperature, the salinity, the turbulent kinetic energy (q^2) and the turbulent length scale (q^2l).

The horizontal diffusivity is calculated along the sigma coordinates following the Smagorinsky formulation (Smagorinsky, 1963). Equations are resolved using a finite differences numerical method. The space and time integration schemes are central finite differences and leap-frog respectively, both of second order precision.

The basic equations used in the model are the continuity equation:

$$\nabla \cdot U_i = 0 \iff \frac{\partial U}{\partial x} + \frac{\partial V}{\partial y} + \frac{\partial W}{\partial z} = 0$$

Where $U_i = iU + jV + kW$ is the velocity, U, V and W are the velocity components in the x, y and z respectively, while the Laplace operator is represent with $\nabla = \frac{\partial}{\partial x} + \frac{\partial}{\partial y} + \frac{\partial}{\partial z}$.

The equations of movement

$$\frac{\partial U}{\partial t} + \frac{\partial U^2}{\partial x} + \frac{\partial UV}{\partial y} + \frac{\partial UW}{\partial z} - fV = -\frac{1}{\rho_o}\frac{\partial P}{\partial x} + \frac{\partial}{\partial z}\left(K_M \frac{\partial U}{\partial z}\right) + F_U$$

$$\frac{\partial V}{\partial t} + \frac{\partial UVU^2}{\partial x} + \frac{\partial V^2}{\partial y} + \frac{\partial VW}{\partial z} + fU = -\frac{1}{\rho_o}\frac{\partial P}{\partial y} + \frac{\partial}{\partial z}\left(K_M \frac{\partial V}{\partial z}\right) + F_V$$

Where ρ_o is the reference density, P the pressure and $P=P(T,S,P)$ is the density of the liquid. The eddy viscosity coefficient is calculated according to the Mellor-Yamada 2.5 turbulent closure scheme (Mellor & Yamada 1982). The terms $\frac{1}{\rho}\frac{\partial P}{\partial x}$ and $\frac{1}{\rho}\frac{\partial P}{\partial y}$ is the pressure gradient in each axis, while pressure is calculated through the hydrostatic approach

$$P = P_{atm} + \rho_o g\eta + g\int_s^0 \rho(x, y, s)ds$$

Where η the free sea surface height, g the gravity acceleration and P_{atm} the atmospheric pressure (steady). The terms fU and fV are the Coriolis force and F_U, F_V are the horizontal diffusion terms:

$$F_U = \frac{\partial}{\partial x}\left(2A_M \frac{\partial U}{\partial x}\right) + \frac{\partial}{\partial y}\left[A_M\left(\frac{\partial U}{\partial y} + \frac{\partial V}{\partial x}\right)\right]$$

$$F_V = \frac{\partial}{\partial y}\left(2A_M \frac{\partial V}{\partial y}\right) + \frac{\partial}{\partial x}\left[A_M \left(\frac{\partial U}{\partial y} + \frac{\partial V}{\partial x}\right)\right]$$

With A_M being the horizontal viscosity parameterized according to Smagorinsky (1963).

Salinity and temperature are treated according to:

$$\frac{\partial S}{\partial t} + \frac{\partial US}{\partial x} + \frac{\partial VS}{\partial y} + \frac{\partial WS}{\partial z} = \frac{\partial}{\partial z}\left[K_H \frac{\partial S}{\partial z}\right] + F_S$$

$$\frac{\partial T}{\partial t} + \frac{\partial UT}{\partial x} + \frac{\partial VT}{\partial y} + \frac{\partial WT}{\partial z} = \frac{\partial}{\partial z}\left[K_H \frac{\partial T}{\partial z}\right] + F_T - \frac{\partial R}{\partial z}$$

With S being the salinity, T the temperature and K_h the vertical turbulent mixing coefficient (Mellor Yamada 2.5 turbulent closure scheme). Terms F_S and F_T represent the horizontal diffusion and are given by:

$$F_S = \frac{\partial}{\partial x}\left(A_H \frac{\partial S}{\partial x}\right) + \frac{\partial}{\partial y}\left(A_H \frac{\partial S}{\partial y}\right)$$

$$F_T = \frac{\partial}{\partial x}\left(A_H \frac{\partial T}{\partial x}\right) + \frac{\partial}{\partial y}\left(A_H \frac{\partial T}{\partial y}\right)$$

With A_H being the horizontal viscosity coefficient, parameterized according to Smagorinsky (1963). Last $\frac{\partial R}{\partial z}$ is the change of solar temperature with depth.

The model was previously applied in the Mediterranean Sea (Zavatarelli & Mellor, 1995; Horton *et al.,* 1997; Drakopoulos & Lascaratos, 1999] and is sub basins like the Adriatic Sea (Zavatarelli & Pinardi, 2003), the Eastern Mediterranean (Korres & Lascaratos, 2003; Petihakis

et al., 2009), the Levantine Basin (Lascaratos & Nittis, 1998), the Cretan sea (Triantafyllou *et al.,* 2003) and the North Aegean Sea (Kourafalou & Tsiaras, 2007).

3.1.2 Biogeochemical model(ERSEM)

The biogeochemical lower trophic level model that was used, is based on the ERSEM (European Regional Seas Ecosystem Model). In the model the organisms are being classified according to their trophic role (consumers, producers, etc.) and size, following the functional group approach. The pelagic food web was slightly modified from the original ERSEM, in order to describe the oligotrophic environment of the Mediterranean Sea.

According to Fig.3 the planktonic food web consists of bacteria, picophytoplankton, nanophytoplankton, diatoms, dinoflagellates, heterotrophic nanoflagellates, microzooplankton and mesozooplankton. The model includes also dissolved inorganic nutrients (phosphate, nitrate, ammonium, silicate) and pools of particulate and dissolved organic matter. The cycles of nitrogen, phosphorus and silicate are coupled with carbon dynamics, as each plankton group has dynamically varying C:N:P:Si pools.

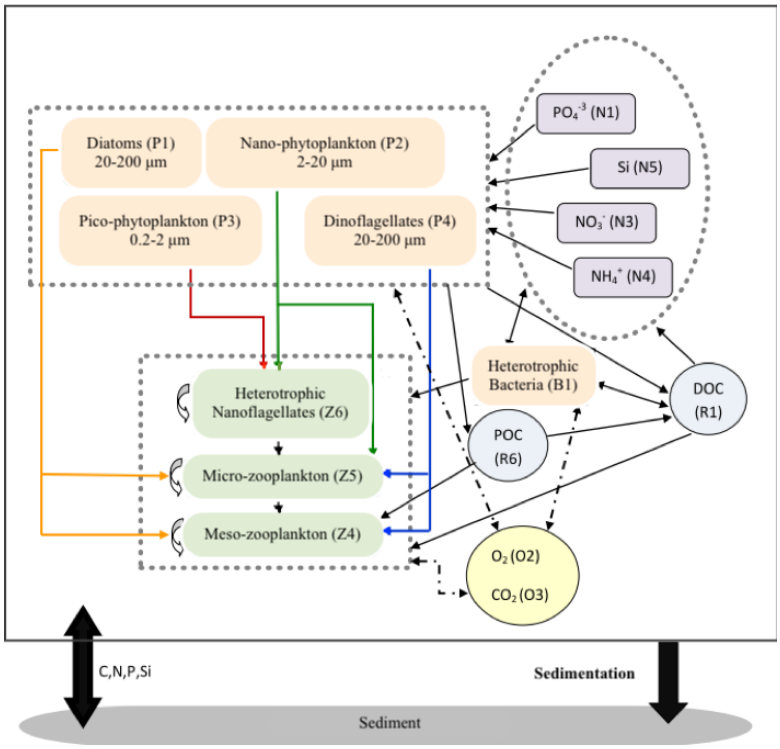

Figure3. ERSEM food web. Arrows represent the fluxes between groups.

The model has also been applied in numerous ecosystems, like that of the North Sea (Radach & Lenhart, 1995; Pätsch & Radach, 1997; Collingridge, 2012), the North Western Mediterranean Sea (Proctor *et al.,* 2003; Elkalay *et al.,* 2012), the Black Sea (Pätsch & Radach, 1997), the Eastern Mediterranean Sea (Allen *et al.,* 2002; Petihakis, [2002, 2012, 2014]; Triantafyllou et al., 2003; Tsiaras *et al.,* 2014), the Arabic Sea (Blackford & Burkill, 2002), the Red Sea (Triantafyllou *et al.,* 2014) and in lagoons (Petihakis et al., 1999; Triantafyllou *et al.,* 2000).

3.2 Individual based model (IBM)

A one-dimensional and then a three-dimensional individual based model (IBM) were developed for the North Aegean Sea ecosystem, aiming to describe the full life cycle of European anchovy (*Engraulis encrasicolus*) and the European sardine (*Sardina pilchardus*), their spatial distribution and their most important energetic features. The model was based on the anchovy model developed by Politikos (2015), on the basis of which the sardine IBM was built, by progressively integrating traits that are known to differ between the two species.

For computational efficiency, both species populations are being divided into Super Individuals (SIs) (Scheffer *et al.,* 1995), with each SI consisting of the individuals that share the same properties like life stage/age class, weight (g), length (mm), age (day) and position (longitude, latitude). SIs that belong at the same life stage or age class have identical characteristics in terms of feeding preferences, mortalities and movement. Given that new SIs are created during spawning, in order to prevent their total number from continuously increasing, when they exceed a certain limit, these of the same age class when found within a predefined distance are merged and their properties averaged.

The model describes the life cycle of both species, from the egg to the adult stage, given that the anchovy and sardine life spans are considered to be 3.5 and 4.5 years respectively. The life span is divided into seven stages/age classes for anchovy (embryo, early larva, late larva, juvenile, adult age-1 to age-3) and eight stages for sardine (with an additional adult age class: adult age-1 to age-4). The number of age classes was defined based on otolith age readings made on samples collected in the field (Somarakis *et al.,* 2012).

The multispecies model includes the following modules, a bioenergetics, a population module, and a movement module with a horizontal and a diel vertical migration (DVM) algorithm.

3.2.1 Bioenergetics

The Wisconsin bioenergetics framework (Ito *et al.,* 2004; Rose *et al.,* 2007) has been adopted to simulate the anchovy and sardine growth for larvae, juvenile and adult stages in the North Aegean Sea. The wet weight increment per unit weight of weight per day for juvenile and adult stages is calculated by the equation:

$$\frac{1}{W_{SI}} \cdot \frac{dW_{SI}}{dt} = [C - (R + EG + SDA + EX + E_{egg})] \cdot \frac{CAL_z}{CAL_f},$$

where W_{SI} is the fish wet weight (g), t the time (days), C the consumption, R the respiration (or losses through metabolism), SDA the dynamic action (or losses because of energy costs of digesting food), EG the egestion (or losses because of faeces), EX the excretion (or losses of nitrogenous excretory wastes) and E_{egg} is the energy allocated to reproduction.

Components of the energy budget ($C, R, EG, EX, SDA, E_{egg}$) are in units of (g prey g fish^{-1} day^{-1}), which are converted to (g fish g fish^{-1} day^{-1}) by using CAL_z which is the caloric equivalent of zooplankton (cal g prey^{-1}) and CAL_f the caloric equivalent of fish (cal g fish^{-1}). More thoroughly, the consumption C_i results from the equation $C_i = \sum_{i=1}^{2} C_{j,i}$

where $C_{j,i} = \frac{C_{max}(\frac{PD_{j,i}v_{j,i}}{k_{j,i}})}{1+\sum_{i=1}^{2}(\frac{PD_{k,i}v_{k,i}}{k_{k,i}})}$, $PD_{j,i}$ is the density of prey type i (i = 1 corresponds to microzooplankton and i =2 to mesozooplankton) (g-prey m^{-3}) for life stage/age class j, $v_{j,i}$ is the preference to prey type i of life stage/age class j (dimensionless) and $k_{j,i}$is the half saturation function (g-prey m^{-3}) for life stage j feeding on prey type i. The respiration R is calculated from the equation

$$R = a_r W_{SI}^{b_r} f_R(T) A \text{ where } f_R(T) = Q_{10}^{\frac{T-T_m}{10}}, A = e^{d_r U} \text{ and } U = a_A W^{b_A} e^{(C_A T)}$$

with a_r being the intercept for respiration, b_r the exponent for respiration, Q_{10} the temperature dependence parameter, T_m the mean annual temperature, d_r the coefficient for R for swimming speed, a_A the intercept U (< 12.0°C), a_A the intercept U (≥12.0°C), a_A the intercept U (≥12.0°C) (during low feeding activity), b_A the coefficient U for weight, c_A the Coefficient U vs. temperature (< 12.0°C) and c_A the Coefficient U vs. temperature (≥12:0°C).

Egestion comes from the equation $F = a_f C$ where a_f is the proportion of food egested, the specific dynamic action $SDA = a_{sda}(C - F)$ where a_{sda} is the specific dynamic action coefficient. Excretion is calculated through $E = a_e(C - F) + b_e$ where a_e is the excretion coefficient and b_e is the proportion of food excreted. Last, specific dynamic action results from consumption and egestion, through:

$$SDA = a_{sda}(C - F)$$

A length-weight relationship is needed to convert weight (*W*) to length (*L*) and allow for the transition from one stage to the other. That piecewise allometric relationship is:

$$W = b_0 + b_1 L + b_2 (L-d_1)(L \geq d_1) + b_3 (L-d_2)(L \geq d_2),$$

where b_0, b_1, b_2 and b_3 are the estimated parameters (non-linear regression), d_1 is the inflexion point, at which the slope changes from the larval to the juvenile stage and d_2 is the length corresponding to the transition from the juvenile to the adult stage (length at first maturity).

Early larvae feed on microzooplankton, late larvae consume micro and mesozooplankton, while juveniles and adults feed only on mesozooplankton. The individuals that each SI represents are assumed to have a vertical distribution (position in the water column) that is maximized around the depth of peak prey availability. Eggs and early larvae are distributed in the surface layer (0-30m), while late larvae, juveniles and adults are assumed to perform diel vertical migrations between the surface (0-30m, night) and the sub-surface (>30m, day).

In order to predict the duration of the embryonic stages (egg+yolk sac larva), which are temperature dependent, we use the equations developed by Gatti, (2017). Parameters for anchovy were adopted from Politikos, (2011) and those for sardine were based on existing literature and are both summarized in Table 1.

Table 1. Equations and parameters of the bioenergetics model

Process	Equations	Parameters Anchovy	Parameters Sardine
Somatic growth	$\frac{1}{W_{SI}} \cdot \frac{dW_{SI}}{dt} =$		

	$\left[C-\left(R+EG+SDA+EX+E_{buffer}\right)\right]\cdot\frac{CAL_z}{CAL_f}$ W_{SI} = fish wet weight (g) t = time (days) C = consumption R = respiration EG = egestion SDA = specific dynamic action EX = excretion E_{buffer}= the energy allocated to reproduction CAL_z = caloric equivalent of zooplankton CAL_f=caloric equivalent of fish	2560 J g^{-1} (zoopl.) 3120J, (<40mm) 3520J, (40≤ Length (mm) ≤ 60) 4048J, (60≤ Length (mm) < 90) 5150J, (90≤ Length (mm))	-//- -//- -//- -//- -//- -//-
Maximum Consumption (C_{max})	$C_{max}=a_c W_{SI}^{b_c} f_C(T) f_C(T) = V^X e^{X(1-V)}$ a_c = Intercept for consumption b_c = Exponent for consumption	a_c= 0.41 b_c= 0.31	-//- -//-
Temperature function	$V=\frac{T_{max}-T}{T_{max}-T_{opt}}$ $S=(lnQ_c)(T_{max}-T_{opt})$ $Y=(lnQ_c)(T_{max}-T_{opt}+2)$ $X=\frac{S^2(1+(1+40/Y)^{1/2})^2}{400}$ Q_c = Slope for temperature dependence T_{opt} = Optimum Temperature (°C) T_{max} = Maximum Temperature (°C)	Q_c = 2.22[a,b], 2.4[c,d] T_{opt}=17.25[a],16.25[b],15.8[c,d] T_{max} = 27	-//- T_{opt}=14.5[a],14.75[b],15.8[c,d] -//-
Consumption (C)	$Ci=\sum_{i=1}^{2} C_{j,i}$	$v_{2,1}$ = 1.0 $v_{3,1}$ = 0.5	-//- -//-

	$C_{j,i} = \frac{C_{max}(\frac{PD_{j,i}v_{j,i}}{k_{j,i}})}{1+\sum_{i=1}^{2}(\frac{PD_{k,i}v_{k,i}}{k_{k,i}})}$ $PD_{j,i}$= density of prey type i i = 1 corresponds to microzooplankton and i =2 to mesozooplankton) (g-prey m^{-3}) for life stage/age class j $v_{j,i}$= vulnerability of prey type i to life stage/age class j (dimensionless) $k_{j,i}$ half saturation function (g-prey m^{-3}) for life stage j feeding on prey type i.	$v_{4,1} = v_{5,1} = v_{6,1} = v_{7,1} = 0$ $v_{2,2} = 0.0$ $v_{3,2} = 0.5$ $v_{4,2} = v_{5,2} = v_{6,2} = v_{7,2} = 1.0$	-//- -//- -//- -//-
Respiration (R)	$R = a_r W_{SI}^{b_r} f_R(T) A$ $f_R(T) = Q_{10}^{\frac{T-T_m}{10}}$ $A = e^{d_r U}$ $U = a_A W^{b_A} e^{(C_A T)}$ a_r = Intercept for respiration b_r = Exponent for respiration Q_{10}= Temperature dependence parameter T_m =Mean annual temperature d_r= Coefficient for R for swimming speed a_A= Intercept U (< 12.0 °C) a_A = Intercept U (≥12.0 °C) a_A = Intercept U (≥12.0 °C) (during low feeding activity) b_A= Coefficient U for weight c_A = Coefficient U vs. temperature (< 12.0 °C) c_A = Coefficient U vs. temperature (≥12:0 °C)	$a_r = 0.003$ $b_r = 0.34$ $Q_{10} = 1.3$ $T_m = 16^{a,b,c,d}$ $d_r = 0.022$ $a_A = 2.0$ (U< 12.0 °C) $a_A = 12.25^{a,b}$, 11.98^{c}, 14.21^{d} (U≥12.0 °C) $a_A = 9.97^{c}$ (U≥12.0 °C) (low feeding activity) $b_A = 0.27^{a,b}$, 0.33^{c}, 0.27^{d} $c_A = 0.149$ (U< 12.0 °C) $c_A = 0.0$ (U≥12:0 °C)	-//- -//- -//- -//- -//- -//- -//- -//- -//- -//-
Egestion (EG)	$F = a_f C$ a_f= Proportion of food egested	$a_f = 0.15^{a,b}$, $0.126^{c,d}$	-//-
Excretion (EX)	$E = a_e(C - F) + b_e$ a_e= Excretion coefficient	$a_e = 0.41$	-//-

	b_e= Proportion of food excreted	b_e = 0.01	-//-
Specific Dynamic Action (SDA)	$SDA = a_{sda}(C - F)$ a_{sdo}= Specific dynamic action coefficient	a_{sda} = 0.10	-//-
Length-weight relationship	$y=b_o+b_1x+b_2(x-d_1)(x>d_1)+b_3(x-d_2)(x>d_2)$ *y, x* (log-transformed fish wet weight and length) b_o = y-intercept b_1 = slope of the function for the larval stage b_2= slope change for the juvenile stage d_1= slope change inflexion point b_3= subsequent slope change for the adult stage d_2 = corresponding length for this slope respectively	 b_o = -6.1158 b_1 = 3.5764 b_2 = -0.616 d_1 = 1.5798 b_3 = 0.7137 d_2 = 1.954	 b_o = -9.229 b_1 = 5.391 b_2 = -2.281 d_1 = 1.699 b_3 = 0.106 d_2 = 2.02
Parameters of the fish distribution function.	$k_f(j, food)$, Vertical distribution steepness parameter *ffc*, Fish biomass conversion factor *qnF*, Fish C:N internal quota *qpF*, Fish C:P internal quota *qnZ5*, Z5 maximum N/C ratio *qnZ4*, Z4 maximum N/C ratio qpZ5, Z5 maximum P/C ratio qpZ4, Z4 maximum P/C ratio	50^b,$40^{c,d}$ $(mgC/m^3)^2$ (calibrated) 147(mgC/g ww) 0.019 (mmol N/mgC) 0.00136 (mmolP/mgC) 0.0167 (mmol N/mgC) 0.015 (mmol N/mgC) 0.001 (mmolP/mgC) 0.00167 (mmolP/mgC)	-//- -//- -//- -//- -//- -//- -//- -//-

[a] Early larval stage (j = 2),[b] Late larval stage (j = 3),[c] Juvenile stage (j = 4),[d] Adult age-classes (j = 5,6,7 & 8 for sardine).

Reproduction

Spawning is regulated by an energy allocation/egg production algorithm, embedded in the bioenergetics equation (Fig.4). This algorithm is different from the one described in

Politikos, (2015). The latter assumed an extreme income breeding mode for the Mediterranean anchovy. The new algorithm is now allowing for breeding pattern to move along the capital-income continuum (McBride *et al.,* 2015). A similar approach was followed in Gatti, (2017). Briefly, the energy available from consumption is first used to satisfy the needs of maintenance (*M*) that accounts for respiration, egestion, specific dynamic action, excretion. The remainder energy (*A*) is then channeled to only growth (increase in weight), if fish is smaller than length at maturity (L_m). This is justified from measurements in European sardine showing that, in juvenile fish, growth is prioritized and immature fish do not store fat (Machias and Tsimenides, 1995). If fish is larger than L_m, the surplus energy (*A*) is channeled to both growth and reproduction. Energy allocated to reproduction is stored, all year round, in the so-called 'reproductive buffer' (Pecquerie *et al.,* 2009). The amount of *A* allocated to reproduction is *(1-k)*A*. The parameter *k* is largely unknown and therefore assumed to be k=0.5 in both species. If A<0, energy already in the reproductive buffer (first) and fish soma (secondly) goes to maintenance (to meet daily maintenance costs) (Fig. 4). Regarding spawning, each SI releases an egg batch (egg SI) on a daily basis, if a (species specific) *SST* criterion is satisfied, fish length is larger than L_m and energy stored in the buffer (E_{buffer}) is sufficient for producing the egg batch.

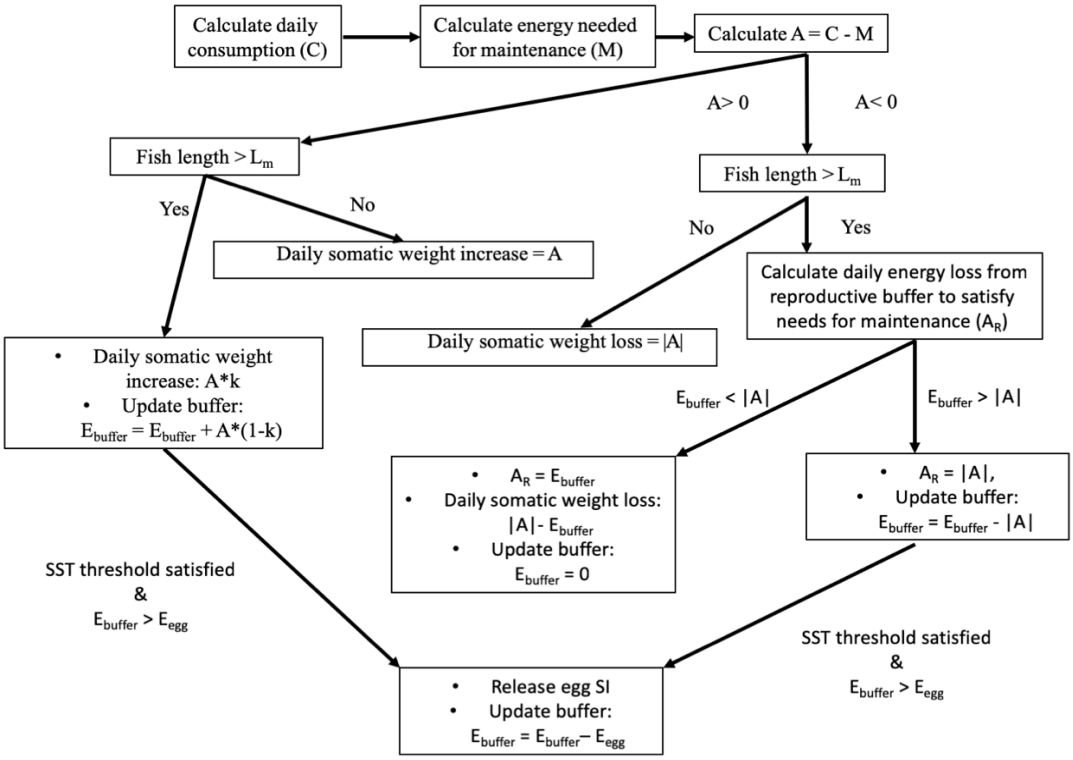

Figure 4. Schematic illustration of the energy allocation and egg production algorithm. SST: Sea surface temperature. L_m: length at maturity. E_{buffer}: energy in reproduction buffer. E_{egg}: batch energy.

The number of eggs released (the population of the egg SI) is equal to the product of daily specific fecundity (*DSF*, number of eggs per gram of the adult SI) and the SI's weight. Different values of *DSF* were adopted for anchovy and sardine, based on published literature (Somarakis *et al.,* 2012; Ganias *et al.,* 2014). The batch energy (E_{egg}) is calculated from *DSF* and egg energy. We used the values of anchovy and sardine egg energy calculated in Gatti *et al.,* (2017) (Table 1).

In the Mediterranean Sea, the two species have different reproductive periods, with sardine spawning from autumn to spring and anchovy from spring to autumn. Therefore a combination of temperature and calendar criterions were adopted for both species. Anchovy

spawns when SST is above 15^{o}C and until the end of September and sardine starts to spawn when SST falls under 16^{o}C and continues until mid-April. During this period, eggs are being released daily, with a total batch energy (E_{egg}) derived from the daily specific fecundity (DSF), which is the number of eggs released per gram of adult SI (Ganias *et al.,* 2014), the weight of the fish and the egg energy of each species (Gatti *et al.,* 2017).

Given the different spawning periods, we also adopted different optimum temperatures for larval consumption (Peck *et al.,* 2013) (Table 2). These were selected so as to lay close to the actual average temperatures that larvae experience. Apart from SST, an additional criterion (not shown in Figure 4) was also applied to define the end of the spawning period. It is known that, in the lack of food, fish stop releasing eggs and start to absorb their gonads (a process known as atresia). If food shortage is prolonged (8-9 days in Northern anchovy) the spawning period of the fish comes to an end (Hunter and Macewicz, 1985). We therefore assumed that if food consumption is insufficient to meet metabolic requirements for 9 consecutive days the SI stops releasing eggs for that particular spawning season.

Last, the embryonic stage (egg+yolk sac larva) durations are temperature dependent and are regulated by the equations developed by Gatti, (2017). Subsequently, the stage transition is length dependent until the juvenile stage and after this is based on calendar criterions.

Table 2. Species particulars

Parameter	Anchovy	Sardine
[a] Length range (mm):		
Early larvae	4-11	5-13
Late larvae	11-42	13-50
Juvenile	42-100	50-105

Adult Stage, age-1	5th March – 4th March (year+1)	1st September – 31th August(year+1)
Adult Stage, age-2	5th March – 4th March (year+1)	1st September – 31th August(year+1)
Adult Stage, age-3	5st March – 1stDecember	1st September – 31th August(year+1)
Adult Stage, age-4	-	1st September – 30th April(year+1)
[a] Length at maturity (Lm, mm)	100	105
[b] Egg energy	0.66	1.11
[c] Daily specific fecundity (eggs g-1)	46	20.1
Batch Energy (g prey per g fish per day)	0.012	0.0086
[d] Spawning period SST threshold	Start: SST >15°C End: October	Start: SST <16°C End: mid-April
Optimum temperatures for consumption	18 (early larvae) 15.85 (late larvae) 15.1 (juveniles/adults)	14.2 (early larvae) 14.2 (late larvae) 15.1 (juveniles/adults)
Half saturation parameters for consumption	0.12 (early larvae) 0.08 (late larvae) 0.14 (juveniles) 0.205 (adults age 1) 0.175 (adults age 2) 0.272 (adults age 3)	0.17 (early larvae) 0.15 (late larvae) 0.0975 (juveniles) 0.157 (adults age 1) 0.19 (adults age 2) 0.19 (adults age 3) 0.2 (adults age 4)
[e] Natural mortalities	0.4,embryos 0.2,early larvae 0.05,late larvae 0.012,juveniles* 0.002, adults	
[e] Fishing mortalities (adults)	0.00136	0.002

[a] Schismenou (2012), [b] Gatti *et al.,* (2017), [c] Somarakis *et al.,* (2012), Ganias *et al.,* (2014), [d]Somarakis (1999), Tsikliras (2007), [e]Politikos (2015), Antonakakis *et al.,* (2011), Giannoulaki *et al.,* (2014).

*The natural mortality of juveniles was calibrated (see text for details).

3.2.2 Population

Mortality

The number of individuals in each SI is computed by taking into account the natural and fishing mortality. Specifically, at each time step, the number of individuals within each SI (*N*) is reduced using the equation:

$$\frac{dN}{dt} = -(M + F) \times N$$

where *M* is the assigned natural mortality and *F* is the fishing mortality rate, applied only to adult SIs (see Table 2).

For the embryonic and larval stages, the adopted *M* values for anchovy were based on published estimates (Somarakis and Nikolioudakis, 2007; Mantzouni *et al.,* 2007; Somarakis et al., 2012). In the case of European sardine, literature information was very limited. The few existing values for egg and early larval mortality, estimated for the Iberian sardine in the Atlantic (Alvarez and Chifflet, 2012) were very similar to the values adopted for the

Mediterranean anchovy. We therefore used the same values of natural mortality for the early life stages of the two species (Table 2).

The natural mortality during the juvenile stage is largely unknown. Yet, mortality during the juvenile stage has a great impact on subsequent population biomass due to the stage's long duration. The natural mortality rate of juveniles was therefore calibrated, so as the simulated anchovy and sardine populations to fluctuate around 40000 t and 25000 t respectively, which are approximately the mean biomasses of the two species in the N. Aegean Sea (based on acoustic data biomass estimations for the period 2003-2008 (Antonakakis *et al.,* 2011; Giannoulaki *et al.,* 2014) (Table 2). The mean natural mortalities of adults were adopted from the aforementioned stock assessment papers (Table 2).

Fishing mortality F(F_{SI} applied to a SI), follows the separability assumption and is determined by the product of three components

$$F_{SI} = F_m \cdot F_{season} \cdot F_{position}$$

where F_m is the mean annual fishing mortality for the age class (Table 2), F_{season} is a proportional term, which parameterizes the seasonality of fishing effort on a monthly basis, calculated from monthly changes in anchovy catches (Fig.5), and $F_{position}$ denotes a flag taking values 0 or 1 to indicate if the current position of the SI is within or outside the known fishing grounds. The fishing grounds of anchovy in the North Aegean Sea include the continental shelf areas of the Thermaikos Gulf, the Thracian Sea and the Strymonikos/Kavala Gulfs (unpublished data).

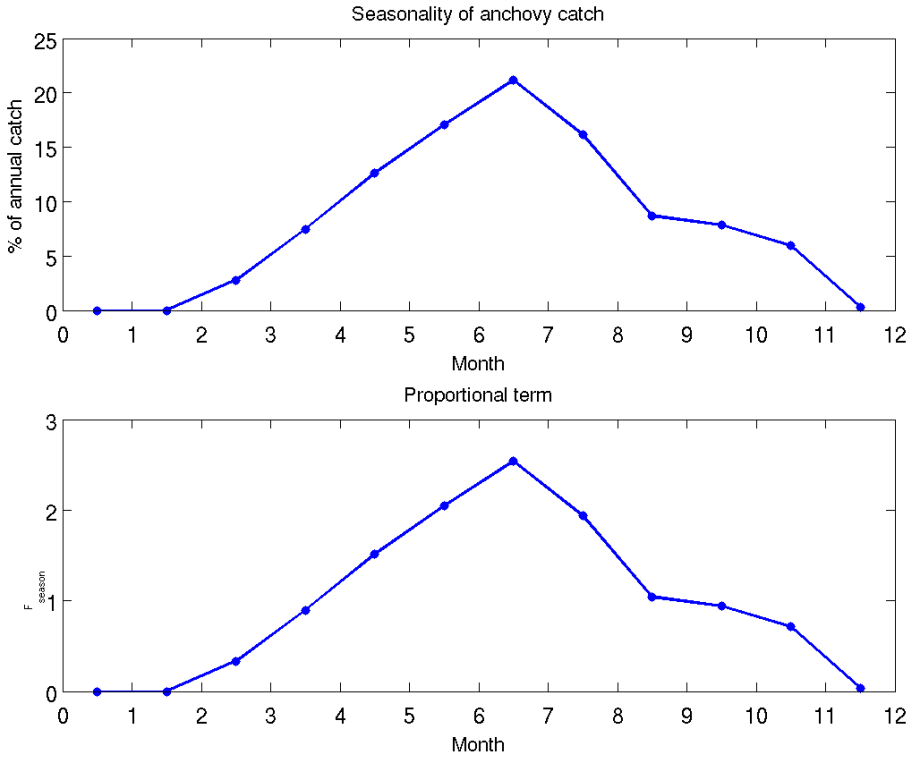

Figure 5. upper panel: Average monthly percentages of anchovy and sardine catches in the North Aegean Sea for the 2003-2008 fishing periods (unpublished data), lower panel: proportional term which parameterizes the seasonality of fishing effort (dimensionless) based on observed seasonality of catches.

Catch

The catch in numbers for each adult fish is calculated using a standard catch equation (Quinn and Deriso, 1999),

$$C_{SI}(t, \delta t) = \frac{F_{SI}}{M_{SI}+F_{SI}} N_{SI} \cdot \left(1 - e^{-(M_{SI}+F_{SI})\delta t}\right),$$

where $CSI_{(x,\ t^{\cdot},\ \delta t)}$ is the catch in numbers of a SI in a time interval [t, t+δt] of length δt and position x. The total yield $CY_{SI}(t^{\cdot},\ \delta t)$ (in grams) for each SI in the time interval [t, t+δt] is calculated as the product of numbers caught and fish weight,

$$CY_{SI}(t^{\cdot},\ \delta t)=c_{SI}(t^{\cdot},\ \delta t)W_{SI}$$

Starvation

Except from natural and fishing mortalities, additional starvation mortality is imposed for all stages (i.e., the SI vanishes) in case that the cumulative weight loss exceeds 35%. This 35% threshold was defined empirically based on residual variation of existing length-weight relationships (see Politikos *et al.,* 2015 for details).

In both the early and adult stages a starvation condition threshold is imposed below which the SI vanishes. We assume that there is a limit of 35% in cumulative weight loss corresponding to the weight estimated from the length-weight relationship. This limit was set empirically after examining available length-weight relationships for larval, juvenile and adult anchovy and was also applied in sardine. Therefore, in the model, we calculate the daily cumulative weight ratio (WR):

$$WR^{t+dt} = WR^{t} + \frac{W^{t+dt}-W^{t}}{W^{t}},$$

where W_{t+dt} is the weight at time step *t+dt* and W_t at the previous time step. If this ratio falls below the threshold value (−0.35) then the fish dies.

3.2.3 Movement

Egg and early larvae stages are considered as passive tracers (Huret *et al.,* 2010) in the model, with their movement governed by hydrodynamic conditions. These are assumed to remain in the first thirty meters of the water column (Politikos *et al.,* 2015), not considering their vertical movements due to buoyancy. Briefly, late larvae, juveniles and adult stages are assumed to perform diurnal vertical migration between the surface layer (0-30m) during the night and the sub-surface layer (>30m) during the day. In the horizontal, fish are assumed to move towards areas with higher food availability, taking into account the ocean current, in order to achieve the desired direction. A random component in the fish movement is also included, while the maximum swimming speed is assumed to be proportional to the fish length. A function of bathymetry is also used to keep adult and juvenile fish from moving towards very deep waters (>300m) or near the coastline, based on existing knowledge of the fish habitats in the N. Aegean.

To prevent fish overcrowding in areas of high zooplankton concentration, fish movement takes into account the fish density in surrounding cells. This is achieved using a "food per capita" gradient, calculated from the ratio of available zooplankton over the fish biomass in neighboring cells. Therefore SIs move towards cells with higher food per biomass concentration, provided that there is no weight loss. In such case, SIs are simply directed to cells with higher food availability.

This was developed on a fish advection-movement module that is based on displacement rules for super individuals (Triantafyllou *et al.,* 2010). In the North Aegean Sea

and in contrast to the Bay of Biscay, there is no published or anecdotal evidence for broad scale migrations of anchovy and sardine, possibly because the eastern Mediterranean is an oligotrophic area and suitable, productive areas are spatially restricted (Somarakis *et al.,* 2012). Also, there is little inter-annual variability in the extent and location of their habitats, as has been recorded and modeled from surveys at sea (Giannoulaki *et al.,* 2008). It is most probable that both species do not move far from productive areas restricting their movement in areas with sufficient amounts of food.

As a corollary, the movement module followed a restricted area approach (Watkins and Rose 2012) allowing the fish SIs to evaluate environmental, bathymetric, growth and population characteristics of surrounding cells and then move to the direction resulting from the combined effects of the aforementioned factors. In this approach, the active life stages (late larval, juvenile, adult) are considered to exhibit active swimming behavior in response to environmental and prey conditions.

Specific criteria are used to determine the movement behavior. On the whole, the fish movement is controlled by the velocity and the direction of the fish. The main factors determining movement are: the currents fields, food availability, bathymetry, swimming speed and density-dependence (biomass of fish in adjacent cells). More specifically, the cruising swimming speed is a function of fish size. The fish are assumed to move along a direction pointing to higher food resources and maintaining position within certain bathymetric ranges, based on their known habitats. The actual swimming velocity of fish is adjusted taking into account the current velocity in order to achieve the desired direction. Moreover, if there is enough food in its current position the fish will only use swimming to compensate the currents and maintain its position, or otherwise search for areas with more food. Schematically, Figure6 illustrates the direction mechanism for fish movement. Finally, a

stochastic term is also added to take into account external factors in the movement process (e.g. predation avoidance).

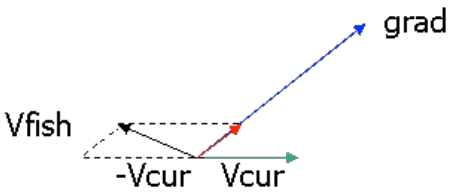

Figure 6. Direction mechanism of fish movement. V_{cur} is the current velocity, V_{fish} is the fish velocity so that it would direct along a gradient (*grad*) towards optimal conditions (food resources bathymetry or other).

Since the fish Super Individual follows a Lagrangian movement and can be located in a continuous horizontal space, whereas the LTL model equations are solved in discrete grid points, an interpolation method has to be implemented so that the hydrodynamic/ecological LTL forcing can be available for each position of the SI. Thus, at each time step, the surrounding points of the SI position within the LTL model grid are identified. The necessary input from the LTL model (e.g. zooplankton biomass, temperature, current velocity and bathymetry) at the SI location is then calculated with bilinear interpolation from the four surrounding points (black x points, Figure 7). For the calculation of the gradients, two extra points are considered (red x-points). These points are defined as the surrounding cells of the current SI's position.

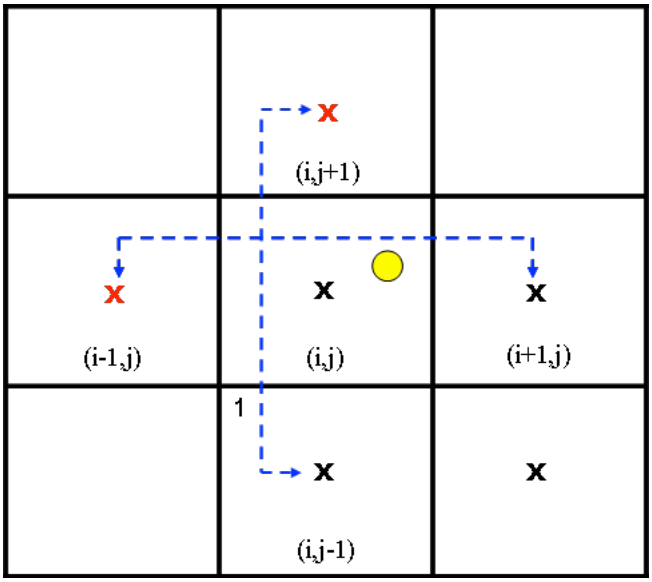

Figure 7. Calculation of the gradient using the surrounding cells.

Passing to the implementation scheme, the updated position of each SI in 2D-Cartesian coordinates $(X_{fish}^{k+1}, Y_{fish}^{k+1})$ at time step *k+1* which was at X_{fish}^{k+1}at time step k, is determined by the equations:

$$X_{fish}^{k+1} = X_{fish}^{k} + (u_{cur} + u_{fish}) \cdot dt + u_{dif} \cdot (2U^{k} - 1) \cdot dt,$$

$$Y_{fish}^{k+1} = Y_{fish}^{k} + (v_{cur} + v_{fish}) \cdot dt + u_{dif} \cdot (2U^{k} - 1) \cdot dt$$

Where u_{cur}, v_{cur} are the current velocities, u_{fish}, v_{fish} denote the realized fish velocity, *dt* is the time step, U^{k}~U[0,1] a random number from the uniform distribution and $u_{dif}=\sqrt{\frac{6difh}{dt}}$ a diffusivity term.

For the implementation of the movement process, as described above, the realized fish velocity (u_{fish}, v_{fish}) that moves the fish horizontally (u − v direction) is calculated by the relationships:

$$u_{fish}=(fish_{cruizing\_speed} - cur_{speed})*((grad^{n}_{u,food} * U_{zoo} grad^{n}_{u,topo} * topo_{fish})$$

$$v_{fish}=(fish_{cruizing\_speed} - cur_{speed})*((grad^{n}_{v,food} * U_{zoo} grad^{n}_{v,topo} * topo_{fish})$$

where $fish_{cruizing\_speed} = S_{cruizing} \cdot fish_{length}$ is the fish swimming speed capability $cur_{speed}=\sqrt{u_{cur}^2 + v_{cur}^2}$ is the magnitude of the current (u_{cur}, v_{cur} are the two horizontal velocity components), $grad^{n}_{u,food}$ is the normalized gradient of topography, U_{zoo} is a function (taking values between zero and one), which slows down the fish when there is enough food and $topo_{fish}$ is a function that relates fish movement with bathymetry.

The graph form of $U_{zoo} = 1-\frac{zoo_{SI}}{zoo_{SI}+k_{zoo}}$, where zoo_{si} is the interpolated forcing zooplankton biomass for the SI and k_{zoo} is a calibrated parameter that controls the steepness of the function U_{zoo} (i.e. it indicated the zooplankton concentration where the U_{zoo} is reduced to 0.5), is shown in Figure 8.

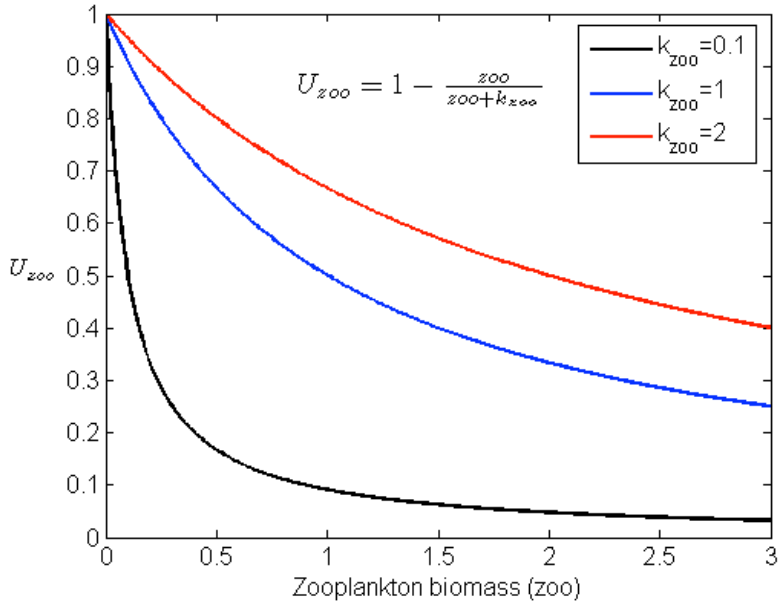

Figure 8. Graph of U_{zoo} for different values of k_{zoo}.

The unit vector of food gradient ($grad_u^n, grad_v^n$) is

$$grad_{u,food}^n = \frac{grad_{u,food}}{\sqrt{(grad_{u\_food})^2+(grad_{v\_food})^2}}, grad_{v,food}^n = \frac{grad_{v,food}}{\sqrt{(grad_{u\_food})^2+(grad_{v\_food})^2}}$$

Where ($grad_u$, $grad_v$) is the zooplankton gradient in *u*-*v* directions, which is calculated in a finite difference grid (Fig. 2) as:

$$grad_{u,food} = \frac{zoo(i+1,j)-zoo(i-1,j)}{du}, grad_{v,food} = \frac{zoo(i,j+1)-zoo(i,j-1)}{dv}$$

Where *zoo(i,j)* indicated the total zooplankton abundance of the *(i,j)* cell.

To avoid the overcrowding of the SIs in areas with high zooplankton availability, the calculation of gradient based on the ratio of the zooplankton to the biomass of the SIs that are present in the surrounding cells was also included and tested. In this case, the gradient is not calculated exclusively from the zooplankton, but from the available zooplankton per gram of fish.

The density-dependence gradient is calculated from the ratios:

$$grad_{u,food}^{ratio} = \frac{\frac{zoo(i+1,j)}{biom(i+1,j)} - \frac{zoo(i-1,j)}{biom(i-1,j)}}{du}$$

$$grad_{v,food}^{ratio} = \frac{\frac{zoo(i,j+1)}{biom(i,j+1)} - \frac{zoo(i,j-1)}{biom(i,j-1)}}{dv}$$

In that way, it is assumed that the SIs share the same food resources and the fish will avoid grid cells in which, although there is enough food, many SIs are present and per capita food availability is decreased. The unit vector of bathymetry gradient ($grad^n_{u,topo}, grad^n_{v,topo}$) is calculated as

$$grad^n_{u,topo} = \frac{grad_{u,topo}}{\sqrt{grad_{u,topo}{}^2 + grad_{v,topo}{}^2}}, grad^n_{v,topo} = \frac{grad_{v,topo}}{\sqrt{grad_{u,topo}{}^2 + grad_{v,topo}{}^2}}$$

Where

$$grad_{u,topo} = \frac{h(i+1,j) - h(i-1,j)}{du}, grad_{v,topo} = \frac{h(i,j+1) - h(i,j-1)}{dv}$$

Where *h(i,j)* is the depth of the water column for the *(i,j)* grid box.

A topography proportion function (*topo*$_{fish}$) which takes values between 0 and 1 is developed to include a mechanism that avoid SIs moving in deep (>300m) or very shallow waters (coastline). In case of deep waters *topo*$_{fish}$ acts on the topography gradient ($grad^n_{u,topo}, grad^n_{v,topo}$) as written in the equation below, by switching the topography gradient direction (minus in the topo fish function) while its value controls the speed up (e.g for high depths, the function the value -1). The function form of the *topo*$_{fish}$ is of the form,

$$topo_{fish} = -\frac{D_{fish}}{D_{fish} + d_{age_{SI}}}, D_{fish} > 200m, \text{ or}$$

$$topo_{fish} = 1 - \frac{D_{fish}}{D_{fish} + d_{age_{SI}}}, D_{fish} < 5\text{m}$$

where D_{fish} is the interpolated depth of the water column at the current location of the SI and $d_{age_{SI}}$ is a depth parameter that controls the steepness of the function. Its value is changed based on SI's age.

The population of the SI at each time step is assumed to have a vertical distribution in the water column, which permits a straight forward calculation of the fluxes between the ecological and fish module. This distribution is dynamically calculated as a function of the available food (zooplankton density) using the function:

$$Ffood(k, stage) = \frac{food^2(k,stage)}{food^2(k,stage)+kfood(stage)},$$

where

$$food(k,stage) = vul1(stage)\ Z4(k) + vul2(stage)\ Z5(k) + vul3(stage)\ Z6(k)$$

is the total available prey for k − layer of the vertical grid and SI life stage. The parameters *vul1(stage) , vul2(stage)* and *vul3(stage)* denote the vulnerabilities of the life stages on the zooplankton groups *(Z4, Z5, Z6)* and *kfood(stage)* is a constant that controls the steepness of the above functions that are maximized around maximum food availability.

Depending on the time of the day, the above distribution is calculated within the surface (0-30m, during the night) or the deeper layer (>30m, daytime), since juveniles and adults accomplish diurnal vertical migrations, staying below the thermocline during daytime whereas during the night they are scattered in the upper water column layers (Plounevez & Champalbert 2000, ANREC 2006).

$$fdis(k, age) = \frac{Ffood(k, stage)}{\sum_{k=1}^{\#of\ layers} Ffood(k, stage)}$$

The above function with depth is calculated for each of the 4 surrounding points of the SI current location (Fig. 9). The assumed SI vertical distribution and all the necessary input from the LTL model (zooplankton biomass, temperature, current velocity) is then calculated with bilinear interpolation from the 4 surrounding points. The current velocity at the SI's position (used for the advection/migration) is calculated at the SI weighted depth average, which can be calculated from:

$$Dep_{SI} = \sum_{k=1}^{\#of\ layers} z(k) \cdot fdis(k, stage)$$

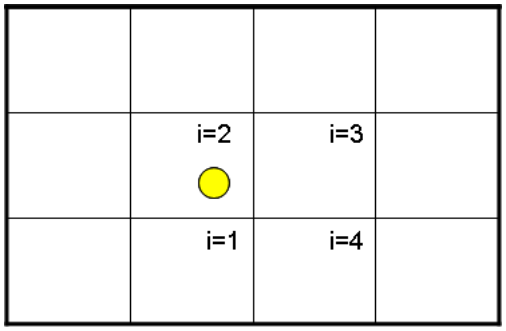

Figure 9. Four surrounding points of SI current location are assumed in order to calculate the distribution function.

Passing to the SI of eggs and early larval stages are treated as passive tracers and the horizontal displacement of each SI due to advection is given by

$$L(x, y) = (u_{si}, v_{si})dt + a \cdot dt$$

where u_{SI} , v_{SI} are the local current velocities, at *x* and *y* directions (in m s^{-1}), *dt* is the time step and a is a random component related to random movement due to other factors (e.g. predation). The local current velocity at the SIs location *(X,Y,Z)* is calculated with bi-linear interpolation from the surrounding current velocities calculated on the hydrodynamic model grid.

3.3 Coupling

3.3.1 Hydrodynamic & Biogeochemical models coupling

The biogeochemical variables are treated by the hydrodynamic model as passive tracers and are adjacent to transport and diffusion. Therefore the total concentration change of a variable (*C*) in time (*DC/Dt*) for a certain grid point is the sum of the concentration change in time in the specific grid point ($\partial C/\partial t$) and a change due to the movement of the liquid and expresses the change of concentration in the direction of the flow and at the speed of the liquid.

$$\frac{DC}{Dt} = \frac{\partial C}{\partial t} + U\frac{\partial C}{\partial x} + V\frac{\partial C}{\partial y} + W\frac{\partial C}{\partial z}$$

The molecular diffusion equation, according to the first Fick (1985) law, is given by:

$$M_x = \frac{\partial}{\partial x}(A_H \frac{\partial C}{\partial x}) + \frac{\partial}{\partial y}(A_H \frac{\partial C}{\partial y}) + \frac{\partial}{\partial z}(K_H \frac{\partial C}{\partial z})$$

Granted that there is no movement of the liquid, then according to the mass preservation equation:

$$\frac{\partial C}{\partial t} = \frac{\partial}{\partial x}(A_H \frac{\partial C}{\partial x}) + \frac{\partial}{\partial y}(A_H \frac{\partial C}{\partial y}) + \frac{\partial}{\partial z}(K_H \frac{\partial C}{\partial z})$$

With the above equation taking the following form in order to express the hydrodynamical and biogeochemical models coupling in the 3D space *(x,y,z)*:

$$\frac{\partial C}{\partial t} = -U\frac{\partial C}{\partial x} - V\frac{\partial C}{\partial y} - W\frac{\partial C}{\partial y} + \frac{\partial}{\partial x}\left(A_H \frac{\partial C}{\partial x}\right) + \frac{\partial}{\partial y}\left(A_H \frac{\partial C}{\partial y}\right) + \frac{\partial}{\partial z}\left(K_H \frac{\partial C}{\partial z}\right) + \sum BF$$

with *U,V,W* representing the velocities field, A_H being the horizontal viscosity coefficient and K_h the vertical turbulent mixing coefficient. $\sum BF$ represents the total biochemical flux for every functional group. The two models are simultaneously integrated (on-line coupled) and the last equation is resolved for each biogeochemical variable for every time step.

3.3.2 Low trophic level and IBM Coupling

In the process of coupling low trophic to higher trophic level models, a series of methods are proposed. The first is by avoiding the complexity of zooplankton dynamics with

the use of a proxy, namely the primary production (Pecquerie *et al.,* 2009) or a transfer function converting primary production to mid-trophic level food availability for a given species (e.g. Lehodey *et al.,* 2010), justified by the relatively constant slopes in log-log biomass size-spectrum relationship. However, the approach may be justified in certain conditions, namely the limits of model validation, but may be inappropriate when extrapolated or when requiring precise food condition, for example varying food diet along lifecycle.

Another approach is by taking the best of existing NPZD models, that is the supposed underlying relationships between functionality and size (e.g. Megrey *et al.,* 2007; Politikos *et al.,* 2011). For instance in ERSEM for the Aegean Sea, in reality each functional type comprises a much wider range of organisms which have broadly the same functional role defined mainly by the corresponding prey – predator relations. Thus the smaller prey size organisms include not only heterotrophic flagellates but also small ciliates and early life stages of bigger animals such as micro and mesozooplankton that forage on the same food source and are themselves preyed upon by the same predator. The second prey type, the microzooplankton includes ciliates and metazoan zooplankton. The last prey type includes mainly mesozooplankton. This is also the approach used by Travers *et al.,* (2009) in their multispecies Individual Based Model.

The NPZD-type model can also be extended to fish (Fennel 2010) that is in a biomass-based framework. Major drawback is that zooplankton bulk biomasses in such models are often weakly validated at present, and size resolution remains weak. To solve the latter, Daewel, (2008) derived zooplankton size-structure from the simulated bulk biomass of a NPZD model using observed size frequency distribution. It was then used to test environmental scenario on several fish species in the North Sea (Daewel et al., 2011).

Another modelling approach consists of focusing on individual-based processes, i.e. the prey-predator interactions, from which a functional response may emerge at the

population level (Huse & Fiksen, 2010). Often the interaction is species-specific, so much data is needed for correct parameterization, while very seldom this is available for more than a prey-predator couple. This approach is mainly used in regions with dominant zooplankton species building the major part of the total biomass. Most models do the coupling in one way, that is from plankton to fish without feedback, although this has proven to be useful to do the full coupling (Travers *et al.,* 2009; Travers & Shin 2010). Indeed, this insures mass conservation (Fennel 2010), and eventually should improve spatiotemporal dynamics of predation on zooplankton (top-down control), which is constant so far in most NPZD models.

So in this modelling setup, the LTL model and the fish IBM model are two-way, dynamically coupled. The heterotrophic biomass (microzooplankton, mesozooplankton) that is consumed by the fish is removed in the LTL model, while fish by-products are fed back to the LTL model, with fluxes due to fish egestion and specific dynamic action being channeled to the organic particulate (detritus) matter pool of the LTL and fluxes due to excretion returning as dissolve organic matter. Moreover, fish individuals within each SI that perform vertical migration(late larvae, juveniles and adults) are assumed to have a vertical distribution following the maximum prey availability. Based on this distribution, the fluxes in terms of zooplankton consumption, as well as released inorganic nutrients and organic matter are calculated for each depth and applied to the LTL model.

More thoroughly, each SI of the fish population, is assumed to be vertically distributed in the water column at the SI location according to the zooplankton concentration. This distribution $F(j,z)$, is a sigmoid function (normalized to 1), of fish life stage j and depth z, is maximized near maximum food availability:

$$F(j,z) = \frac{food(j,z)^2}{food(j,z)^2 + k_f(j,food)}$$

With $Z_4(z)$, $Z_5(z)$ corresponding to meso and microzooplankton respectively and

$$food(j,z) = pref_4(j) * Z4(z) + pref_5(j) * Z5(z)$$

being the total available prey at depth *z* for life stage *j* over the zooplankton groups with the corresponding feeding preferences $pref_4(j)$ and $pref_5(j)$. Finally, $k_f(j,food)$ is a parameter, which controls the steepness of the distribution function.

As already mentioned, all stages besides eggs and early larvae are assumed to perform diurnal vertical migrations, staying below the thermocline (>30m) during daytime and in the upper water column layer during the night (0–30m). Thus, $F(j,z)$ is calculated within the 0–30 m layer or below that, depending on the time of the day. The vertical distribution of zooplankton is first calculated in the SI surrounding grid points of the LTL grid and is then bi-linearly interpolated at the SI location and the inverse procedure is followed when calculating the returned fluxes to the LTL model. Thus, using the distribution function that represents the fish vertical spreading at the SI location, the fluxes in terms of zooplankton consumption, released inorganic nutrients and organic matter are calculated at all depths of the water column and applied to the surrounding LTL model grid points.

The fish derived fluxes are calculated for each depth z as:

$$Flux(j,z) = Flux_{Fish} * F(j,z)$$

where $Flux_{Fish}$ is the total flux from the fish SI in terms of consumed zooplankton or released inorganic nutrients/organic matter and *F(j,z)* is the distribution function. Therefore, the fish zooplankton consumption and released by-products are similarly distributed in the water column, based on the assumed vertical distribution of the fish.

Given the different units of the fish (g wet weight) and the LTL (mgC/m^3, mmol N, P/m^3) models, the fish biomass (*f_biom*) is translated to carbon (*fc_biom*), nitrogen (*fn_biom*) and phosphorus (*fp_biom*) average (a different weight is applied on the flux of each depth, based on the vertical distribution *F(j, z)*) concentrations in the water column of the LTL grid cell, where the fluxes are applied:

$$fc\_biom(mgC/m^3) = f\_biom(g\ ww) * ffc(mgC/g\ ww)/vol(m^3),$$

$$fn\_biom(mmol\ N/m^3) = qnF(mmol\ N/mgC) * fc\_biom(mgC/m^3),$$

$$fp\_biom(mmolP/m^3) = qpF(mmolP/mgC) * fc\_biom(mgC/m^3),$$

where *ffc* is a conversion factor from fish gram ww to mgC, based on the carbon content of anchovy dry weight, assuming that dry weight is 32% of wet weight (Tudela and Palomera, 1999), (*qnF, qpF*) is the assumed ratio of the nitrogen and phosphorus over carbon pools in the fish biomass and *vol* is the water column volume at the LTL grid cell (*dx * dy * depth*), where the fluxes are applied.

The returned fluxes are then calculated as:

$$Flux_{carbon}(Z4, Z5) = fc\_biom * CON(Z4, Z5),$$

$$Flux_{nitrogen}(Z4, Z5) = fc\_biom * CON(Z4; Z5) * qnZ4; 5;$$

$$Flux_{phosphorus}(Z4, Z5) = fc\_biom * CON(Z4; Z5) * qpZ4; 5,$$

$$Flux(ammonia, phosphate) = fn, p\_biom * EX,$$

$$Flux(POC, N, P) = fc, n, p\_biom * (EG + SDA),$$

where *Z4, Z5* are the mesozooplankton and microzooplankton LTL groups respectively and *CON(Z4,Z5), EX, EG* and *SDA* are respectively the *Z4,Z5*consumption, excretion, egestion and dynamic action rates (day^{-1}) calculated by the fish bioenergetic model. Since the fish biomass has different C:N:P internal quotas (*qnF,qpF*) from the consumed zooplankton (*qnZ4,5, qpZ4,5*), the excess carbon, nitrogen or phosphorus is assumed to be excreted as dissolved organic matter following Broekhuizen, (1995), so that the fish can maintain a constant C:N:P internal quota.

3.4 Genetic Algorithm

The bioenergetics module was calibrated against the available length- and weight-at-age field data by applying a heuristic optimization technique based on a genetic algorithm (GA). GAs are inspired from the principles of natural selection and they are effective when dealing with large and complicated search spaces or when there is no other analytical solution for the problem.

GAs are often characterized as population based evolutionary processes, starting with a population of candidate solutions (called chromosomes) that are evolved in time via a number of cycles (called generations) and genetic operations (i.e., crossover and mutation) towards a specific goal that is described by a problem-specific optimization function (called fitness function). Chromosomes consist of genes, which in our application are the model

parameters to be tuned. For every generation, the fitness function is evaluated for every chromosome estimating in this way the quality of the candidate solution (e.g., highest score indicates better solution). While passing from one generation to another, solutions that achieve the highest score are selected to survive. The process is continued until some termination criteria are fulfilled or a user-defined number of generations is reached (Soufan *et al.,* 2015). Here, for simplicity and in order to achieve reproducibility of our results, we deployed a simple genetic algorithm adopted by the implementation described in Kleftogiannis, (2015).

More thoroughly, the GA follows state-of-the-art implementation principles. Our chromosomes contain genes that correspond to the number of model parameters. For simplicity we used binary (e.g., 0 or 1) chromosome representation. For every parameter we used 10 bits and for coding-decoding the actual parameters values we follow the bellow formula:

$$Value = \frac{(Val_{Max} - Val_{Min}) * Val_{Init}}{2^{(number\ of\ bits-1)}} + 1$$

Where the maximum and minimum values (Val_{Max}, Val_{Min}) define the range of the parameter and Val_{init}, is the starting point of the simulation. The size of the population was set to 100 chromosomes. Increasing the population size does not necessarily improve the performance as there is no guarantee that the algorithm will be able to find any better solution (Soufan *et al.,* 2015).

In our implementation the population was initiated randomly and all parameters are

within a pre-defined range. In the first generation we also forced one chromosome to have all of its parameters equal to the upper bound of the corresponding range and similarly one chromosome to have all of its parameters equal to the lower bound of the corresponding range.

Regarding the genetic operators, the crossover produces new offsprings by combining genes of two chromosomes. We used two-point crossover, which is a typical crossover option for many GA applications. The following example illustrates the two-point crossover operation over a pair of chromosomes with 10 genes:

Population state at generation **n**

Chromosome_1 (Parent_A): [10 ***1 1 1 1 1*** *0 1 1]*

Chromosome_2 (Parent_B): [1 1 ***1 0 0 0 1*** *1 0 1]*

Population state at generation **n+1** after applying two-point crossover

Chromosome_1' (Child_A): [10 ***1 0 0 0 1*** *0 1 1]*

Chromosome_2' (Child_B): [1 1 ***1 1 1 1 1*** *1 0 1]*

The mutation operator modifies specific genes of a given chromosome. The simplest mutation operator is the bit-string that switches specific genes at random positions (i.e., 1 becomes 0 and 0 becomes 1). The following example illustrates the bit-string mutation operation over a chromosome with 10 genes:

Chromosome_2' state at generation **n+1** before mutation

Chromosome_2' [1 1 1 1 1 **1** 1 1 01]

Chromosome_2' state at generation **n+1** after applying mutation

Chromosome_2' [1 1 1 1 1 **0** 1 1 01]

Both mutation and crossover operators simulate the natural pressure on the population and regulate the information exchange across different generations. Following state-of-the-art solutions proposed in the literature we fixed mutation rate to 0.8 for our experimentation.

The evolution of the population follows a tournament selection, where the best chromosomes in the population are selected to serve as parents of new children. The GA operators including selection, mutation and crossover are then carried over in an iterative process through a predefined number of generations. In addition, the utilized selection scheme applies elitism. Elitism keeps the best solutions of the population at a given generation to the next generation. For the rest of our experimentation we define those generation specific best solutions as sub-optimal solutions of the process. In our implementation we keep the best two solutions of the population for every generation. Notably, extensive usage of elitism sometimes may lead to premature convergence.

Since the objective was to tune the model and achieve average weights-at-age for each species as close as possible to field data, we introduced a simple fitness function:

$$Fitness = 1/\sqrt{\sum (prediction - reference)^2}$$

This fitness function takes into account the Euclidean distance between weight data and the predicted weight of the species for one or more predefined dates. Thus, given two weight outputs for a specific age, derived from different model runs using different parameter values, the higher ranked output is the one that has smaller distance with respect to the reference weight.

Regarding the termination criteria, we set a maximum number of generations equal to 1000. To reduce the execution time, the algorithm is equipped with an additional stopping criterion, which considers the population as converged (i.e., steady-state) if there is no difference in the average fitness value of the population for 150 consecutive generations.

The genetic algorithm was applied to the stage-/age-specific half saturation coefficients (see equation for consumption in Table 1), that regulate food consumption (Huret *et al.,* 2019). For this purpose, we used an IBM version that included only one super-individual from each species. By experimenting with the GA setup, we compared a simultaneous parameter tuning (all stage-/age-specific half saturation coefficients) to a sequential parameters tuning. The later involved the tuning of the half saturation constant first for the larvae, then for the juveniles etc. until the terminal adult age class. The sequential tuning approach proved more successful in predicting the available growth data.

4. Experiments and results

4.1 Model Setup

In the one-dimensional model configuration, the biogeochemical model is forced by temperature and daily vertical diffusivity profiles, averaged for the 2003 – 2008 period, over the Thracian Sea. These were obtained off-line from a 3-D simulation of the hydrodynamic model (Tsiaras *et al.,* 2014). Given that the coupling with hydrodynamics is only one-way, using the full 3-D hydrodynamic output would be preferable. This is because a 1-D hydrodynamic model does not resolve horizontal processes and has important limitations in areas where lateral water inputs (Black Sea Water, rivers etc) are very important. Water column properties (temperature, salinity) are therefore not realistically simulated with a 1-D hydrodynamic model. A monthly varying input of dissolved inorganic nutrients (phosphate, nitrate, ammonium, silicate) was adopted at the surface layer to mimic river/Black Sea Water (BSW) nutrient inputs in the Thracian Sea. This nutrient input follows the seasonal variability of riverine/BSW inputs, peaking during spring and is tuned so that the simulated plankton productivity (Chl-a, zooplankton) is similar to the one simulated with the 3-D version of the biogeochemical model (Tsiaras *et al.,* 2014).

For the needs of the three-dimensional simulations, a long-term hindcast simulation was performed over 2000-2009 period. The atmospheric forcing was obtained from HIRHAM model re-analysis (Christensen *et al.,* 1996). Initial fields and open boundary conditions for the biogeochemical and hydrodynamic models were obtained from a Mediterranean basin

scale model simulation over 2000-2009 period, (Kalaroni *et al.,* 2020). The coupled model was initially integrated for a 5-year spin-up period. Mean (1995 – 1999) river nutrient load data for major N. Aegean Rivers (Evros, Axios, Aliakmonas, Strymon, Pinios, Nestos, see Figure 1) were adopted from Skoulikidis (2009). The Dardanelles water exchange is parameterized using a two-layer (inflow of Black Sea Water and outflow of Aegean water) open boundary condition (Nittis *et al.,* 2006), with seasonally varying concentrations of dissolved inorganic nutrients (Tuğrul *et al.,* 2002) and annual mean concentrations of ammonium, dissolved and particulate organic matter (Polat and Tugrul, 1996). An input of phytoplankton is also adopted, based on a monthly climatology of available SeaWiFS (Sea-viewing Wide Field-of view Sensor) Chl-a data (O'Reilly *et al.,* 1998).

The fish model was initialized on 1st January 2000, as in Politikos, (2015), taking into account of the species mean estimated biomasses and main habitat areas (Giannoulaki *et al.,* 2013) that are found in Thermaikos Gulf, Strymonikos Gulf, Thracean Sea and in the BSW inflow area, east of Limnos Island (Figure 1). An initial number of 1000 SIs was assigned, for each of three anchovy (juveniles, age-1, age-2) and four sardine (juveniles, age-1, age-2, age-3) age classes, with reference weights per age.

4.2 LTL Model results

The coupled hydrodynamic/biogeochemical model has been extensively validated in previous modeling efforts (Kourafalou and Tsiaras, 2007; Tsiaras *et al.,* [2012, 2014]; Petihakis *et al.,* 2014). The main hydrodynamic and biogeochemical features in the N. Aegean are briefly discussed below.

The mean near surface circulation and salinity, chlorophyll and mesozooplankton concentrations are shown in Figure 10. The model captures the main aspects of the circulation in the N. Aegean, known from observational studies and previous modelling efforts (Kourafalou and Tsiaras, 2007; Tsiaras *et al.,* [2012, 2014]; Petihakis *et al.,* 2015). An overall cyclonic circulation is simulated, driven by the inflowing Levantine water from the South and the inflow of brackish Black Sea Water at Dardanelles strait. The latter branches around Limnos Island, creating a semi-permanent anti-cyclone in the North East (Zervakis and Georgopoulos, 2002; Olson *et al.,* 2007), or following a South-Western pathway that carries BSW to the South Aegean. An anti-cyclonic circulation is also simulated in Sporades basin (Androulidakis and Kourafalou, 2011; Olson *et al.,* 2007).

The anti-cyclonic circulation in the Northeast Aegean may be considered as a favorable factor for the anchovy/sardine habitat (Giannoulaki *et al.,* 2005), as it increases the residence time of nutrient rich waters of river and Black Sea origin and also contributes to the retention of eggs/larva in the area. Nutrient inputs from River and BSW discharge sustain an increased plankton production, in an otherwise oligotrophic Aegean Sea, especially in coastal river influenced areas.

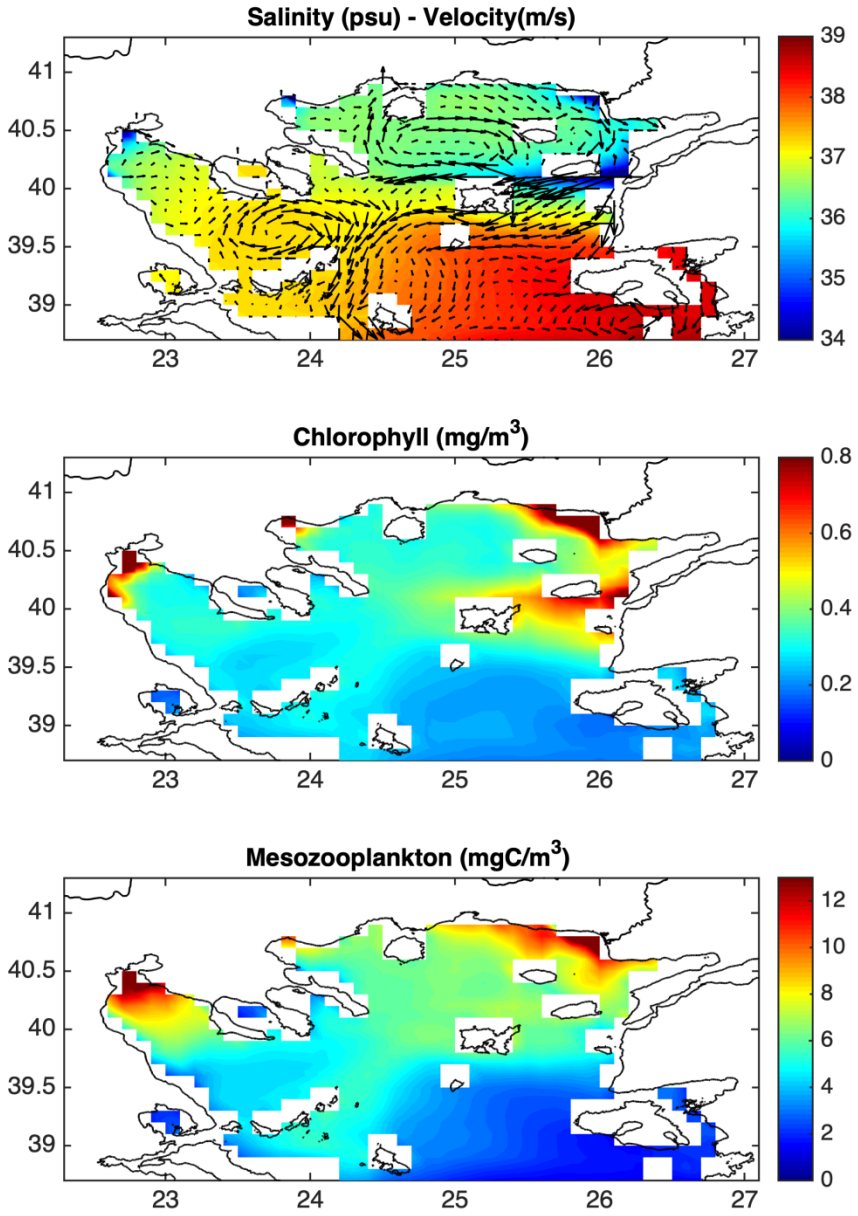

Figure 10. Main spatial surface ecological variables (yearly averaged).

Phytoplankton concentration peaks during winter (~March), following the entrainment of sub-surface nutrients from increased vertical mixing and nutrient inputs from BSW and river runoff that peak over the same period. Mesozooplankton, the main prey of anchovy/sardine, follows the phytoplankton bloom with a 1-2 month delay (Fig. 11), peaking during April-May period.

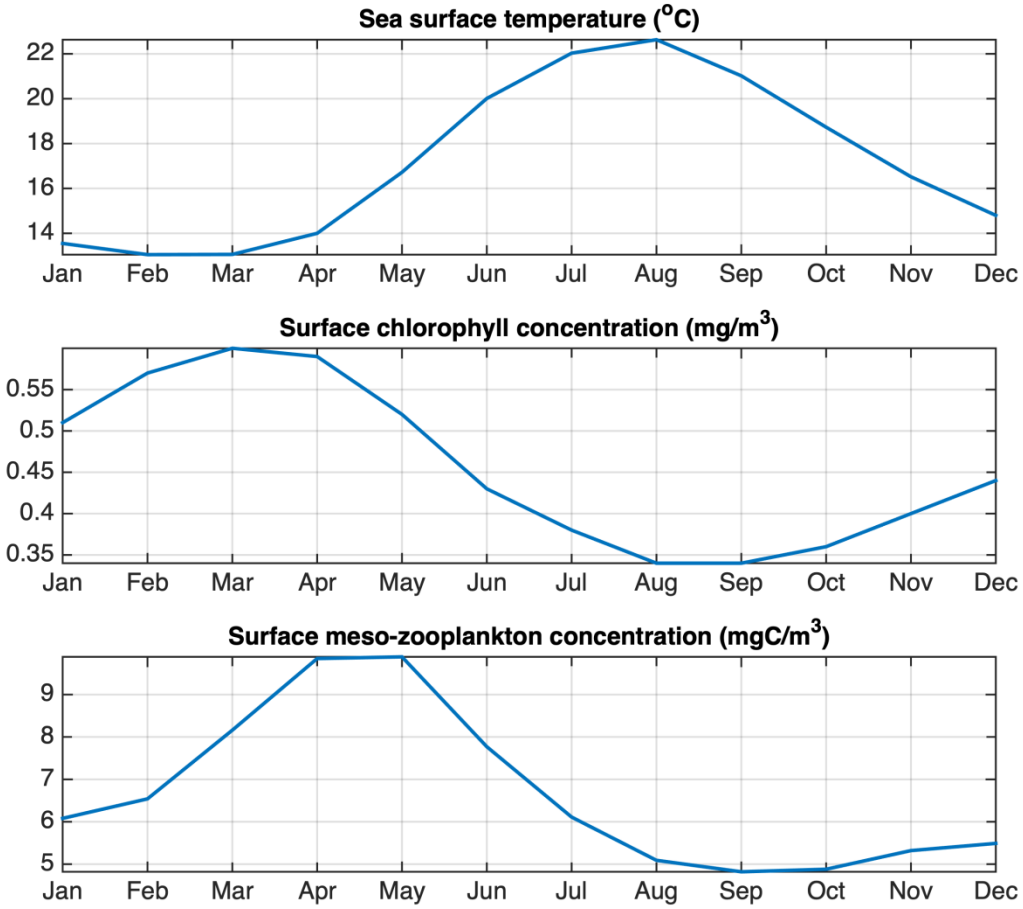

Figure11. Main surface ecological variables (seasonal).

4.3 IBM results

4.3.1 1D model

Initially a one-dimensional version of the model was constructed in order for the preliminary tuning to take place and the main aspects of the bioenergetic modules to be studied. To that aim, field data were used, including length-weight measurements and

length/weight-at-age estimates. For anchovy, these data are described in Politikos, [2011, 2015] and Huret, (2019). For sardine, we used data available from Schismenou (2012) and Schismenou, (2016) for larvae and juveniles, and data from the acoustic and daily egg production surveys carried out in the N. Aegean Sea from 2003 to 2008 (Somarakis *et al.,* 2012).

Additionally, we studied the monthly variation of the somatic condition of two species using length-weight measurements made on fish collected from the commercial purse seine fleet from 2003 to 2008. No samples were available for January and February, which is a closed period for the purse seine fishery (Machias *et al.,* 2008). Size-adjusted monthly mean weights were estimated for each species using a general linear model approach. The rationale for studying the monthly variation of fish condition (which reflects energy storage [see Brosset, (2017) and references therein] was to compare its changes with model predictions for the seasonal zooplankton cycle and fish breeding patterns (income-capital).

For this purpose, a 'capital index' similar to the one developed in Gatti, (2017) was computed for each age class:

$$(dE_{buffer} - \sum_{s}^{e} A_R) \Big/ \sum_{s}^{e} E_{egg}$$

It corresponds to the quotient of the division between the energetic loss from the reproductive buffer between the start (*s*) and the end (*e*) of the spawning season (after the subtraction of the cumulative emergency maintenance costs paid from the reproductive buffer, as described in Figure 4) and the cumulative energy spent for egg production during

the spawning season. The higher is the capital index, the closer is the species to the capital breeding pattern, i.e. it is more dependent on stored energy for the production of eggs.

For the needs of these experiments, the anchovy-sardine IBM, with a time-step 1200 sec, was run for a 30 year period in order to evaluate its performance in terms of population and reproductive characteristics of the two species in the North Aegean Sea. The first ten years were considered as model spin up. Hence, only the remaining period (11-30 years) was taken into account for model evaluation and analysis.

Subsequently, we used the model to test the sensitivity of the anchovy and sardine populations to (a) changes in fishery exploitation rates, and (b) changes in the timing of the existing 2.5 months closure period. In the first set of simulations, we examined the effect of changing the levels of fishing mortality on the populations of anchovy and sardine as well as on their mesozooplankton prey. The fishing mortality of each species was allowed to vary, so that the Paterson's exploitation rate (*E.R. = fishing mortality/[natural mortality + fishing mortality]*) fluctuated around 0.4 (0.23 to 0.51 and 0.32 to 0.46 for anchovy and sardine respectively). The value of 0.4 as empirically defined by Patterson, (1992), is currently considered as the exploitation rate corresponding to the maximum sustainable yield for the Mediterranean small pelagic fish stocks (STECF 2017) and is a reference point for their management, i.e. stocks exploited above 0.4 are considered overexploited. In the second set of simulations, we examined the effect of changing the timing of the existing 2.5 months purse-seine fishery ban, now scheduled between 15 December and end of February, by shifting it by one month along the year, i.e. 15 January-March, 15 February-April etc.

Somatic condition

The mean monthly somatic condition of anchovy and sardine in the Thracian Sea (estimated from the field samples) appears to follow closely the seasonal variability of the simulated mesozooplankton concentration (Fig. 12). Although no samples were available in the January-February period to estimate somatic condition, results showed that the latter increased from December to spring in both species (more sharply in anchovy with the summer spawning period, more slowly in the winter spawning sardine). Interestingly, somatic condition starts to decrease sharply after July, i.e. approximately one month after the strong decrease in the simulated mesozooplankton concentration.

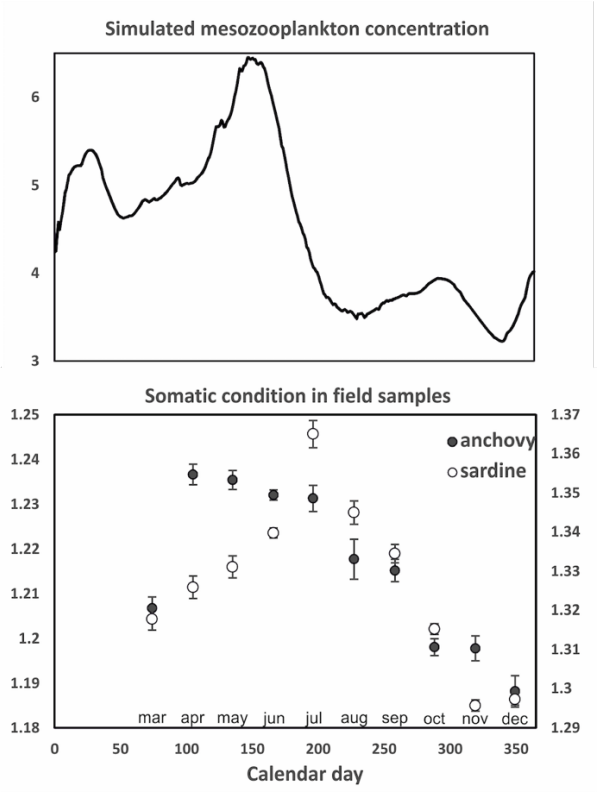

Figure 12. Top panel: Simulated average mesozooplankton concentration (mgC m^{-3}) in the water column (0-100m) against calendar day. Bottom panel: length-adjusted monthly mean weight (somatic condition) of fish samples collected onboard the Thracian Sea purse seine fleet in 2003-2008.

The application of the genetic algorithm to tune the half saturation coefficients resulted in growth trajectories that were in close agreement with available lengths- and weights-at-age data from field samples, in both larvae (Fig. 13) and adults (Fig. 14).

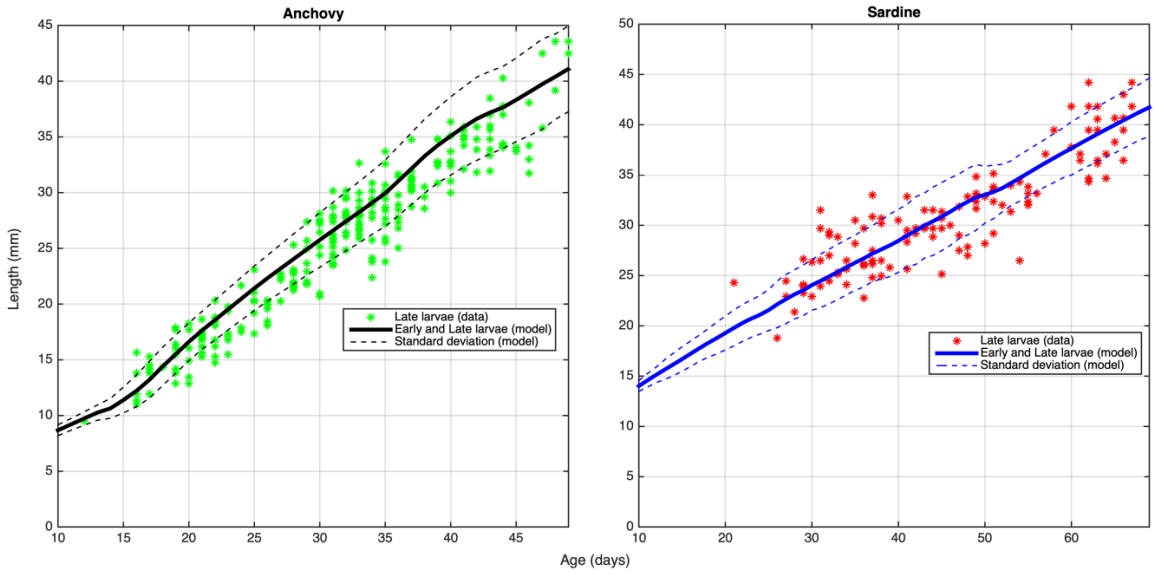

Figure 13. Mean length-at-age (±SD) of anchovy and sardine larvae, calibrated using the genetic algorithm and field data (Schismenou 2012, Schismenou *et al.,* 2013, 2016).

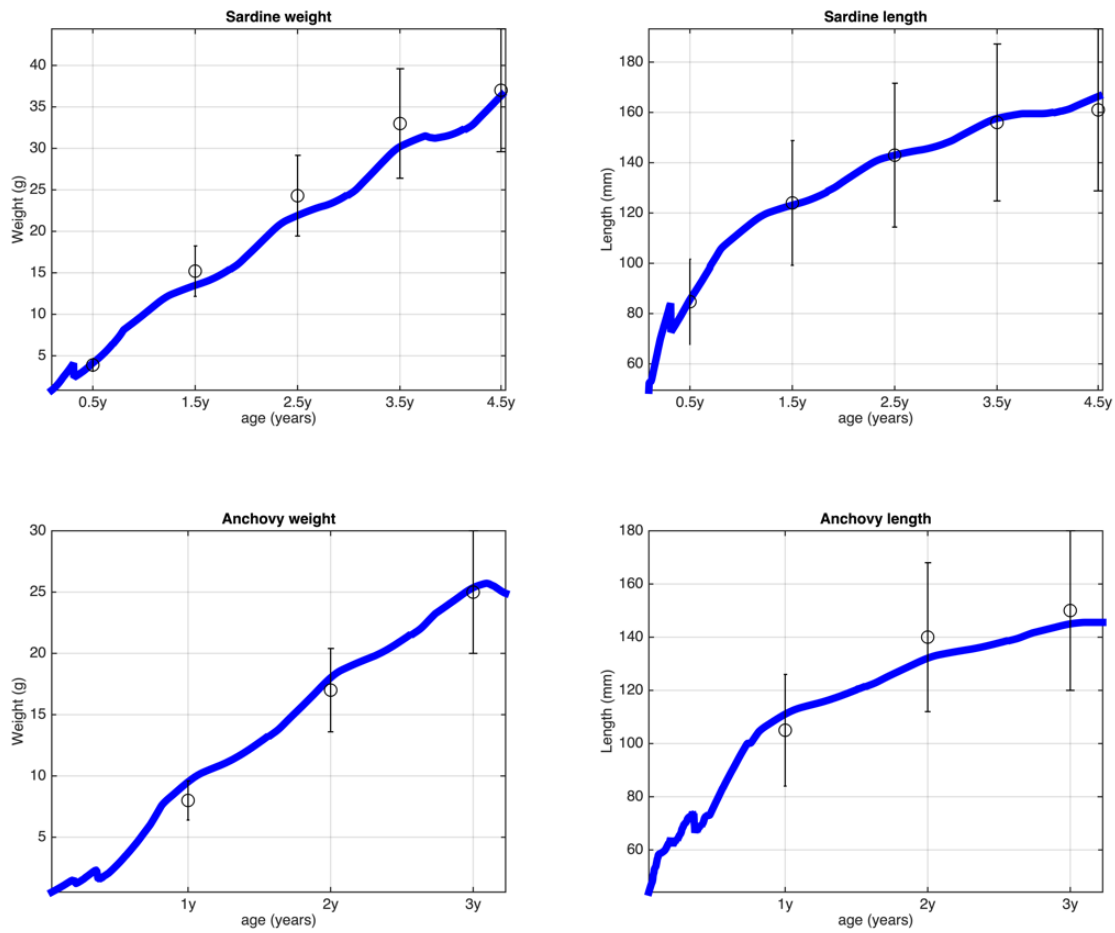

Figure 14. Evolution of mean weight and mean length of fish, calibrated using the genetic algorithm and mean weight- and length-at-age of adult fish (±SD) estimated from samples collected during the acoustic and egg production surveys in the North Aegean Sea, 2003 – 2008 (Somarakis *et al.,* 2012).

Finally, after the 10-years spin-up period, the modelled biomasses of the anchovy and sardine populations fluctuated around 40000 t and 25000 t respectively, i.e. the adopted reference biomass values (Fig. 15).

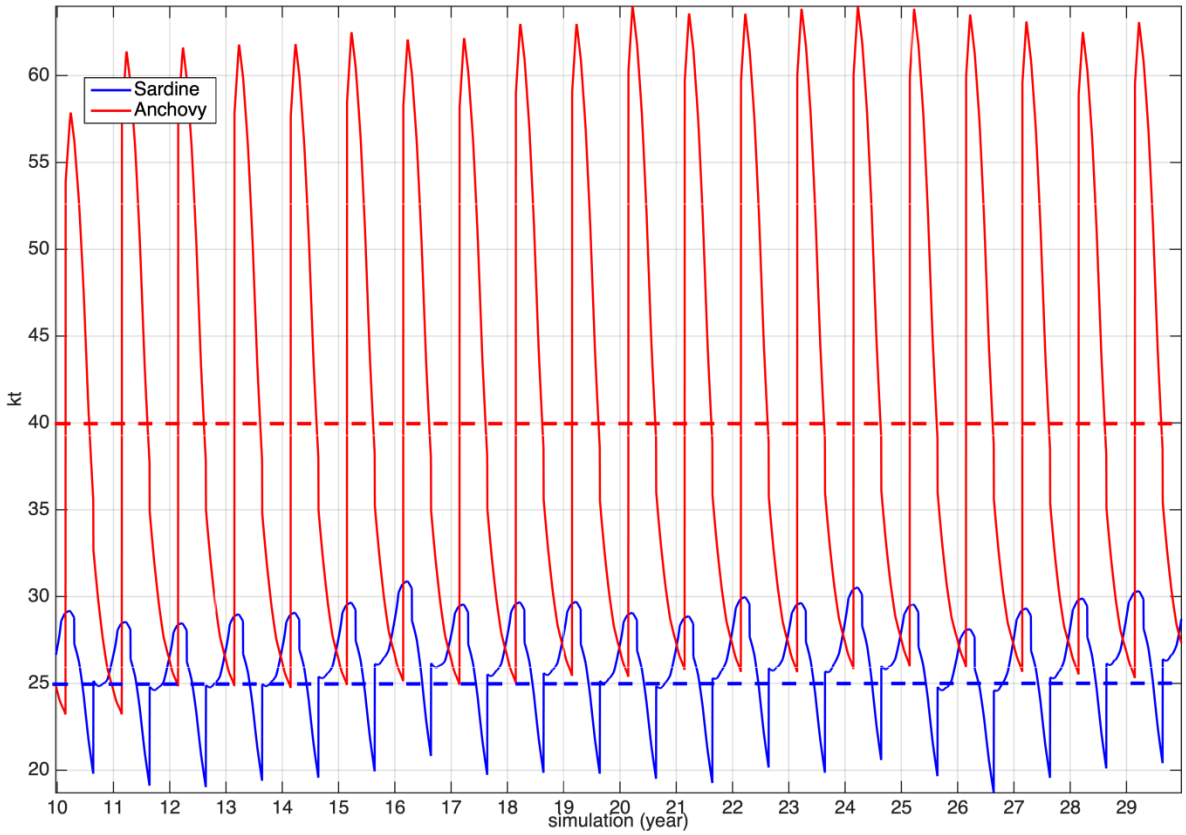

Figure 15. Model-simulated anchovy and sardine biomass. The mean biomasses of the two species in the N. Aegean Sea (based on acoustic data biomass estimations for the period 2003-2008) are also shown.

Model outputs regarding the spawning period and daily egg production of the two species were in agreement with known patterns (Fig. 16): Anchovy starts spawning in late April and its population continues to release eggs up to late September, but with decreasing numbers, especially after early summer, when SST reaches high values (Fig. 11) and the mesozooplankton concentration decreases (Fig. 12). No obvious difference in spawning timing/duration was observed between recruit (age-1) and repeat spawners (age 2+) (Fig. 16). In sardine, spawning starts in November and lasts until the end of April, i.e. spawning mainly coincides with the period of increase in mesozooplankton concentration (Fig. 12). The model

also predicts that, in sardine, recruit spawners have a delayed and shorter spawning period than the repeat spawners.

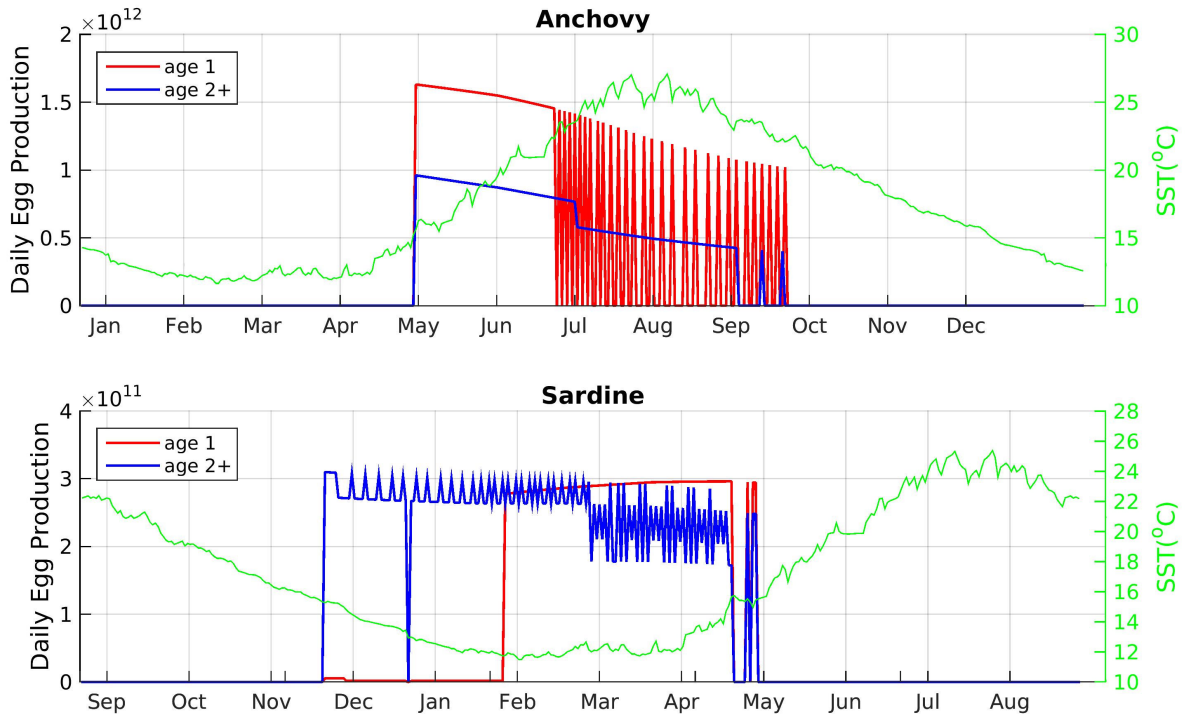

Figure16. Model-simulated daily egg production (total number of eggs produced by the population) for recruit (age 1) and repeat spawners (age 2+). The seasonal evolution of sea surface temperature (SST) is also shown.

In contrast to expectations (Somarakis *et al.,* 2019), the mean values of the 'capital index' are much higher in anchovy than in sardine (Table 3). This implies that the sardine in the North Aegean Sea derives most energy for egg production from direct food intake rather than energy stored prior to the spawning period. Indeed, the field estimates of mean monthly condition (Fig. 12) indicated that sardine has the lowest somatic weight in autumn prior to the start of its winter spawning season.

Table 3. Mean value of the capital index per age class.

	Age 1	Age 2	Age 3	Age 4
Anchovy	0.47	0.71	0.75	-
Sardine	0.006	0.28	0.34	0.09

Changes in fishery exploitation rates

Changing the fishing mortality imposed on the two species, so as to vary the Patterson's exploitation rate above and below the 0.4 reference point (Fig. 17), showed that the biomass of each individual species is relatively insensitive to changes in the exploitation rate of the other species and concomitant changes of its biomass. However, an obvious effect of the combined fishing rates on the two species could be seen on mesozooplankton, which is the fish prey. Sustainable exploitation of both species (E.R. <0.4) results in the decrease of mesozooplankton availability and overexploitation (E.R.>0.4) leads to the increase of mesozooplankton concentration.

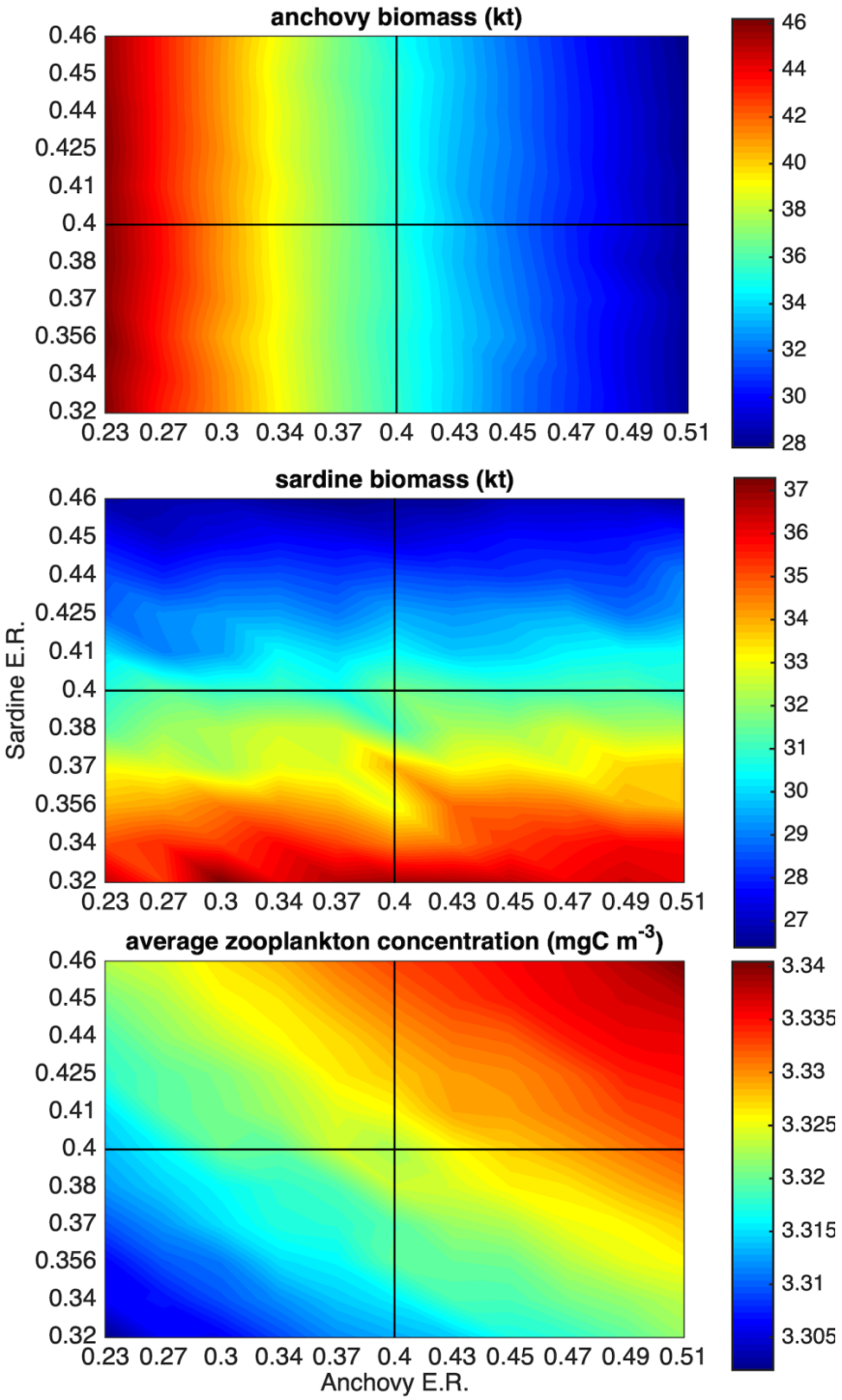

Figure 17. Biomass of anchovy and sardine and mean mesozooplankton concentration for different combinations of exploitation rate (E.R.) of the two species. E.R. = 0.4 is the reference point (maximum sustainable yield proxy) currently used in the management of small pelagic fish stocks in the Mediterranean Sea.

Changes in the timing of the fishery closure period

Shifting the timing of the fishery ban affects the biomass of both species (Fig. 18); however suitable timing (i.e., leading to the increase in average biomass) differs between anchovy (spring) and sardine (autumn). In both species, the most favorable closure period is the period of (and around) peak recruitment, as evidenced by the decline of mean fish weight in the population (Fig. 18, lower panel). When protecting the recruiting fish prior and/or during the initial phase of their first spawning period population biomass is positively affected, clearly owing to the increased annual population fecundity (Fig. 18, middle panel). In other words, due to the numerical dominance of recruit spawners in the population (>70% in both species, not shown), allowing a higher number of them to spawn results in the increase of egg production and the subsequent increase of population biomass.

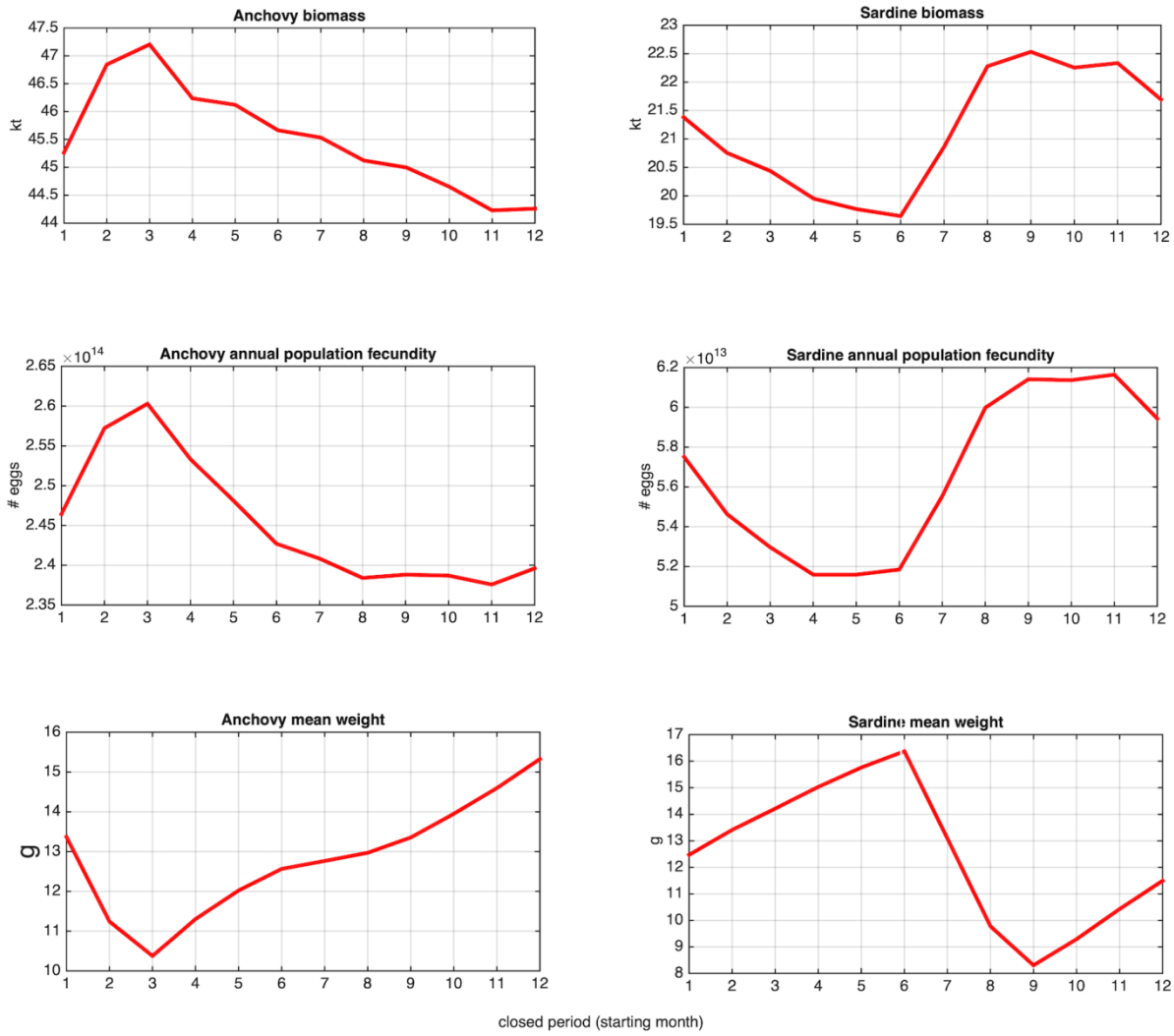

Figure 18. Mean anchovy and sardine biomass (upper panel) and annual population fecundity (middle panel) in relation to the timing of the 2.5 months fishing ban. Months 1, 2, 3,… etc correspond to closed period 15 Jan-Mar, 15 Feb-Apr, 15 Mar-May, …etc. The mean weight of individuals during the respective closed period is also plotted (lower panel).

4.3.2 3D model

With the addition of a movement-migration module, a 3-D fully coupled model was created and used for the direct linking of growth, mortality, movement and spawning

processes to the detailed spatial and temporal scales of the hydrodynamic/biogeochemical model (e.g. Rose *et al.*, 2015).

In the three-dimensional version of the anchovy and sardine model, the basic species attributes that are used for model calibration, are once more the early and adult stages growth in terms of body length and weight respectively and additionally, the evolution and spatial distribution of biomass and the production of eggs. The abundance (biomasses) and the physiology (weight and length per age) data, used for validation, were the same with those used for the one-dimensional model. It should be noted that in biomass estimates, the instrument's distinctive ability allows the recognition of the fish that are over 80mm in length. Therefore in the model derived biomasses, all adult stages together with juveniles with lengths over 80mm are included.

Growth

The simulated growth was validated against field sample length data for the late larval stage and weights data for the juveniles and adult stages. The simulated life history trajectories show good agreement with the data for both larval (Fig. 19) and adult stages (Fig. 20). A noticeable difference between the two species simulated adults weight evolution appears in summer and especially in July, with anchovy weight showing a weaker increase, as compared to sardine. This is in agreement with the species somatic condition data (Gkanasos *et al.,* 2019), where anchovy weight during July remains unchanged, or presents small deviations compared to June, while sardine weight significantly increases during the same

period. This is mainly due to the fact that anchovy spawns during summer, thus channeling a significant percentage of the energy stored, to reproduction, instead of somatic growth.

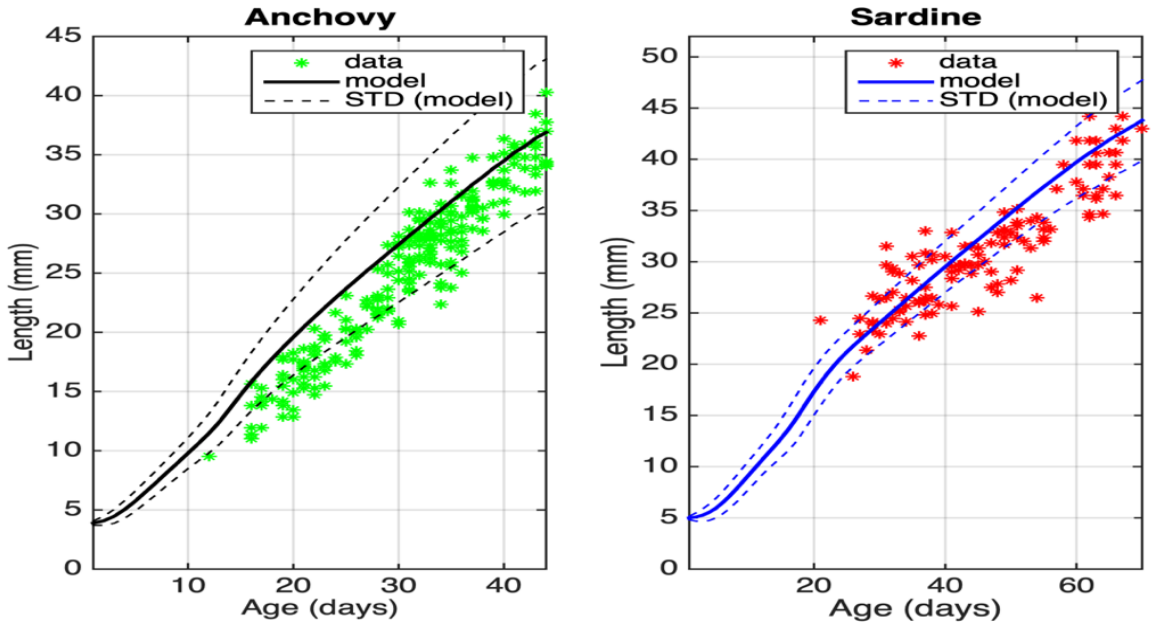

Figure 19. Mean late larvae lengths (±SD) against field data

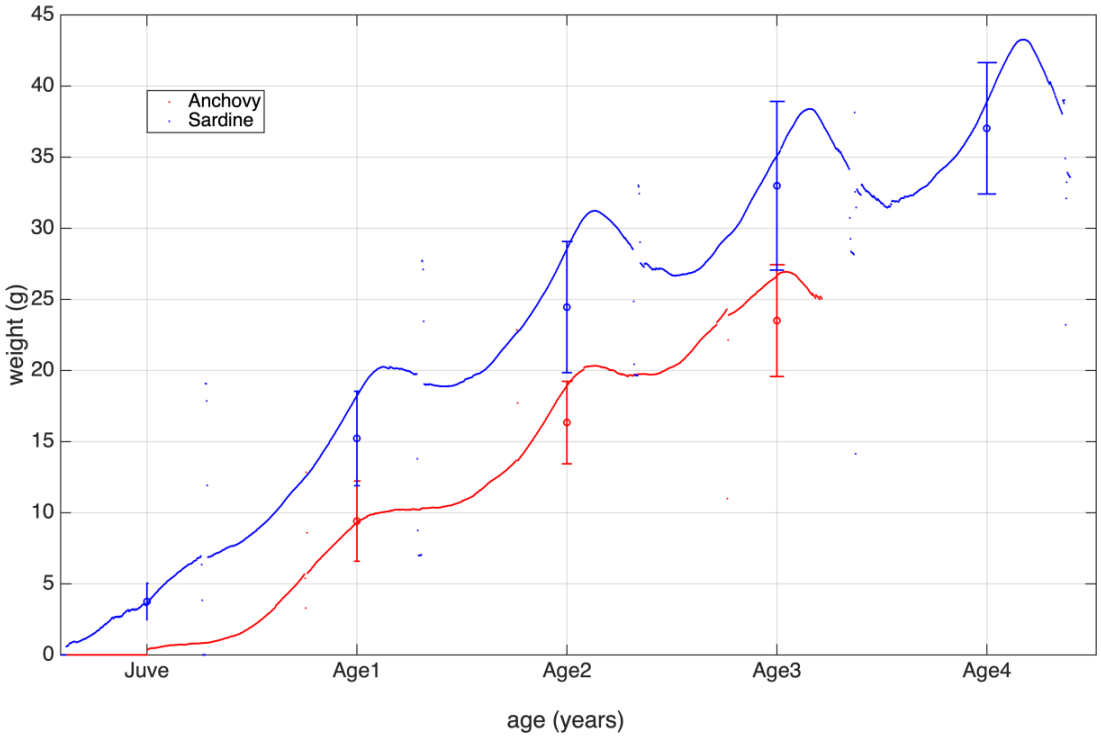

Figure 20. Species modeled weight per age against field data (±SD)

Biomass

Data from acoustic surveys during 2003-2008 period were used for the validation of the model derived biomass (Fig. 21). The data indicate a stronger variability in the estimated sardine biomass, as opposed to the relatively weaker inter-annual fluctuation for anchovy. Model results present a similar fluctuation for anchovy biomass, which is in most cases within the range of observations, but fail to capture the observed increasing trend for sardine and its particularly high biomass during 2006 (despite the large variations) and 2008.

Major differences between the two species simulated biomass seasonal variability include the emergence of two-yearly anchovy peaks (in January and in June), as well as the maintenance of a relatively high biomass during the intermediate period. Sardine peaks only during June-July period and is significantly lower during the rest of the year. For anchovy, the first peak is mainly attributed to the recruitment of juveniles above 80mm,while the second may be attributed to the adult's optimum somatic condition from April to July (Gkanasos *et al.,* 2019). On the other hand, sardine biomass peak (June-July) occurs during a period, where increased juvenile abundance and optimum somatic state timely coincide.

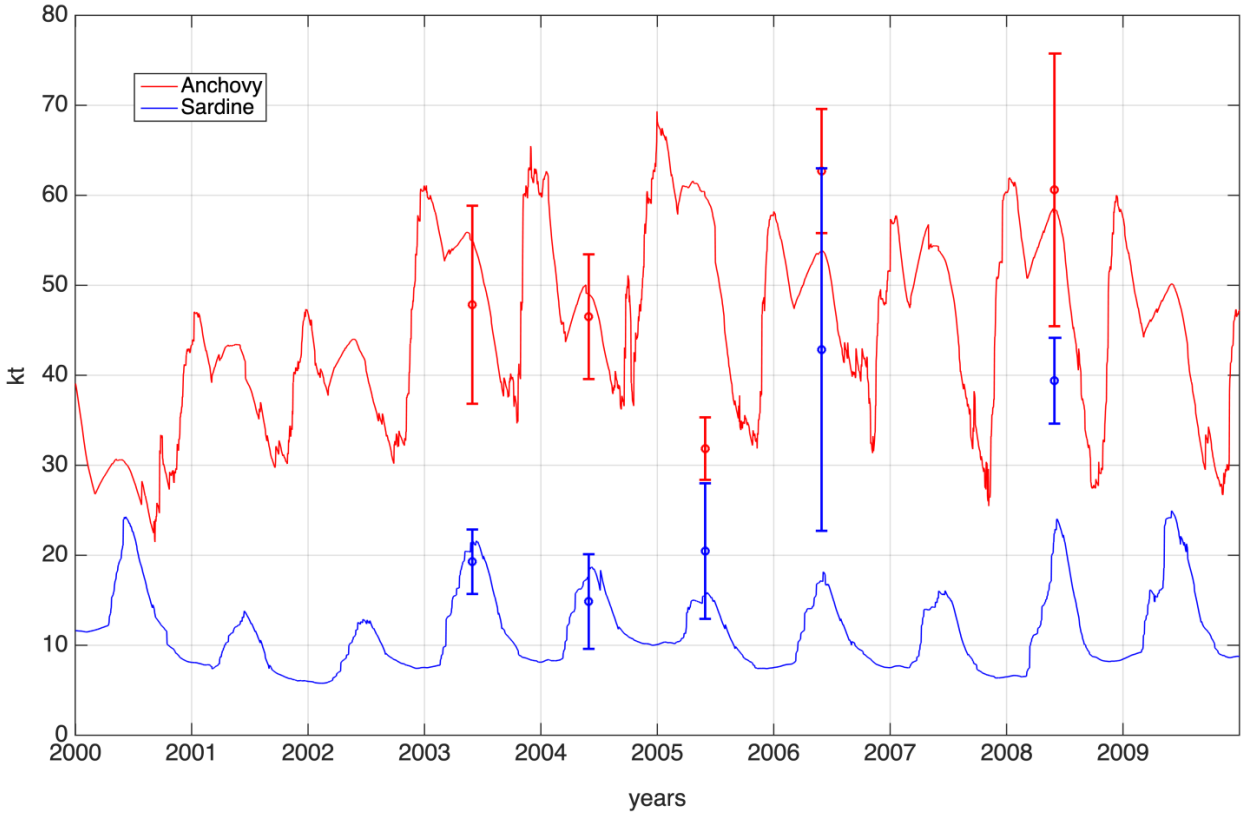

Figure 21. Biomass evolution (stages: juveniles (> 80mm) and adults), against data from acoustic surveys for the years 2003-2008.

From the simulated spatial distribution of biomass (Fig. 22), both species appear to cover the N. Aegean continental shelf (h<150m), showing higher concentrations in Thermaikos Gulf, Strymonikos Gulf and the Thracean Sea coastal areas, which is in reasonably good agreement with the biomasses estimates from acoustic surveys data and literature (Giannoulaki *et al.,* 2005). Areas showing higher fish biomass are characterized by relatively higher primary production and zooplankton concentrations, which is related to the BSW and river nutrient loads, as discussed above (see Figure 10).

The main model deviation from the data is found on the east of Limnos Island, where the observed patches of relatively high biomass are not reproduced by the model. We should note that this area lies in the pathway of BSW, discharged from the Dardanelles straits and is

characterized by very strong currents that result in the off-shore advection of fish eggs/larvae that prevents the establishment of an important adult population. Therefore, this model deviation might be related to an overestimation of BSW induced currents and/or an underestimation of mesozooplankton carried by BSW (not adopted in the model) and deserves further investigation. Although the sardine stock is much smaller (~20kt), as compared to anchovy (~45kt), it seems to be spatially less restricted, particularly in the southwestern part of the basin (near Sporades and around Limnos Island) and this is in agreement with the data.

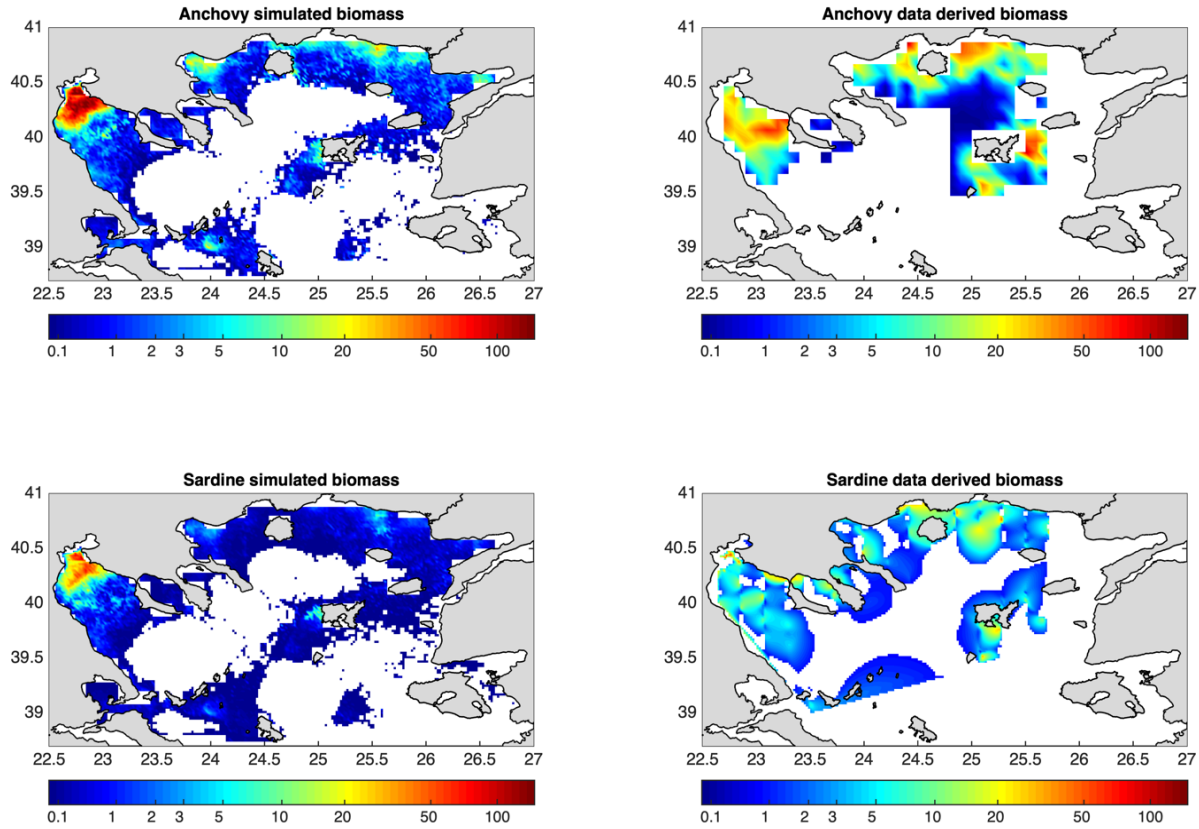

Figure 22. Anchovy (top) and Sardine (bottom) simulated (left) biomass against acoustic surveys (right) mean June (2003 - 2009), biomass (tons sq. miles -1)

Egg production

Daily egg production surveys indicated the presence of sardine eggs from November to April and anchovy eggs from May to September. To describe the different spawning periods for the two species in the model, a combination of temperature and calendar criterions were used. Thus, the spawning period was assumed to start when SST is higher than 15^{o}C or lower than 16^{o}C for anchovy and sardine respectively. The end of the spawning period was set on specific dates for both species.

The simulated egg production for sardine presents a much weaker variability, as compared to anchovy, which is consistent with its income breeding reproduction pattern (Gkanasos *et al.,* 2019). The slightly increasing egg production during the spawning period (Autumn-Spring) follows the corresponding increase of zooplankton (Fig. 11). The anchovy egg production presents a steep peak in May-June period (Fig. 23) and then drops until the offset of the spawning period in September. The pattern of the curve is in accordance to the capital breeding mode of anchovy in the N. Aegean (Gkanasos *et al.,* 2019), since the energy stored during the food abundant previous period is channeled to a peak egg productivity, that fades out in relation to the poor feeding conditions during the summer.

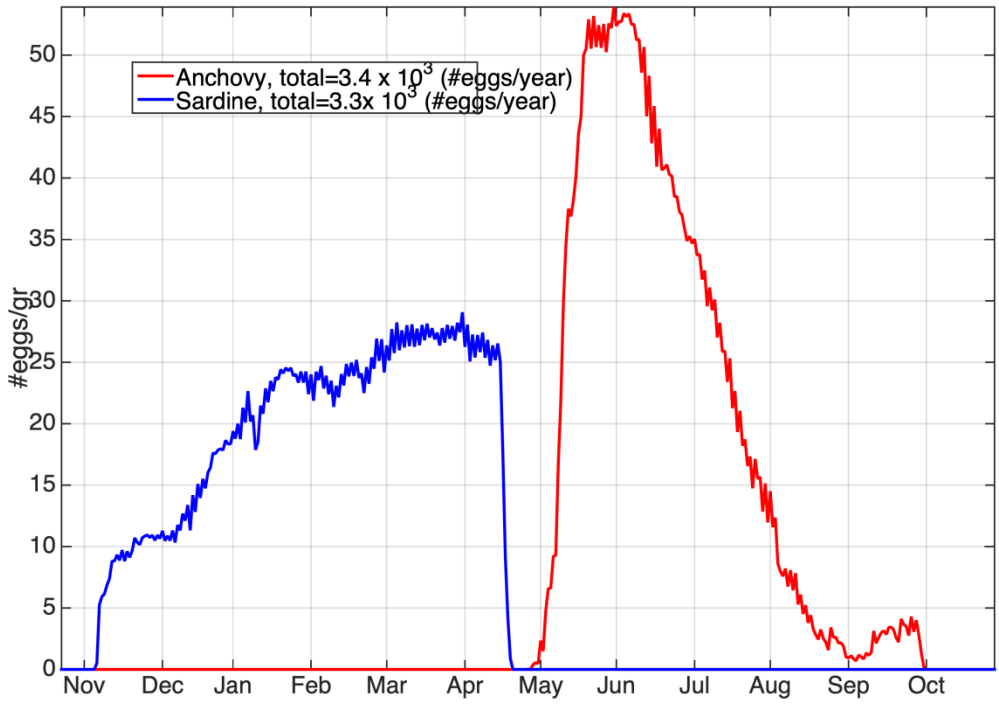

Figure 23. Normalized daily egg production for the years 2000-2009.

Data on the spatial distribution of eggs are only available for anchovy (Fig. 24), since surveys were only during summer period. The simulated anchovy egg abundance is higher in areas of increased biomass, such as Thermaikos Gulf, the Thracean Sea and Strymonikos Gulf, closely following the simulated adult biomass distribution (Fig. 23), which is generally in agreement with in-situ data. The main model deviation is the overestimation of egg abundance in Thermaikos Gulf and this might be attributed to an overestimated egg production, following the slight overestimation in the adult biomass (Fig. 22) and the relatively weaker near surface circulation, as compared to the more exposed Thracean Sea that results in the weaker off-shore dispersion of eggs.

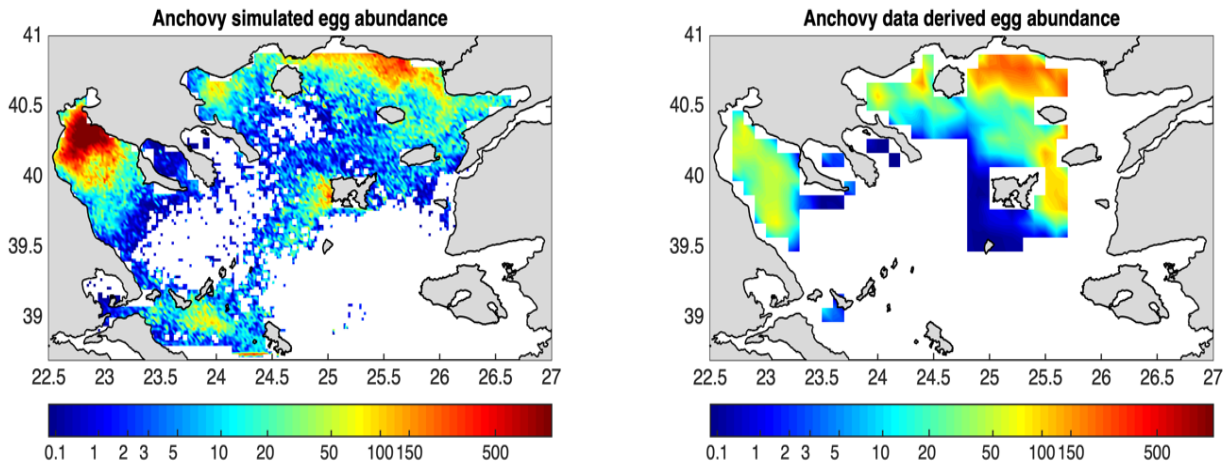

Figure 24. Anchovy mean June (2003 - 2006), biomass (tons/sq. miles) and egg production (eggs/m^2).

Resources competition

In order to investigate a possible species interaction, resulting from resource competition, two additional experiments were performed, with the existence of only one species in the model at a time. So while in the reference simulation, the annual mean biomass for the two species were ~45kt for anchovy and 11.5kt for sardine, when the two species were separately simulated, their biomasses were 47kt and 42kt for anchovy and sardine respectively (Table 4). The fact that a similar mean biomass is simulated for the two species implies that this is mainly related to the available resources (i.e. zooplankton), sustaining the fish stock. The resource competition is also revealed by the important increase of mesozooplankton biomass with decreasing fish biomass in the different simulations (Table 4).

It is interesting to note that a higher total fish biomass is simulated in the two-species simulation (56.5kt), as compared to the single-species simulations (42-47kt). This might be related to the intra-specific density-dependence, as the two-species have a complementary

spawning period (sardine: autumn-winter, anchovy: spring-summer) and share the same resources, but their peak feeding on zooplankton is on a different period. Thus, in the single-species simulation the pressure exerted from fish to zooplankton is relatively higher, resulting in lower biomass. Given that identical natural mortalities are used for the two species and egg production is also linked to available resources, it may be no surprise in terms of population dynamics that the two species eventually obtain a very similar biomass. However, when the two species share the same resources, anchovy appears to achieve a much higher biomass, preventing the increase of sardine stock. Sardine appears to be strongly benefited from an anchovy retreat and is highly dependent from the food resources limitation in the area due to the anchovy existence. This suggests that anchovy is currently better acclimatized in the N. Aegean and is the dominant species, as compared to sardine. In order to verify this finding, an additional simulation was performed with the two species initialized with inverted biomasses and the outcome was again similar to the reference simulation, characterized by higher anchovy biomass.

Table 4. Simulated species biomasses (annual mean and during sampling period) and mesozooplankton concentration in single and multispecies experiments.

	Two-species	Single Species (anchovy)	Single Species (sardine)
Anchovy biomass	45 (59)	47 (61)	-
Sardine biomass	11.5 (19)	-	42 (60)
Total biomass	56.5	47	42
Mesozooplankton (0-100m)	1.93	1.95	2.12

Given that the fishing pressure on the two species is similar in the N. Aegean and the annual egg production (per fish weight) is comparable, the reason behind the dominance of anchovy might be attributed to the difference between the two species larval growth. Larval length data show that summer anchovy larvae present higher growth rates as compared to winter sardine larvae. Even among anchovy larvae (Schismenou *et al.,* 2013), those that are found during winter present significantly lower growth (0.63mm d^{-1}), than those of summer (0.8mm d^{-1}), while sardine (winter) larvae are also positively correlated with temperature (Schismenou *et al.,* 2016). Faster growth and smaller anchovy transformation length (42mm instead of 50mm for sardine), in turn leads to reduced stage mortality, resulting to increased species population.

In the model, given the similarities of the two species and the lack of sufficient data on the effect of temperature on energetic rates, the same temperature dependence is adopted for anchovy and sardine, except for the optimum temperatures for larvae food consumption (see Table 1). These are assumed to be close to their mean ambient temperatures during the two different seasons (autumn-winter for sardine, spring-summer for anchovy), following the "optimal growth temperature hypothesis". The fish growth for each stage of both species is mainly regulated from the consumption half-saturation parameters (see Table 1) that are tuned in order to obtain a best fit with the available growth data (Fig. 4-5). Thus, a relatively higher half-saturation coefficient is adopted for sardine larvae, in order to reproduce the observed lower growth during autumn-winter period. Indicatively, sardine half-saturation parameters for the early and late larval stages are respectively 42% and 88% higher as compared to those fitted for anchovy.

Temperature sensitivity

The effect of temperature increase (dT, +1 oC and +2 oC) on the mean anchovy and sardine biomass is shown in Figure 25. In the two-species simulations, anchovy biomass decreased with increasing temperature (from -37% for dT = +1oC to -64% for dT = +2oC). In contrast, sardine biomass increased by ~ +5% in both experiments. In single-species simulations, when the temperature increase was applied on all stages (larvae/juveniles and adults, t. on all st.), both species biomasses decreased (from -25% for dT = +1oC to -51% for dT = +2oC for anchovy and from -13% for dT = +1oC to -32% for dT = +2oC for sardine). These experiments show that temperature increase negatively affects both species, but this is masked in the case of sardine in the two-species simulation due to the lower resource competition when anchovy biomass decreases. The negative effect of temperature on fish growth results from the dome shaped consumption temperature dependence and the (exponential) increase of metabolic costs (mainly respiration) with temperature.

The single species experiments highlight the fact that temperature increase affects anchovy more than sardine. A comparison among the species corresponding ages, shows that both anchovy adults and early stages are significantly more affected than those of sardine. The anchovy spawning period coincides to the maximum yearly sea temperature. Therefore the already elevated energetic demands of the anchovy adults during this period, are even more charged due to the temperature increase, thus affecting the somatic condition and the subsequent egg production. The effect of temperature is not that obvious on sardine adults, since these already are in a good somatic condition when spawning. Anchovy larvae period of occurrence also partially coincides to the maximum yearly temperature, so once again these stages are more affected by the temperature increase as compared to those of sardine.

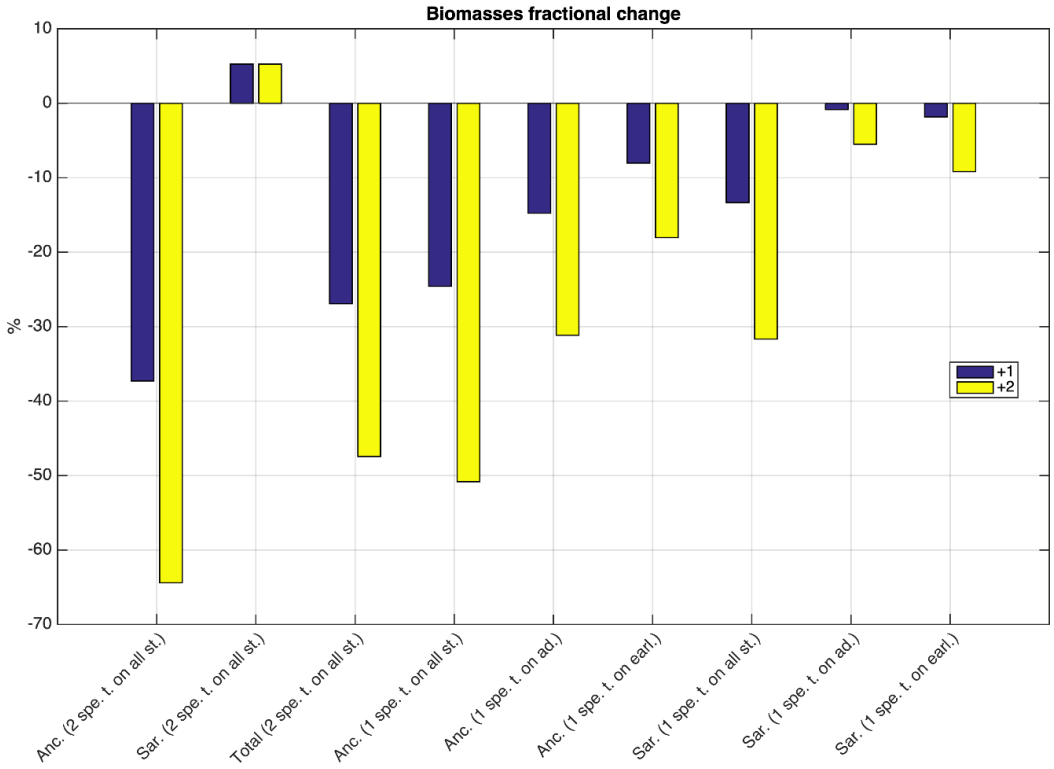

Figure 25. Temperature effect on biomasses. Experiments abbreviations: Both species (2 spe.), or single species (1 spe), with temperature effect applied on early stages (t. on earl.), on adult stages (t. on ad.), or on all stages (t. on all st.).

Temporal variations in fishery

The sustainability of the fishing effort is a major concern for small pelagic fish like anchovy and sardine. Therefore, among the different measures for their preservation, the alteration of the closed fishing period should also be considered. The result of this action must be twofold, since the resulting increase of species abundance must take under consideration the socioeconomic aspect of the fishing activity that must either remain stable or sustainably increased. In order for the experiments with different closed fishing periods to be comparable, they should yield the same amount of total annual catches. To this end, a

proportional term which parameterizes the seasonality of fishing effort (dimensionless) based on observed seasonality of catches, was calibrated.

The result was a series of simulation experiments towards testing the efficiency of different closed periods for fishing. Five two-month closed fishing periods were tested (months 3-4, 5-6, 7-8, 9-10, 11-12) against a reference period (months 1-2) that closely corresponds to the actual closed fishing period for purse-seiners in Greece (closed fishing period 15th of December –1st of March).

The highest increase in anchovy adult population (+19%) and biomass (+13%) occurs when the fishery is closed during May and June (Fig. 26). This is the period when anchovy egg production peaks during its spawning period (late April – mid September). Anchovy biomass and adult population increase slightly when the fishery is closed in March-April. This is a period characterized by elevated somatic growth and recruitment of new adults (Gkanasos *et al.,* 2019).

Increase in sardine population (+8%) and biomass (+10.75%) is observed only if the fishery is closed during September and October (Fig. 26). This period coincides with the onset of recruitment (September 1st) and the spawning season (November). Thus, banning the fishing activity during this period, increases the number of spawning adults and consequently the sardine biomass.

Consequently, the combination of those two periods would assist both species augmentation; however, due to socioeconomic reasons only one period should be selected. Thus, as both species are of similar size and simultaneously fished, the increase in the total biomass of both species must be considered. This is maximum when species are not fished during May and June. In this scenario, the total biomass is increased by 8% compared to the

reference period (fishery closed in January-February), due to the increase of the total species population (+14%) compared to the reference period.

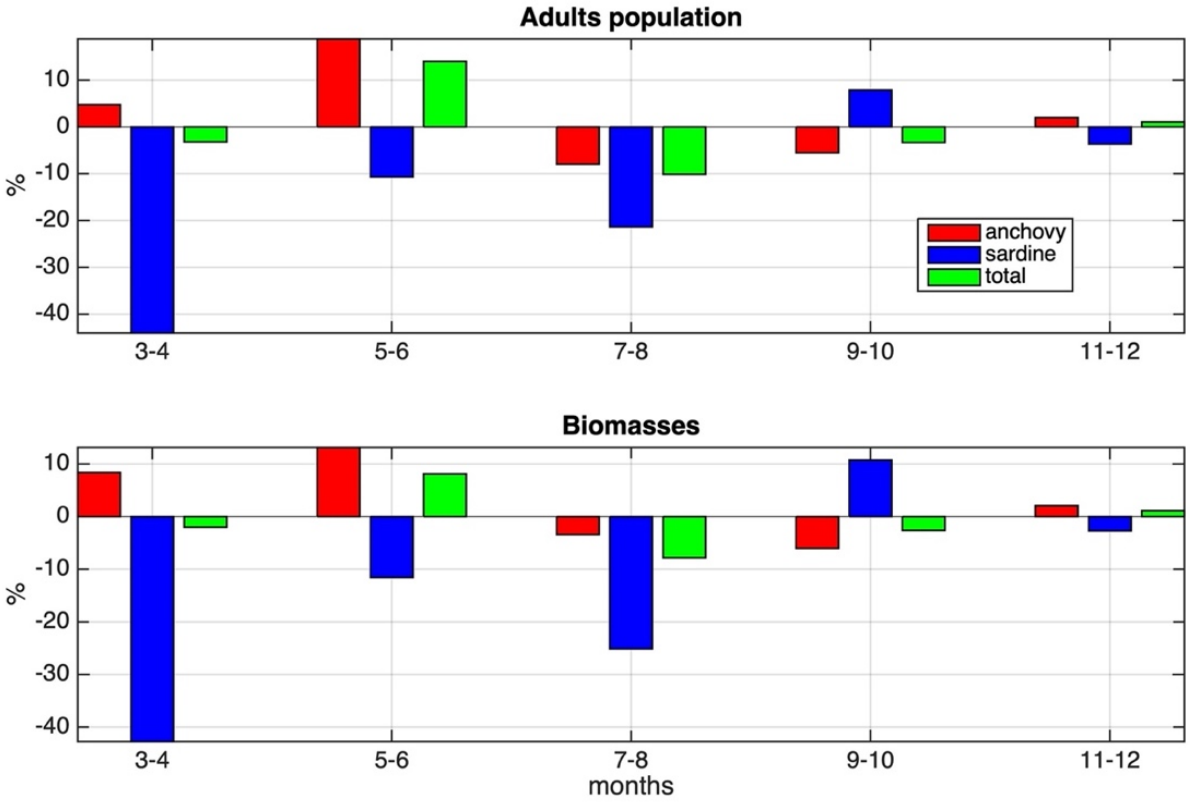

Figure 26. Adults population and biomasses fractional changes over the reference simulation, in changing closed fishing period experiment.

Spatial variations in fishery

In this set of experiments, changes in anchovy and sardine biomass due to changes in the fishing grounds are studied. To this aim, three simulation experiments with different fishing grounds, all of them sub-areas of the reference one were tested. According to these,

fishing is prohibited in i) sea areas with bottom depth under 50m, ii) in Thermaikos Gulf, or iii) in the Thracean Sea (Fig. 27).

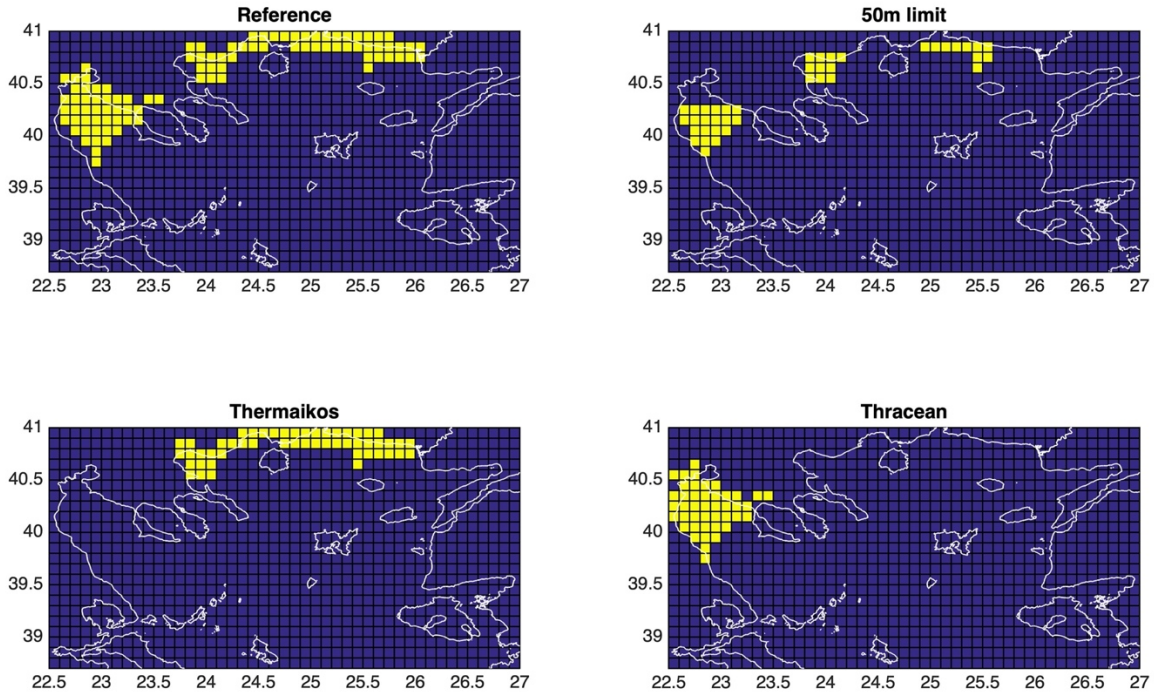

Figure 27. Maps of different fishing areas. Fishing points in yellow.

Results show that total adult population and biomass increased only when fishing was prohibited in areas with bottom depths below 50m; however, catches decreased. In this scenario, the total biomass increased by 21%, which is attributed to the anchovy biomass boost (Fig. 28). This biomass gain was mainly due to the increase of age-1 adult population (Fig. 29), that apparently reside closer to the shore. In the rest of the scenarios, the total adult population and biomass remain about the same. According to model simulations, total catches decrease due to the closure of Thermaikos Gulf or of areas <50m and remain about the same with the closure of the Thracean Sea (Fig. 28).

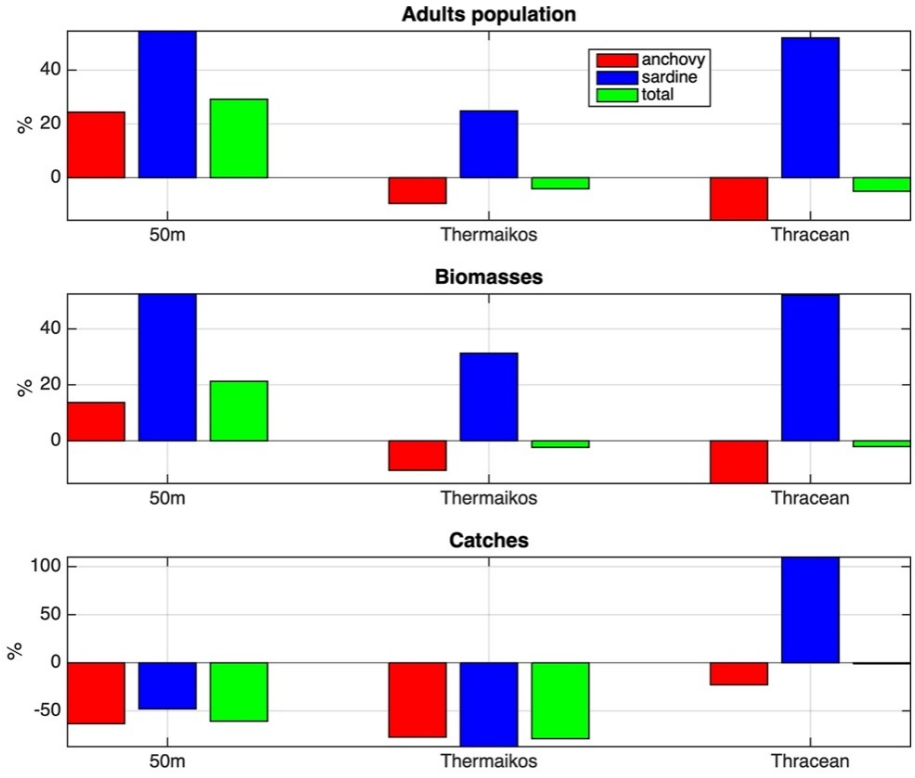

Figure 28. Adults population, biomass and annual catches fractional changes over the reference simulation, in changing closed fishing areas experiment.

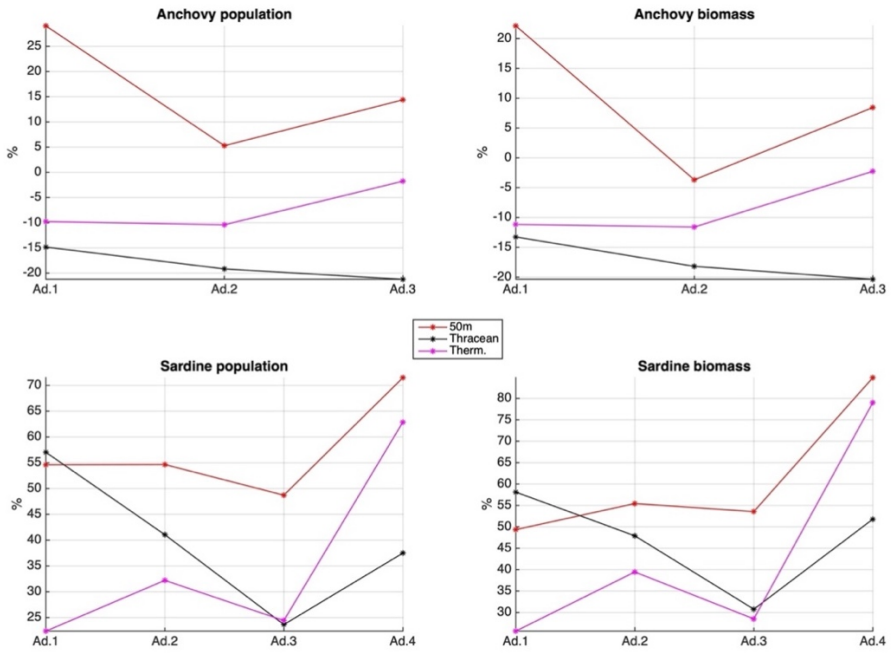

Figure 29. Fractional changes per age (Ad.1, Ad.2, Ad.3, Ad4) of adults populations and biomasses, in changing closed fishing areas experiment, over the reference simulation.

The results display differences in the habitats of anchovy and sardine. The fact that anchovy population and biomass is only increased when fishing is banned coastally (sea bottom<50m), shows a species preference to shallow waters. On the contrary, sardine seems to be more spread across the continental shelf, a conclusion driven by the fact that in all scenarios, a boost in abundance emerges.

Advocate to that is the unexpected sardine catch increase when banning fishery in the Thracean Sea. This is probably attributed to the fact that in this scenario, sardine population boost leads to a corresponding egg production increase. The circulation pattern in the area, carries eggs westwards favoring sardine in all areas and not just in the Thracean Sea and thus resulting to more catches in total. This phenomenon is not repeated when banning fishery in the Thermaikos Bay, since the circulation does not favor the transport of eggs eastwards.

5. Modeling the impact of Climate Change

The objective of the following section, is to assess the effect of changes in specific climatic drivers on the pelagic ecosystem and small pelagic fish populations through a series of simulations. Small pelagic fish populations are closely linked to environmental conditions (abundance of phyto/zooplankton, temperature, ocean circulation). The variability of primary production in the Aegean Sea is driven primarily by lateral (rivers, Black Sea water) nutrient inputs and the entrainment of deep-water nutrients through vertical mixing. So the impact of future climate changes (e.g. temperature rise, decrease in river output) on the productivity and, subsequently, on small pelagic fishes is investigated by simulating scenarios adopting future climate conditions.

Climatic scenarios

Two simulations were performed, adopting present (1980-2000) and future (2080-2100) climatic conditions under the IPCC-A1B scenario (Chust *et al.,* 2014). The atmospheric forcing for these climate simulations was obtained from SINTEX-G (INGV-SXG, Gualdi *et al.,* 2007) fully coupled global atmosphere-ocean general circulation model. The open boundary conditions for the biogeochemical and hydrodynamic models were obtained from a Mediterranean basin scale model simulation over the same periods (Stergiou *et al.,* 2016). Both river and BSW discharge and nutrient inputs were the same in the two simulations.

The application of present (1980-2000) and future (2080-2100) climatic conditions under the IPCC-A1B scenario showed that in the future climate scenario, sea surface temperature (SST) is increased by +1.12^{o}C on average, while sea surface salinity (SSS) is also slightly increased (+0.09 psu on average), resulting in an overall increase of stratification (indicated by a decrease of mixed layer depth by ~6%). The latter results in a decrease of phytoplankton (-4.6%), followed by a decrease of microzooplankton (-6%) and mesozooplankton (-6.9%) biomass (Fig. 30 & Table 5). These changes refer to a simulation of the biogeochemical model, without the fish, as the simulated microzooplankton (prey of larvae) and particularly mesozooplankton (prey of late larvae, juveniles and adults) biomass is significantly influenced from the total fish biomass, based on the model two-way coupling. Thus, changes in this "uncoupled" simulation may be considered indicative of the impact of climate change on plankton productivity that would be otherwise masked in a two-way coupled simulation, where plankton mortality from fish consumption is also changing. We should note that river and BSW discharge and nutrient inputs are kept unchanged is the present/future simulations.

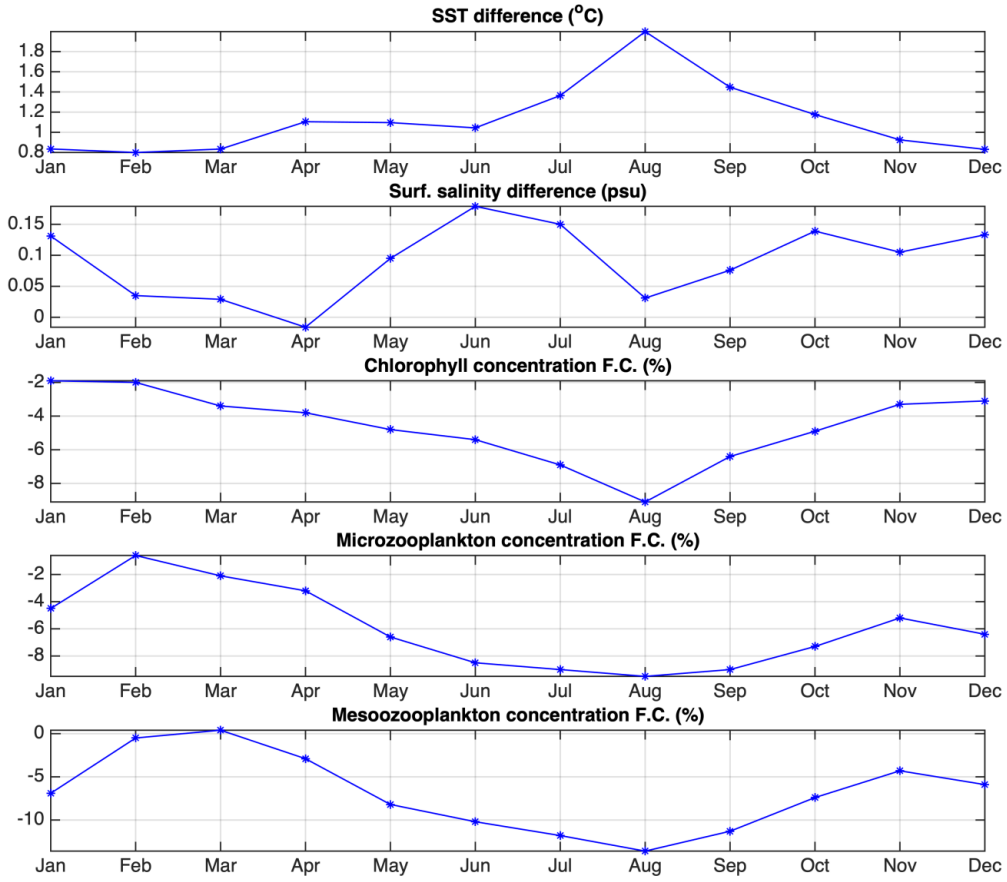

Figure 30. "Future" and "Present" scenarios ecological indices differences and fractional changes.

Table 5. Biomasses and ecological variables alterations for the two periods.

	1980-2000	**2080-2100**	**Future – Present**		
			annual	**Nov. – Apr.**	**May – Oct.**
SST (°C)	18.61	19.73	+1.12	+0.89	+1.35
Salinity (psu)	36.44	36.53	+0.09	+0.07	+0.11
Microzooplankton	6.9 (mgC/m^3)	6.55(mgC/m^3)	-6%	-3.7%	-8.3%
Mesozooplankton	8.71 (mgC/m^3)	8.17(mgC/m^3)	-6.9%	-3.3%	-10.4%
Biomasses (kt) 2 spe. 1 spe (anchovy) 1 spe (sardine)	Anc.: 59.5 sar.: 33 81 89	Anc.: 25, sar.: 44 32 44	Anc.: -57%, sar.:+33% -60% -51%		

The temperature increase and reduction of food resources result in a significant anchovy biomass decrease by -57% (Table 5). On the other hand, sardine biomass is increased by 33%, which is partly related to resource competition, as sardine benefits from anchovy biomass reduction, as discussed above. When the two species are separately simulated, not sharing the same resources, sardine appears also negatively affected, showing an important, though slightly smaller, reduction (-51%), as compared to anchovy. It is noticeable that sardine annual mean biomass (44 kt) is higher than anchovy (25 kt) in the two-species simulation, which suggests a potential change of the environmental factors that favor anchovy in the N. Aegean making it the dominant species. To further investigate this finding, temperature and zooplankton biomass changes in the future climate were compared during the two periods (Table 5) that may be considered as representative for spawning and larval growth for anchovy (May-October) and sardine (November-April). The temperature increase and food reduction during May-October appears significantly higher, as compared to November-April period. Therefore, anchovy faces a combination of more adverse conditions (+1.35^{o}C temperature increase and 8%-10% food reduction) during its spawning period, as compared to sardine (+0.89^{o}C temperature increase and ~ -3.4% food reduction), which might explain the simulated dominance of the latter in the future climate conditions.

The projected results for anchovy and sardine biomass in the future climate scenario are more or less consistent with results in the temperature sensitivity experiments. The climate change projected warming is roughly comparable with the dT=+1^{o}C temperature increase experiments, showing an anchovy biomass decrease by -37% and a sardine biomass increase by +5% in the two-species simulation (see Fig. 25). These changes were amplified (anchovy -57%, sardine +33%) in the future climate scenario by the differential decrease of food availability during the two species spawning periods, considering also resource

competition that favors sardine. Comparing the single species simulations, the reduction of both anchovy (-60%) and sardine (-51%) biomass in the future climate scenario appear much stronger as compared to the -25% and -13% reductions in the temperature sensitivity. This can be partly attributed to the zooplankton decrease. Another factor that must be taken into account is the longer duration (20 years) of the future climate scenarios, resulting in a magnified effect, as compared to the temperature sensitivity (10 years).

Scenarios of changing river nutrient inputs.

The river nutrient inputs are an important component of the N. Aegean nutrient budget (Tsiaras *et al.,* 2012) and have a great impact on plankton productivity, especially in the coastal, river influenced areas. In this section, simulations with different nutrient loads from the main rivers in the area were performed. These originated from three different socio-economic scenarios (BAU: Business As Usual [BAU30], PT: Policy Target [PT30] and DB: Deep Blue [DB30]) and are based on future projections build upon hydrological/nutrient emission modelling of the Mediterranean drainage basin (Ludwig *et al.,* 2010).

In Figure 31, the nutrients load from the three different socio-economic scenarios as compared to the reference simulation, are presented. Nitrates (NO_3) load is reduced in Evros, Strymon and Aliakmon rivers in all scenarios, while in Axios & Nestos and Pinios rivers nitrates are increased compared to the reference simulation. Phosphorus (PO_4) is limited in all scenarios and rivers besides that of Pinios in the BAU30 scenario.

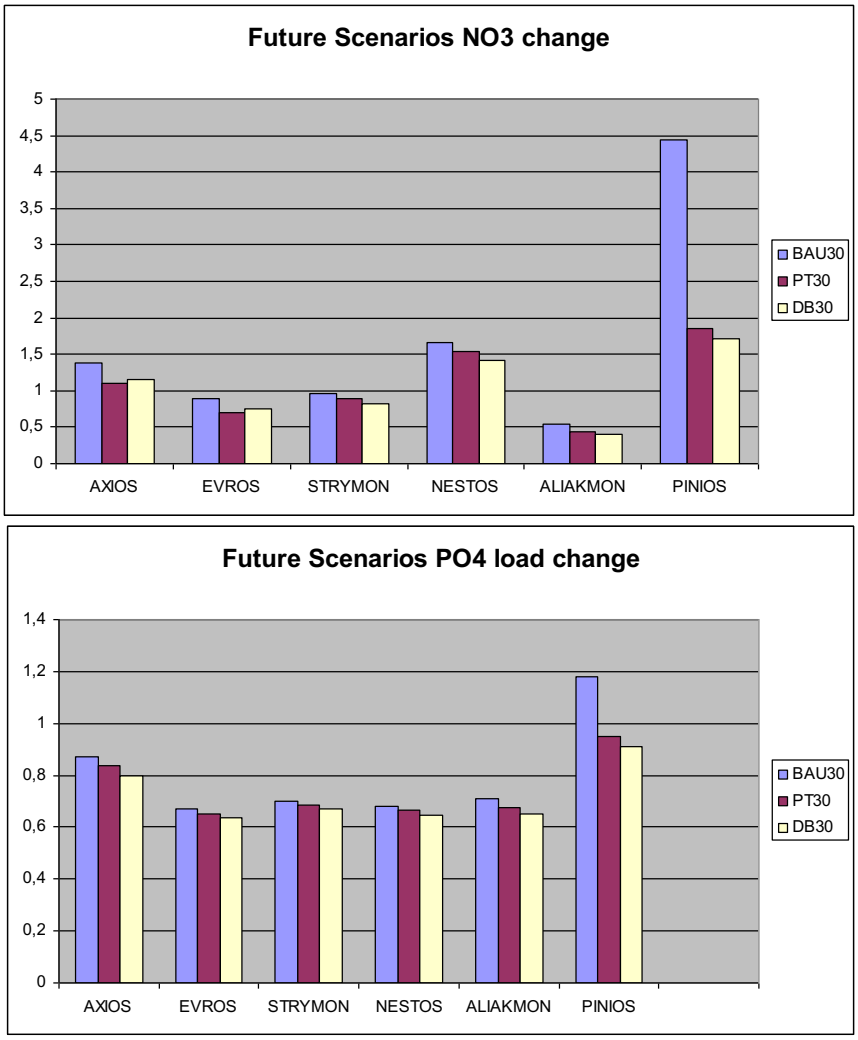

Figure 31. Relative change (Future Scenario/Reference) in nitrate (top) and phosphate (bottom) river nutrient loads of 2030 period scenarios BAU, PT, DB for major N. Aegean Rivers.

These changes in river inputs lead to a cumulative nutrients reduction in all scenarios, which in turn cause reduced simulated surface chlorophyll and zooplankton concentrations in the North Aegean Sea, with the exception of Thermaikos Gulf. The increase of nitrogen inputs from Axios and Pinios rivers, especially in the first two scenarios (BAU30 & PT30), results to an increased simulated phytoplankton and zooplankton biomass in Thermaikos Gulf (Fig. 32), an area that is currently characterized by nitrogen limitation (Tsiaras *et al.,* 2014).

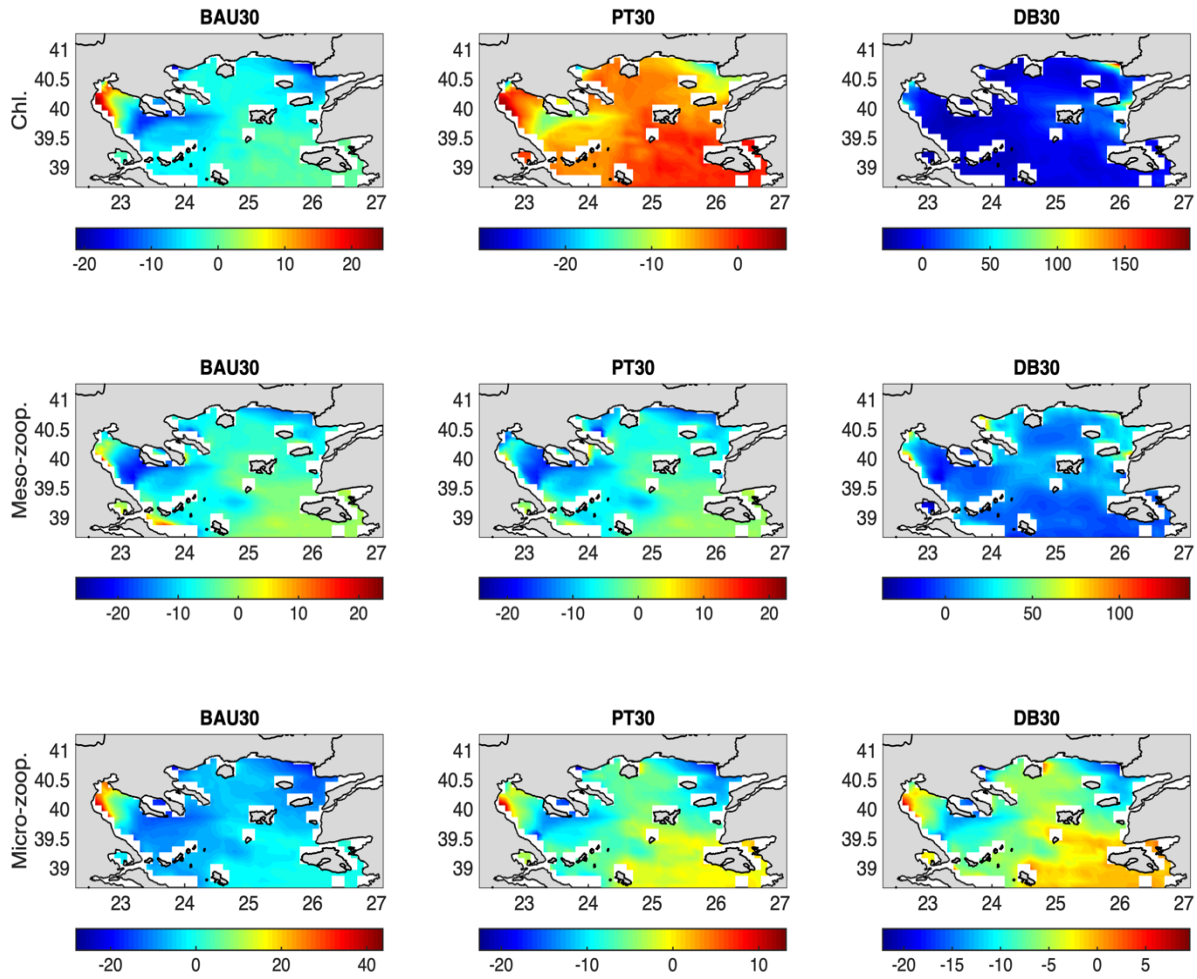

Figure 32. Model simulated chlorophyll, meso and micro-zooplankton biomass fractional change (%) of the three scenario simulations, over the reference simulation.

Overall, simulated micro and meso-zooplankton concentration is reduced (Table 6), affecting early life stage survival and egg production and resulting in reduced fish biomass. Anchovy exhibits the largest biomass decrease (60, 56 and 54%, in all scenarios respectively). Sardine is affected as well, but to a lesser extent (12, 14.4 and 12.9%, in all scenarios respectively), probably favored by the decrease in anchovy biomass due to resource competition.

Table 6. Anchovy and sardine biomass and fractional changes of ecological variables over the reference simulation, for the three scenarios.

	BAU30	**PT30**	**DB30**
Nitrates	-6.6%	-17%	-20,6%
Phosphates	-36%	-37%	-39%
Chlorophyll	-10%	-11.5%	-12%
Microzooplankton	-8%	-10%	-10%
Mesozooplankton	-9.5%	-9.5%	-9.3%
Anchovy biomass (kt)	23.5 (-60%)	25.8 (-56%)	27.2 (-54%)
Sardine biomass (kt)	16.7 (-12%)	14.4 (-24%)	12.9(-32%)

Scenarios of changing Black Sea water/nutrient inputs.

The low-salinity Black Sea Water (BSW) is enriched in particulate and dissolved organic matter (Sempere *et al.,* 2002), contributing, along with river nutrient inputs to an increased primary and secondary production in the N. Aegean Sea (Siokou *et al.,* 2002). In this section, two scenarios were performed, with increased/reduced (±25%) BSW discharge in order to investigate its influence on the North Aegean Sea ecosystem and the resulting effects on anchovy and sardine stocks.

In terms of surface salinity, the effect of changing BSW inflow is apparent in the Thracean Sea due to the dominant anticyclonic circulation in the area. The enhanced (x1.25) BSW inflow results to a stronger southwestard current with water of BSW origin towards Thermaikos Gulf and Sporades Islands (Fig. 33).

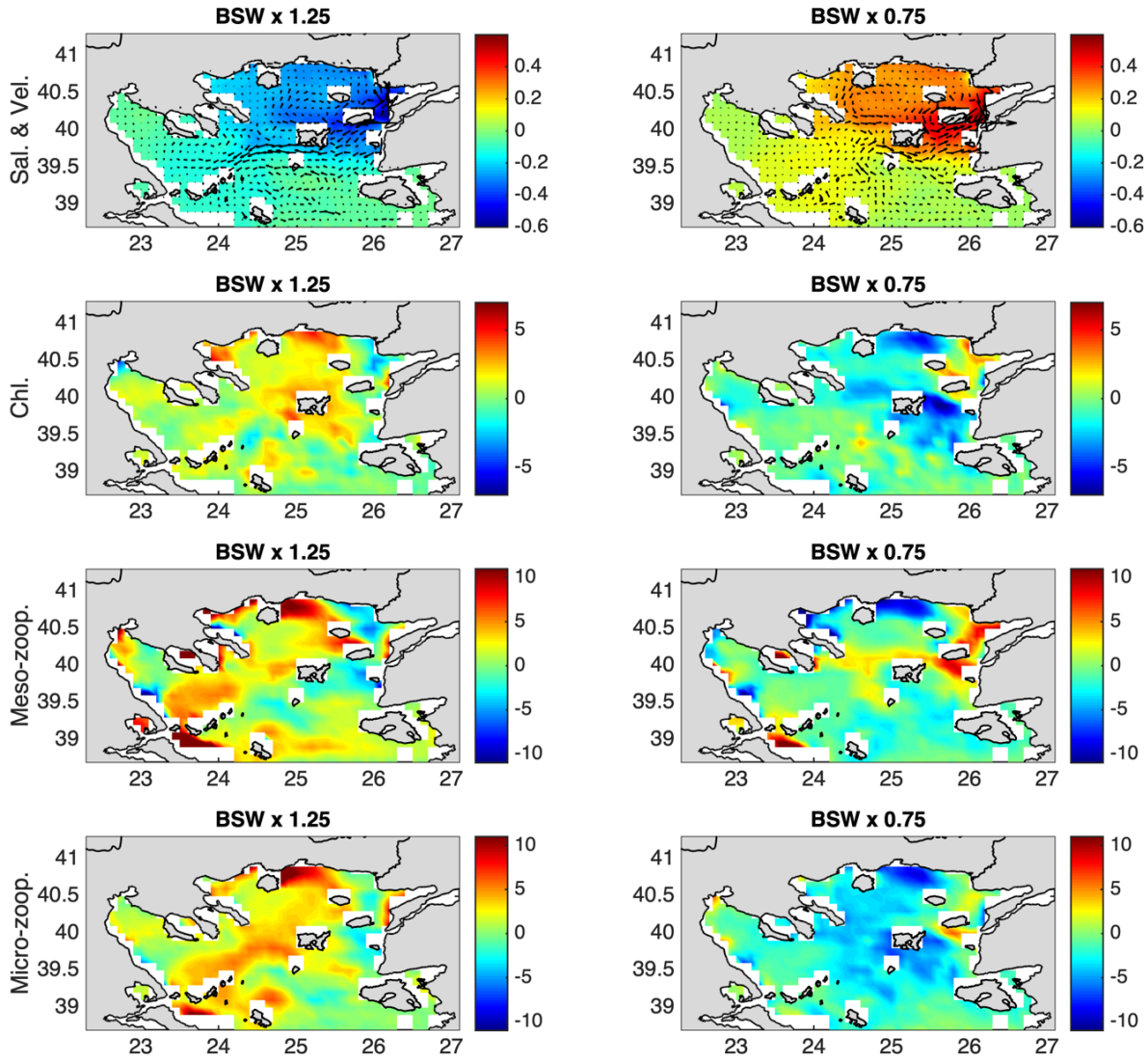

Figure 33 Model simulated surface salinity (psu) and surface velocity (m/sec) differences and chlorophyll, meso & micro-zooplankton biomass fractional changes (%) of the simulation experiments with increased (left) and decreased (right) BSW discharge, over the reference simulation.

In the increased BSW inflow scenario, the enhanced input of inorganic nutrients and organic matter triggers an increase of primary production, leading to a corresponding increase of micro and meso-zooplankton concentrations (Table 7). The opposite is observed in the reduced BSW inflow simulation experiment. However, despite the increased

zooplankton concentration in the increased BSW inflow scenario, anchovy biomass decreases (-9%), while in the reduced BSW scenario, anchovy biomass remains about the same (-0.2%). On the other hand, sardine biomass seems to be mainly regulated by resource competition with anchovy, showing an increase in both cases.

Table 7. Ecological variables and fish biomass fractional changes over the reference simulation for the two BSW scenarios.

	BSW x 1.25	**BSW x 0.75**
Nitrates	+0.9%	-1.1%
Phosphates	0%	0%
Chlorophyll	+1.5%	-1.5%
Microzooplankton	+2.9%	-3.2%
Mesozooplankton	+2.3%	-0.8%
Anchovy biomass (kt)	53.8 (-9%)	58 (-0.2%)
Sardine biomass (kt)	21.5 (+13%)	20.5 (+8%)

This discrepancy in anchovy and sardine simulated biomass is caused by the amplification of the southwestward current due to the increased BSW flow that occurs during Autumn, Summer and especially during Spring (Table 8), as the low-salinity BSW discharge is a major circulation forcing mechanism for the entire N. Aegean (Olson *et al.,* 2007). This augmented circulation during the peak of the anchovy spawning season, drifts anchovy eggs away from the spawning grounds, thus significantly affecting reproduction and consequently the species biomass. During winter, the speed of the current does not significantly change and sardine eggs remain unaffected.

Table 8. Surface current velocity fractional changes over the reference simulation for the two BSW scenarios.

	BSW x 1.25	**BSW x 0.75**
Winter	-0.9%	-2%
Spring	+7.7%	-1%
Summer	+4.3%	-5.7%
Autumn	+3.2%	-5%

In conclusion, in the reduced BSW outflow scenario, anchovy and sardine biomass slightly deviate from the reference biomass, while in the increased BSW outflow experiment, sardine is benefited by the decrease in anchovy biomass due to the elevated surface velocities that carry anchovy eggs away from the favorable spawning grounds.

6. Discussion

The one-dimensional full life cycle IBM model developed and evaluated in this study describes the population dynamics of two species. It includes all processes necessary to simulate growth, egg production and population dynamics and it is two-way coupled with the LTL model. It should be noted here that, in non-upwelling systems like the North Aegean Sea, in which a strong vertical heterogeneity in temperature and zooplankton develops during the thermally stratified period, it is important to incorporate a diel vertical migration (DVM) behavior in the fish model because temperature and food availability, and consequently consumption and metabolic rates, will change between day and night. In our region anchovy and sardine have a very similar DVM with fish moving above the thermocline during the night and below it, during the day (Giannoulaki *et al.,* 1999; Tsagarakis *et al.,* 2012). The simple vertical migration algorithm developed in Politikos*,* (2015) and also used here, accounts for the consequences of DVM behavior on consumption and respiration due to thermal stratification and the formation of deep chlorophyll/zooplankton maxima.

In developing the model for sardine we started with the already existing parameterization for anchovy (Politikos *et al,* [2011, 2015]), changing only those parameters that are known to differ between the two species, i.e. the length-weight relationships, the length ranges of early life stages and number of age classes, but most importantly, their reproductive characteristics, i.e. spawning period, fecundity and egg size. The genetic algorithm applied to tune the bioenergetics model resulted in simulating growth trajectories that were very close to size-at-age data from the field.

Genetic algorithms have previously been applied by Huse and Giske, (1998) and Okunishi, (2009) for tuning the weights of an artificial neural network used for habitat choice, energy allocation and spawning strategy/spawning migration, respectively. In our study, tuning the bioenergetics model involved the adjustment of the half saturation parameters so that the simulated fish growth matched the mean size-at-age data estimated from field samples. This computationally demanding process was effectively tackled by a heuristic optimization technique based on a genetic algorithm. The deployed algorithm minimizes the execution time and produces solutions close to optimal (i.e. if not the overall best from all feasible solutions, it finds one very close to the best). Our experimentation showed that the best tuning is achieved, when applying the process sequentially from the younger to older stage/age rather than when concurrently considering all stages/ages, which can be attributed to the dependence of each life stage on previous growth history. The deployed method was very effective and accurate and depending on available hardware, it could be applied to tune more fish processes such as population parameters and temperature dependence.

When calibrating parameters, such as the half saturation constants, one assumes that food consumption is adapted to local prey availability (Huret *et al.,* 2019). Given the similarity of the two species in the North Aegean Sea, e.g. the similar lengths-/weights-at-age (Figure 14), as well as the lack of information on how temperature affects their energetic rates, we adopted the same parameterization for temperature dependences, except for the optimum temperatures for food consumption, which were stage specific and were assumed to be close to the average temperature of the larval, juvenile and adult habitats (Peck *et al.,* 2013). In this logic, the major difference between the two species was that the optimum temperature for consumption was lower in sardine larvae (that grow in winter-spring) and higher for anchovy larvae (that grow in summer). This is somewhat consistent with the 'optimal growth

temperature hypothesis': Takasuka, (2007) demonstrated that the larvae of anchovy and sardine have different temperature optima for growth in the NW Pacific, which might be an explanation for the anchovy and sardine population alternations in this region.

Field data on somatic condition showed that both anchovy and sardine increase their energy reserves from winter to early summer, when the simulated mesozooplankton concentration is also increasing (Figure 12). However, from mid-summer onwards, somatic condition declines sharply, lagging the modelled mesozooplankton decline by approximately one month. This finding was unexpected. Several other sardine stocks have been shown to increase their condition all along the summer months, exhibiting maximum condition and lipid storage prior to the onset of gonadal maturation in autumn (Ganias *et al.,* 2014; Somarakis *et al.,* 2019, and references therein). These sardine stocks are mostly capital breeders using primarily stored energy to produce eggs (Somarakis *et al.,* 2019). In contrast, both the observed seasonal variation of somatic condition and the calculation of the capital index from the model simulation suggest that the sardine stock in the North Aegean Sea is closer to the income breeding mode. On the contrary, anchovy, which starts to spawn in a period of increased zooplankton concentration and continues to release eggs in the subsequent period of maximal surface temperatures/sharply decreasing food availability, is primarily a capital breeder. This can be attributed to the peculiar pelagic production cycle and stressful summer temperatures in the oligotrophic Aegean Sea, where the first half of the year (winter-spring) is the period of increasing zooplankton concentration, in contrast to other ecosystems like those inhabited by the Atlantic anchovy and sardine stocks in which the zooplankton concentration is high in spring-summer and very low in the autumn-winter period (Huret *et al.,* 2019). Indeed, in the Bay of Biscay, European anchovy is primarily income whereas European sardine, capital breeder (Gatti *et al.,* 2017). The indications that the North

Aegean Sea anchovy is mostly capital breeder contradict an earlier suggestion, based on data from the early 90's, that it is income breeder (Somarakis, 2005). Recent papers suggest that the period of maximal SPF energy storage in the Mediterranean has changed in recent years (from autumn to early summer) probably reflecting a change in the phenology of plankton production (Brosset *et al.,* [2015, 2017]). As shown by the modelling study of Gatti*,* (2017), and supported by a review paper on fish breeding patterns (McBride *et al.,* 2015), the capital-income mode can be plastic in many species; fish can move along the capital-income breeding continuum, in response to their physiological condition and the match-mismatch between the production of food and the production of eggs.

The energy allocation and reproduction algorithm developed, resulted in spawning periods that were consistent with observed spawning periods of the two species in the Eastern Mediterranean (Ganias *et al.,* 2007; Somarakis *et al.,* 2014, 2019). In both anchovy and sardine, the onset of the spawning period is determined by its SST threshold. The end of spawning simply results from the exhaustion of reserves from the reproductive buffer and energy intake insufficient to meet the needs of maintenance towards the end of summer. It should be noted here that because the model is 1-D, temperature or other thresholds imposed concurrently to all SIs result in the abrupt starting and ending of spawning periods. The simulated egg production highlighted that sardine age-1 (recruit spawners) start to spawn later than repeat spawners (age 2+) and have a shorter spawning period. This is well documented for sardine in the Eastern Mediterranean (Ganias *et al.,* 2007) and elsewhere (Ganias *et al.,* 2014 and references therein), but has never been reported for anchovy in the Eastern Mediterranean, nor resulted from the model simulations. This difference can be explained from the contrasted trophic conditions that anchovy and sardine experience before the onset of their first spawning period, i.e. high food concentration in spring vs low in autumn

and the subsequent delay in reaching the size at maturity and acquiring energy for reproduction in sardine, but not in anchovy.

The current application assumes that the fraction of energy allocated to reproduction is equal to the fraction allocated to growth. This choice was considered reasonable given the lack of information on energy allocation. Furthermore, there is some evidence that the fraction k is plastic: Tank experiments in Japanese anchovy have demonstrated that energy allocation to reproduction versus growth changes depending on per capita food availability (Tsuruta and Hirose, 1989).

A 1-D fish model is also particularly useful in testing simple management scenarios, especially when spatially explicit fisheries data (e.g. catches, fishing effort) are scant or unreliable, as is the case for Greek and most other Mediterranean stocks (Damalas, 2017). Testing management options with coupled full life cycle models is attractive because the bottom-up control of population fluctuations is directly taken into consideration.

The current model formulation assumed that the diet of the two species is alike. This assumption is supported by recent trophodynamic studies showing that, in contrast to upwelling systems, the daily ration and diet composition of anchovy and sardine in the N. Aegean Sea are remarkably similar (Nikolioudakis *et al.,* [2011, 2012, 2014]). Although adult sardines ingest phytoplankton as well, the contribution of phytoplankton to dietary carbon is negligible (Costalago and Palomera 2014; Nikolioudakis *et al.,* 2012) and copepods are the main energy source for both species (Nikolioudakis *et al.,* 2014). Despite the high diet overlap and, consequently, food competition between anchovy and sardine in the N. Aegean Sea, the simulations with varying fishing mortalities showed that the biomass of each species was insensitive to changes in the biomass of the other species caused by changes in its exploitation rate. This implies that the simulated mesozooplankton concentration suffices to support the

populations of the two species with no obvious trophic competition. Interestingly, what could be seen from the two-species simulations and the two-way coupling of the fish with the lower trophic level model was the top-down control of mesozooplankton by anchovy and sardine. The combined fishing rates on the two species affected the concentration of mesozooplankton, with sustainable exploitations leading to the decrease of mesozooplankton and unsustainable exploitations to its increase. This can eventually have implications for the pelagic ecosystem and fishery in the area. Removal of small pelagic fish may open up ecological space for other species competing with small pelagics for the same zooplankton prey such as jellyfish (Richardson *et al.,* 2009). For example, in the Benguela system, off the coast of Namibia, overfishing of the sardine stocks in the 60s and 70s led to the outbreak of jellyfish such as *Chrysaora* (Lynam *et al.,* 2006). Episodes of anchovy *Engraulis encrasicolus* collapse and ctenophore *Mnemiopsis leidyi* explosion occurred in the Black Sea and the Caspian Sea (Shiganova 1998; Daskalov *et al.,* 2007).

Testing the effect of timing of the 2.5-month closed period highlighted that the most effective timing for both species is the recruitment period which, however, is different for anchovy (spring) and sardine (autumn). The simulations showed that protecting the numerically dominant recruits prior and/or during the initial phase of their first spawning season contributes to the increase in population fecundity and subsequently the increase in population biomass. The current timing of the fishing ban (15 December-February) seems to be more suitable (although not optimal) for sardine and less effective for anchovy. The periods 15 February-April or 15 March-May seems to be the most beneficial for anchovy.

It should be noted here that our simulations were based on fixed natural mortality rates and averaged environmental conditions. However, natural mortalities can vary greatly in time and space in relation to a variety of ecological factors, such as water temperature, fish

condition and size of prey and predator stocks. Such variability as well as inter-annual variability in environmental conditions were not considered in this study and the results of the analyses represent average conditions.

Summarizing, the 1D anchovy-sardine IBM developed and calibrated in this study reproduced well the main characteristics of the two stocks in the N. Aegean Sea. The model was useful in assessing the breeding pattern of the stocks as well as the outcomes of simple management measures.

The next step included the development of a three-dimensional IBM model, describing the full life cycle of anchovy and sardine in the North Aegean Sea. This was also two-way coupled to a 3-D lower trophic model, providing the prey (microzooplankton, mesozooplankton) and physical properties (temperature, currents) of the fish habitat.

The anchovy and sardine simulated growth, biomass and spatial distribution were once again validated against available data over the 2000-2009 period, showing a reasonable agreement. More thoroughly, the somatic growth evolution was found within the range of field data, both in terms of larval lengths and juvenile/adult weights. The evolution of modelled anchovy biomass yields the interannual variability during the reference period, while that of sardine is very stable and does not project the biomass increase (although with very high uncertainty) during the years 2006 and 2008. The two species biomass spatial distribution was also in relatively good agreement with data from acoustic surveys, showing high concentrations in the more productive river influenced coastal areas (Thermaikos and Strymonikos Gulf, Thracean Sea) and along the pathway of BSW (Limnos island and Sporades). The main model deviation from the data was the underestimation of the observed population in the vicinity of BSW discharge (east of Limnos Isl.), probably due to an overestimation of currents that result in the off-shore advection of fish eggs/larvae and/or an underestimation

of mesozooplankton carried by BSW that is not adopted in the model. The simulated anchovy egg abundance was in general agreement with data (not available for sardine), being slightly overestimated in Thermaikos Gulf, following an overestimation of the adult population and the increased egg retention due to weaker circulation, as compared to the more exposed Thracean Sea.

This time, sensitivity experiments revealed an important effect of resource competition, with both anchovy and sardine reaching a similar biomass in single-species simulations. This contradicts the findings from the one-dimensional setup, where simulated zooplanktonic concentration seemed to cover the demands of both populations. We now believe that the spatially variable distribution of the food and the predators caused trophic competition that is not shown in a horizontally averaged simulation. In other words the three-dimensional setup better resembles the actual conditions and differ from a homogenous state.

The dominance of anchovy, in the two-species reference simulation (even when initial biomasses are inverted), given the very similar adopted mortalities, may be attributed to its increased larval growth during summer-autumn, as compared to the reduced growth of sardine larvae during winter-spring period. Higher larval growth rate of anchovy leads to reduced cumulative larval mortalities and a corresponding increased species population, as compared to sardine that appears to be strongly benefited from an anchovy retreat.

In the context of the expected global warming, the impact of increasing temperature on the fish metabolism and resulting biomasses of the two species was investigated with a series of sensitivity experiments. Single-species simulations showed that both species are negatively affected by the increasing temperature, with anchovy biomass being more drastically reduced due to the higher summer energetic demands for both adults (deteriorated somatic condition

and thus egg production) and larvae (growth). This is not the case for sardine that spawns during winter, in an already elevated somatic condition and thus is more affected by the larval stages. In the two-species simulations, sardine appears to benefit from an anchovy biomass decrease due to resource competition, showing a slight increase with temperature.

Finally, the impact of climate change on the two-species biomass was investigated with two simulations, adopting present (1980-2000) and future (2080-2100) climatic conditions under the IPCC-A1B scenario. An increase of sea surface temperature (+1.12^{o}C on average) was simulated in the future climate scenario, combined with a slight increase (+0.09 psu on average) of salinity, resulting in an overall increase of stratification. This resulted in a reduction of zooplankton biomass (-6.5% on average). The temperature increase and reduction of food resources resulted in a significant anchovy biomass decrease (-57%), while sardine biomass was increased by 33%. This different response is partly attributed to resource competition, as sardine benefits from anchovy biomass reduction. Single-species simulations showed that both species biomasses are expected to decline, with sardine showing a slightly smaller reduction. The reason for that, lies in the stronger temperature increase and zooplankton reduction, during the anchovy egg production and larval growth period, as compared to the rest of the year. Therefore the pressure on anchovy is greater, for both the adults (spawning period) and the early stages (growth reduction with increasing temperature), a phenomenon that with the addition of the resources competition (when the two species coexist), leads to a sardine predominance, in the two species experiment.

Changes similar to the above, like temperature increase and zooplankton changes, were described by Hermann, 2014 and Hidalgo, 2018, in their works for the Mediterranean Sea and concluded that these will result in an overall species decline. More specifically they

speculate a positive effect on winter-spawning species like sardine, against competitive summer spawning species like anchovy.

All scenarios with changing river inputs, lead to a nutrient reduction with consequences in the primary and secondary production in the area (excluding Thermaikos Bay). Both species biomasses were reduced as a result of the reduced egg production and early life stages survival. Anchovy is the dominant species in terms of abundance and was the most affected, while sardine was favored from the reduced resource competition.

Changes in the Black Sea Water inflow from the Dardanelles Straight showed that a reduction would cause small deviations of populations, while an increase would trigger biomass alterations. Elevated surface velocities seem to drift anchovy eggs away from the spawning grounds, resulting to a species biomass drop that instead benefits sardine through resources competition.

Towards a more sustainable exploitation of both species, the effects of potential alterations on the closed fishing period were studied and exhibited that in general both species benefit when not fished before or during the onset of their spawning periods. Anchovy biomass increases when adults are in elevated somatic growth (March-April) and sardine is favored when not fished during September and October, i.e. the period of adult recruitment.

The effort towards more sustainable fishing efforts lead to the investigation of its effect in specific fishing ground subdomains. Results showed that when species are not fished in coastal areas (sea bottom depth < 50m), both species are benefited since this area gathers a major part of the spawning activity. Another interesting result was the increase in total sardine catches despite the lack of fishing activity in the Thracean Sea. This resulted from the

local biomass increase, causing an egg production boost that due to the westward circulation (sardine is more spatially spread than anchovy), elevated the total sardine biomass.

Future work will be more expanded, incorporating the entire Mediterranean and the Black Seas. For this cause, different parameterization of the species for each respective area of abundance will be required. Differences between the Eastern and Western part of the Mediterranean will be studied and connections to world indexes (AMO, NAO) will be investigated.

The addition of more species, including predators of anchovy and sardine, will assist to a deeper study of trophic interactions. Also, species performing lessepsian migration are considered a danger to the Mediterranean Sea ecosystem. Their study through the integration in the multispecies model, could assist in focused actions towards controlling their spread.

Last, the future incorporation of a more spatially resolved and proportional to the local population fishing activity, by incorporating socioeconomic data, is another step towards the realization of a true end to end model.

7. References

1. Adloff, F., Somot, S., Sevault, F., Jordà, G., Aznar, R., Déqué, M., Herrmann, M. *et al.,* 2015. Mediterranean Sea response to climate change in an ensemble of twenty first century scenarios. Climate Dynamics, 45(9–10): 2775–2802. (also available at https://doi. org/10.1007/s00382-015-2507-3).

2. Agostini, V. and Bakun, A., 2002. `Ocean triads' in the Mediterranean Sea: physical mechanisms potentially structuring reproductive habitat suitability (with example application to European anchovy, Engraulisencrasicolus). Fisheries Oceanography, 11(3), pp.129-142.

3. Alheit, J., Roy, C., & Kifani, S. (2009). Decadal-scale variability in populations. In D. Checkley, J. Alheit, Y. Oozeki, & C. Roy (Eds.), Climate Change and Small Pelagic Fish (pp. 64-87). Cambridge: Cambridge University Press. doi:10.1017/CBO9780511596681.007

4. Allen, J.I., Somerfield, P.J., Siddorn, J., 2002. Primary and bacterial production in the Mediterranean Sea: a modelling study. J. Mar. Syst. 33/34, 473–495.

5. Alvarez P., Chifflet M. 2012. The fate of eggs and larvae of three pelagic species, mackerel (Scomber scombrus), horse mackerel (Trachurus trachurus) and sardine (Sardina pilchardus) in relation to prevailing currents in the Bay of Biscay: Could they affect larval survival? Sci. Mar. 76: 573–586.

6. Alvarez-Berastegui, D., Hidalgo, M., Tugores, M.P., Reglero, P., Aparicio-González, A., Ciannelli, L., Juza, M. *et al.,* 2016. Pelagic seascape ecology for operational fisheries oceanography: modelling and predicting spawning distribution of Atlantic bluefin tuna in Western Mediterranean. ICES Journal of Marine Science, 73(7): 1851–1862. (also available at https://doi.org/10.1093/icesjms/fsw041).

7. Androulidakis, Y. and Kourafalou, V., 2011. Evolution of a buoyant outflow in the presence of complex topography: The Dardanelles plume (North Aegean Sea). Journal of Geophysical Research, 116(C4).

8. Antonakakis, K., Giannoulaki, M., Machias, A., Somarakis, S., Sanchez, S., Ibaibarriaga, L. *et al.,* (2011). Assessment of the sardine (SardinapilchardusWalbaum, 1792) fishery in the eastern Mediterranean basin (North Aegean Sea). Mediterranean Marine Science, 12(2), p.333.

9. Arakawa, 1972. Design of the UCLA general circulation model. Numerical integration of weather and climate. University of California, Dept. of Meteorology, Rep. 7, 116 pp

10. Bakun A., Babcock E.A., Lluch-Cota S.E., Santora C., Salvadeo C.J. 2010. Issues of ecosystem-based management of forage fisheries in ‘‘open’’ non-stationary ecosystems: the example of the sardine fishery in the Gulf of California. Rev Fish Biol Fisheries 20: 9–29.

11. Baretta, J.W., W. Ebenhoh and P. Ruardij (1995), The European regional seas ecosystem model, a complex marine ecosystem model, Netherlands Journal of Sea Research, 33, 233-246.

12. Benedetti, F., Guilhaumon, F., Adloff, F. & Ayata, S.D. 2017. Investigating uncertainties in zooplankton composition shifts under climate change scenarios in the Mediterranean Sea. Ecography, 41(2): 345–360. (also available at https://doi.org/10.1111/ecog.02434).

13. Blackford, J.J., Burkill, P.P.P., 2002. Planktonic community structure and carbon cycling in the Arabian Sea as a result of monsoonal forcing: the application of a generic model. J. Mar. Syst. 3, 239–267. http://dx.doi.org/10.1016/S0924-7963(02)00182-3

14. Blumberg, A.F. and Mellor, G.L., (1983), Diagnostic and prognostic numerical circulation studies of the South Atlantic Bight. J. Geophys. Res., 88(C8), 4579-4592.

15. Broekhuizen N, Haeth MR, Hay SJ, Gurney WSC, 1995. Modelling the dynamics of the North Seas mesozooplankton. Netherlands Journal of Sea Research 33, 381-406.

16. Brosset, P., Ménard, F., Fromentin, J., Bonhommeau, S., Ulses, C., Bourdeix, J., *et al.,* (2015). Influence of environmental variability and age on the body condition of small pelagic fish in the Gulf of Lions. Marine Ecology Progress Series, 529: 219-231.

17. Brosset, P., Fromentin, J., Van Beveren, E., Lloret, J., Marques, V., Basilone, *et al.,* (2017). Spatio-temporal patterns and environmental controls of small pelagic fish body condition from contrasted Mediterranean areas. Progress in Oceanography, 151: 149-162.

18. Catalan, I. *et al.,* 2010. Growth and feeding patterns of European anchovy (Engraulis encrasicolus) early life stages in the Aegean Sea (NE Mediterranean). ESTUARINE COASTAL AND SHELF SCIENCE, 86(2), pp.299-312.

19. Checkley, D., Asch, R. and Rykaczewski, R., 2017. Climate, Anchovy, and Sardine. Annual Review of Marine Science, 9(1), pp.469-493.

20. Checkley Jr., DM, Bakun A, Barange M, Castro LR, Freon P, Guevara R, Herrick Jr. SF, McCall AD, Ommer R, Oozeki Y, Roy C, Shannon L, Van der Lingen CD. 2009. Synthesis and perspective. Climate change and small pelagic fish. (Checkley Jr. DM, Alheit J, Oozeki Y, Roy C, Eds.).:344-351., Cambridge, UK; New York: Cambridge University Press

21. Christensen, J H; Bøssing Christensen, O; Lopez, P; van Meijgaard, E; and Botzet, M (1996): The HIRHAM4 Regional Atmospheric Climate Model. Scientific Report 96-4, Danish Meteorological Institute.

22. Chust, G., Allen, J. I., Bopp, L., Schrum, C., Holt, J., Tsiaras, K., Zavatarelli, M., Chifflet, M., Cannaby, H., Dadou, I., Daewel, U., Wakelin, S. L., Machu, E., Pushpadas, D., Butenschon, M., Ar- tioli, Y., Petihakis, G., Smith, C., Garaçon, V., Goubanova, K., Le Vu, B., Fach, B. A., Salihoglu, B., Clementi, E., and Irigoien, X.: Biomass changes and trophic amplification of plankton in a warmer ocean, Global Change Biol., 20, 2124– 2139, doi:10.1111/gcb.12562, 2014.

23. Collingridge, K., 2012. Modelling risk areas in the North Sea for blooms of the invasive comb jellyfish Mnemiopsis Leidyi. CEFAS Summer Proj. 9, 21–36.

24. Costalago, D., Palomera, I. (2014). Feeding of European pilchard (Sardina pilchardus) in the northwestern Mediterranean: from late larvae to adults. Scientia Marina 78: 41-54.

25. Courant, R.;Friedrichs, K.;Lewy, H. (March 1967), 1928.On the partial difference equations of mathematical physics, IBM Journal of Research and Development, 11 (2): 215–234

26. Daewel, U., Peck, M.A., Kuhn, W., St John, M.A., Alekseeva, I., Schrum, C., 2008. Coupling ecosystem and individual-based models to simulate the influence of environmental variability on potential growth and survival of larval sprat (Sprattus sprattus L.) in the North Sea. Fisheries Oceanography 17, 333–351.

27. Daewel, Ute, Peck, Myron A. & Schrum, Corinna, 2011. Life history strategy and impacts of environmental variability on early life stages of two marine fishes in the North Sea: an individual-based modelling approach. Canadian Journal of Fisheries and Aquatic Sciences, 68(3), pp.426-443.

28. Damalas D. 2017. A brief reflection on the Mediterranean fisheries: bad news, good news and no news. Journal of Fisheries Research 1: 27-30.

29. Daskalov, G., Mamedov, E. (2007). Integrated fisheries assessment and possible causes for the collapse of anchovy kilka in the Caspian Sea. ICES Journal of Marine Science, 64: 503-511.

30. Drakopoulos, P., Lascaratos, A., 1997. Modelling the Mediterranean sea: climatological forcing. J. Mar. Syst. 20, 157–173

31. Elkalay, K., Khalil, K., Thomas, H., Bozec, Y., Ruardij, P., Baar, H. De, 2012. Biogeochemical 1D ERSEM ecosystem model applied to recent carbon dioxide and nutrient

data in the North Sea. Developments in Environmental Modelling, pp. 275–294 http://dx.doi.org/10.1016/B978-0-444-59396-2.00017-1.

32. Fennel, W., 2010. A nutrient to fish model for the example of the Baltic Sea. JOURNAL OF MARINE SYSTEMS, 81(1-2), pp.184-195.

33. Frangoulis, C., Psarra, S., Zervakis, V., Meador, T., Mara, P., Gogou, A., Zervoudaki, S., Giannakourou, A., Pitta, P., Lagaria, A., Krasakopoulou, E., Siokou-Frangou, I., 2010. Connecting export fluxes to plankton food-web efficiency in the Black Sea waters inflowing into the Mediterranean Sea. J. Plankton Res. 32, 1203–1216.

34. Ganias, K., Somarakis, S., Nunes, C., 2014. Reproductive potential. In: Biology and Ecology of Sardines and Anchovies. CRC Press, Taylor & Francis Group, Boca Raton, pp. 79–121.

35. Ganias, K., Somarakis, S., Koutsikopoulos, C. and Machias, A. (2007). Factors affecting the spawning period of sardine in two highly oligotrophic Seas. Marine Biology 151: 1559-1569.

36. Garcia, A. & Palomera, I., 1996. Anchovy early life history and its relation to its surrounding environment in the Western Mediterranean basin. SCIENTIA MARINA, 60, pp.155-166.

37. Gatti, P., Petitgas, P. and Huret, M. (2017). Comparing biological traits of anchovy and sardine in the Bay of Biscay: A modelling approach with the Dynamic Energy Budget. Ecological Modelling, 348: 93-109.

38. Giannoulaki, M., Machias, A., Tsimenides, N. (1999). Ambient luminance and vertical migration of the sardine Sardina pilchardus. Marine Ecology Progress Series, 178, pp.29-38.

39. Giannoulaki M, Machias A, Somarakis S, Tsimenides N (2005). The spatial distribution of anchovy and sardine in the northern Aegean Sea in relation to hydrographic regimes. Belgian Journal of Zoology 135 (2), 151.

40. Giannoulaki M., Valavanis V.D., Palialexis A., Tsagarakis K., Machias A., Somarakis S., Papaconstantinou C. (2008) Modelling the presence of anchovy Engraulis encrasicolus in the Aegean sea during early summer, based on satellite environmental data. Hydrobiologia 612: 225- 240.

41. Giannoulaki M., Ibaibarriaga L., Antonakakis K., Uriarte A., Machias A., Somarakis S., *et al.,* 2014. Applying a two-stage Bayesian dynamic model to a short-lived species, the anchovy in the Aegean Sea (Eastern Mediterranean): Comparison with an integrated catch at age stock assessment model. Mediterranean Marine Science 15: 350-365

42. Gkanasos, A., Somarakis, S., Tsiaras, K., Kleftogiannis, D., Giannoulaki, M., Schismenou, E., Sofianos, S. and Triantafyllou, G., 2019. Development, application and evaluation of a 1-D full life cycle anchovy and sardine model for the North Aegean Sea (Eastern Mediterranean). PLOS ONE, 14(8), p.e0219671.

43. Gualdi, S. *et al.,* (2007) Changes in tropical cyclone activity due to global warming: results from a high-resolution coupled general circulation model. Journal of Climate 21, 5204-5228.

44. Herrmann, M., Estournel, C., Adloff, F. & Diaz, F. Impact of climate change on the western Mediterranean Sea pelagic planktonic ecosystem and associated carbon cycle. J. Geophys. Res. 119, 5815–5836 (2014).

45. Hidalgo, M., Mihneva, V., Vasconcellos, M., & Bernal, M. (2018). Climate change impacts, vulnerabilities and adaptations: Mediterranean Sea and the Black Sea marine fisheries. In M. Barange, T. Bahri, M. C. Beveridge, K. Cochrane, S. Funge-Smith & F. Poulain (Eds.), Impacts of Climate Change on Fisheries and Aquaculture: Synthesis of Current Knowledge, Adaptation and Mitigation Options (pp. 139–159). Rome, Italy: FAO Fisheries and Aquaculture. Technical Paper No. 627, 628 Pp. FAO.

46. Horton, C., Clifford, M., Schmitz, J., Kantha, L.H., 1997. A real-time oceano-graphic nowcast/forecast system for the Mediterranean sea. J. Geophys. Res. 102 (C11), 25123–25156

47. Hunter JR, Macewicz B (1985) Measurement of spawning frequency in multiple spawning fishes. In: Lasker R (ed) An egg production method for estimating spawning biomass of pelagic fish: application to the northern anchovy, Engraulis mordax. NOAA Tech Rep NMFS 36:79–93

48. Huret, M., Petitgas, P., Woillez, M., 2010. Dispersal kernels and their drivers captured with a hydrodynamic model and spatial indices: A case study on anchovy (Engraulis encrasicolus) early life stages in the Bay of Biscay. Prog. Oceanogr. 87, 6–17.

49. Huret, M., Tsiaras, K., Daewel, U., Skogen, M.D., Gatti, P., Petitgas, P., *et al.,* 2019. Variation in life-history traits of European anchovy along a latitudinal gradient: a bioenergetics modelling approach. Marine Ecology Progress Series, 617-618: 95-112.

50. Huse, G. and Giske, J. (1998). Ecology in Mare Pentium: an individual-based spatio-temporal model for fish with adapted behaviour. Fisheries Research, 37: 163-178.

51. Huse, G. & Fiksen, O., 2010. Modelling encounter rates and distribution of mobile predators and prey. PROGRESS IN OCEANOGRAPHY, 84(1-2), pp.93-104.

52. Ito, S., Megrey, B., Kishi, M., Mukai, D., Kurita, Y., Ueno, Y., *et al.,* (2007). On the interannual variability of the growth of Pacific saury (Cololabis saira): A simple 3-box model using NEMURO.FISH. Ecological Modelling, 202: 174-183.

53. Ito, S., Rose, K., Megrey, B., Schweigert, J., Hay, D., Werner, F., *et al.,* (2015). Geographic variation in Pacific herring growth in response to regime shifts in the North Pacific Ocean. Progress in Oceanography, 138: 331-347.

54. Kalaroni, S., Tsiaras, K., Petihakis, G., Economou-Amilli, A. and Triantafyllou, G., 2020. Modelling the mediterranean pelagic ecosystem using the POSEIDON ecological model. Part II: Biological dynamics. Deep Sea Research Part II: Topical Studies in Oceanography, 171, p.104711.

55. Katara, I., Pierce, G., Illian, J. and Scott, B., 2011. Environmental drivers of the anchovy/sardine complex in the Eastern Mediterranean. Hydrobiologia, 670(1), pp.49-65.

56. Kitchell, J., Stewart, D. Weininger, D. (1977). Applications of a Bioenergetics Model to Yellow Perch (Perca flavescens) and Walleye (Stizostedion vitreum vitreum). Journal of the Fisheries Research Board of Canada, 34: 1922-1935.

57. Kleftogiannis, D., Theofilatos, K., Likothanassis, S. and Mavroudi, S. (2015). YamiPred: A Novel Evolutionary Method for Predicting Pre-miRNAs and Selecting Relevant Features. IEEE/ACM Transactions on Computational Biology and Bioinformatics, 12: 1183-1192.

58. Kooijman, S. (2010). Dynamic energy budget theory for metabolic organisation. Cambridge University Press. Cambridge

59. Korres, G., Lascaratos, A., 2003. An eddy resolving model of the Aegean and Levantine basins for the Mediterranean Forecasting System Pilot Project (MFSPP): implementation and climatological runs. Analles Geophysicae, MFSPP – Part I 21 (Special Issue), 205–220.

60. Kourafalou, V. H. & K. Tsiaras, 2007. A nested circulation model for the North Aegean Sea. Ocean Science 3: 1–16

61. Krom M, Herut B, Mantoura CFR (2004) Nutrient budget for the Eastern Mediterranean: implications for phosphorus limitation. Limnol Oceanogr 49:1582–1592

62. Lascaratos, A. and Nittis, K., 1998. A high-resolution three-dimensional study of intermediate water formation in the Levantine Sea, J. Geophys. Res., 103(C9), 18 497–18 511

63. Lehodey, P., Murtugudde, R. & Senina, I., 2010. Bridging the gap from ocean models to population dynamics of large marine predators: A model of mid-trophic functional groups. PROGRESS IN OCEANOGRAPHY, 84(1-2), pp.69-84.

64. Ludwig, W., .Dumont, E., Meybeck, M., Heussner, S., (2009) River discharges of water and nutrients to the Mediterranean and Black Sea: major drivers for ecosystem changes during past and future decades? Prog Oceanogr 80: 199–217

65. Ludwig, W., Bouwman, A.F., Dumont, E., Lespinas, F., 2010. Water and nutrient fluxes from major Mediterranean and Black Sea rivers: Past and future trends and their implications for the basin-scale budgets. Global Biogeochemical Cycles. doi: 10.1029/2009GB003594.

66. Lynam, C., Gibbons, M., Axelsen, B., Sparks, C., Coetzee, J., Heywood, B., et al (2006). Jellyfish overtake fish in a heavily fished ecosystem. Current Biology, 16: R492-R493.

67. Machias A, Tsimenides N (1995) Biological factors affecting the swimbladder volume of sardine (Sardina pilchardus). Marine Biology 123:59-867

68. Machias A., Stergiou K.I., Somarakis S., Karpouzi V.S., Kapantagakis A. (2008) Trends in trawl and purse seine catch rates in the north-eastern Mediterranean. Mediterranean Marine Science 9: 49-65

69. Macias, D.M., Garcia-Gorriz, E. & Stips, A. 2015. Productivity changes in the Mediterranean Sea for the twenty-first century in response to changes in the regional atmospheric forcing. Frontiers in Marine Science, 2: 79 [online]. [Cited 11 March 2018]. https://doi.org/10.3389/fmars.2015.00079

70. Mantzouni, I., Somarakis, S., Moutopoulos, D.K., Kallianiotis, A., Koutsikopoulos, C., 2007. Periodic, spatially structured matrix model for the study of anchovy (Engraulis encrasicolus) population dynamics in N Aegean Sea (E. Mediterranean). Ecological Modelling 208: 367–377.

71. McBride, R., Somarakis, S., Fitzhugh, G., Albert, A., Yaragina, N., Wuenschel, M., *et al.,* (2015). Energy acquisition and allocation to egg production in relation to fish reproductive strategies. Fish and Fisheries 16: 23-57.

72. Megrey, B., Rose, K., Klumb, R., Hay, D., Werner, F., Eslinger, D., *et al.,* (2007). A bioenergetics-based population dynamics model of Pacific herring (Clupea harengus pallasi) coupled to a lower trophic level nutrient–phytoplankton–zooplankton model: Description, calibration, and sensitivity analysis. Ecological Modelling, 202: 144-164.

73. Mellor, G. L. & T. Yamada, 1982. Development of a turbu- lence closure model for geophysical fluid problems. Review Geophysics and Space Physics 20: 851–875.

74. Morote, E. *et al.,* 2010. A comparison of anchovy (Engraulis encrasicolus) and sardine (Sardina pilchardus) larvae feeding in the Northwest Mediterranean: influence of prey availability and ontogeny. ICES Journal of Marine Science, 67(5), pp.897-908.

75. Nikolioudakis, N., Palomera, I., Machias, A. and Somarakis, S. (2011). Diel feeding intensity and daily ration of the sardine Sardina pilchardus. Marine Ecology Progress Series 437: 215-228.

76. Nikolioudakis, N., S. Isari, P. Pitta and S. Somarakis. 2012. Diet of sardine Sardina pilchardus: an 'end-to-end' field study. Mar. Ecol. Progr. Ser. 453: 173–188.

77. Nikolioudakis, N., Isari, S. and Somarakis, S. (2014). Trophodynamics of anchovy in a non-upwelling system: direct comparison with sardine. Marine Ecology Progress Series 500: 215-

78. Nittis, K., Perivoliotis, L., Korres, G., Tziavos, C., & Thanos, I., 2006. Operational monitoring and forecasting for marine environmental applications in the Aegean Sea. Environmental Modelling and Software, 21(2), 243–257.

79. Oguz, T., Salihoglu, B. and Fach, B. (2008). A coupled plankton–anchovy population dynamics model assessing nonlinear controls of anchovy and gelatinous biomass in the Black Sea. Marine Ecology Progress Series 369: 229-256.

80. Okunishi, T., Yamanaka, Y. and Ito, S. (2009). A simulation model for Japanese sardine (Sardinops melanostictus) migrations in the western North Pacific. Ecological Modelling 220: 462-479.

81. Olson, D., Kourafalou, V., Johns, W., Samuels, G. and Veneziani, M., 2007. Aegean Surface Circulation from a Satellite-Tracked Drifter Array. Journal of Physical Oceanography, 37(7), pp.1898-1917.

82. O'Reilly, J., Maritorena, S., Mitchell, B.G., Siegel, D., Carder, K.L., Garver, S., Kahru, M., McClain, C., 1998. Ocean color chlorophyll algorithms for SeaWiFS. J. Geophys. Res. 103 (24) 937–24,953.

83. Patterson, K. R., 1992. An improved method for studying the condition of fish, with an example using Pacific sardine Sardinops sagax (Jenyns). Journal of Fish Biology, 40: 821–831.

84. Pätsch, J., Radach, G., 1997. Long-term simulation of the eutrophication of the North Sea: temporal development of nutrients, chlorophyll and primary production in comparison to observations. J. Sea Res. 1101

85. Pecquerie, L., Petitgas, P. and Kooijman, S. (2009). Modeling fish growth and reproduction in the context of the Dynamic Energy Budget theory to predict environmental impact on anchovy spawning duration. Journal of Sea Research 62: 93-105.

86. Peck, M., Reglero, P., Takahashi, M. and Catalán, I. (2013). Life cycle ecophysiology of small pelagic fish and climate-driven changes in populations. Progress in Oceanography 116: 220-245.

87. Pethybridge, H., Roos, D., Loizeau, V., Pecquerie, L. and Bacher, C. (2013). Responses of European anchovy vital rates and population growth to environmental fluctuations: An individual-based modeling approach. Ecological Modelling 250: 370-383.

88. Petihakis, G., Triantafyllou, G., Koutsoubas, D., Allen, J.I., Dou- nas, C., 1999. Modelling the annual cycles of nutrients and primary production on a lagoon dynamical system. Marine Environmental Research 48, 37–48.

89. Petihakis, G., Triantafyllou, G., Allen, I.J., Hoteit, I., Dounas, C., 2002. Modelling the spatial and temporal variability of the Cretan Sea ecosystem. J. Mar. Syst. 36, 173–196. http://dx.doi.org/10.1016/S0924-7963(02)00186-0.

90. Petihakis, G., Drakopoulos, P., Nittis, C., Zervakis, V., Christodoulou, C., Tziavos, C., 2007. M3A system (2000–2005) — operation and maintenance. Ocean Sci. 3, 117–128. - 305 - http://dx.doi.org/10.5194/os-3-117-2007

91. Petihakis, G., Triantafyllou, G., Tsiaras, K., 2009. Eastern Mediterranean biogeochemical flux model—simulations of the pelagic ecosystem. Ocean Sci.

92. Petihakis, G., Triantafyllou, G., Korres, G., Tsiaras, K., Theodorou, A., Pollani, A., 2012. Ecosystem modelling: towards the development of a management tool for a marine coastal system part-II, ecosystem processes and biogeochemical fluxes. J. Mar. Syst. 94, S49–S64. http://dx.doi.org/10.1016/j.jmarsys.2011.11.006.

93. Petihakis, G., Tsiaras, K., Triantafyllou, G., Kalaroni, S., Pollani, A., 2014. Sensitivity of the N. Aegean Sea ecosystem to Black Sea water inputs. Mediterr. Mar. Sci. 790–804

94. Petihakis, G., Tsiaras, K., Triantafyllou, G., Kalaroni, S., Pollani, A., 2014. Sensitivity of the N. Aegean Sea ecosystem to Black Sea water inputs. Mediterr. Mar. Sci. 790–804

95. Pikitch, E., Boersma, P.D., Boyd, I.L., Conover, D.O., Cury, P., Essington, T., et al, 2012. Little fish, big impact: managing a crucial link in ocean food webs. In: Lenfest Ocean Program, Washington, DC, p. 108.

96. Plounevez, S. & Champalbert, G., 2000. Diet, feeding behaviour and trophic activity of the anchovy (Engraulis encrasicolus L.) in the Gulf of Lions (Mediterranean Sea). Oceanologica Acta, 23(2), pp.175-192.

97. Polat, C., Tugrul, S., 1996. Chemical exchange between the mediterranean and black sea via the Turkish straits, CIESM science series. Bull. Inst. Oceanogr. 2 (17), 167–186.

98. Politikos, D.V., Triantafyllou, G.N., Petihakis, G., Tsiaras, K., Somarakis, S., Ito, S-I., et al, 2011. Application of a bioenergetics growth model for European anchovy (Engraulis encrasicolus) linked with a lower trophic level ecosystem model. Hydrobiologia, 670, 141-164.

99. Politikos, D., Somarakis, S., Tsiaras, K.P., Giannoulaki, M., Petihakis, G., Machias, A., *et al.,* 2015. Simulating anchovy's full life cycle in the northern Aegean Sea (eastern Mediterranean): A coupled hydro-biogeochemical-IBM model. Progress in Oceanography, 138: 399-416.

100. Quinn II T.J., Deriso R.B. (1999) Quantitative Fish Dynamics. Oxford University Press, New York.

101. Proctor, R., Holt, J., Allen, J., Blackford, J., 2003. Nutrient fluxes and budgets for the North West European Shelf from a three-dimensional model. Sci. Total Environ. 314-316, 769–785. http://dx.doi.org/10.1016/S0048-9697(03)00083-4

102. Radach, G., & Lenhart, H. -J., 1995. Nutrient dynamics in the North Sea: Fluxes and budgets in the water column derived from ERSEM. Netherlands Journal of Sea Research, 33(3-4), 301–335.

103. Regner, S., 1996. Effects of environmental changes on early stages and reproduction of anchovy in the Adriatic Sea. SCIENTIA MARINA, 60, pp.167-177.

104. Rose K.A., F. Werner, B.A. Megrey, M.N. Aita, Y. Yamanaka and D. Hay (2007) Simulated herring growth responses in the Northeastern Pacific to historic temperature and zooplankton conditions generated by the 3-dimensional NEMURO nutrient-phytoplankton-zooplankton model. Ecological Modelling 202: 184-195.

105. Rose, K.A., Fiechter, J., Curchitser, E.N., Hedstrom, K., Bernal, M., Creekmore, S., *et al.,* 2015. Demonstration of a fully-coupled end-to-end model for small pelagic fish using sardine and anchovy in the California Current. Prog. Oceanogr. 138: 348–380.

106. Sánchez-Garrido, J., Werner, F., Fiechter, J., Rose, K., Curchitser, E., Ramos, A., García Lafuente, J., Arístegui, J., Hernández-León, S. and Rodríguez Santana, A., 2019. Decadal-scale variability of sardine and anchovy simulated with an end-to-end coupled model of the Canary Current ecosystem. Progress in Oceanography, 171, pp.212-230.

107. Sánchez-Garrido, J., Werner, F., Fiechter, J., Rose, K., Curchitser, E., Ramos, A., García Lafuente, J., Arístegui, J., Hernández-León, S. and Rodríguez Santana, A., 2019. Decadal-scale variability of sardine and anchovy simulated with an end-to-end coupled model of the Canary Current ecosystem. Progress in Oceanography, 171, pp.212-230.

108. Saraux, C., Van Beveren, E., Brosset, P., Queiros, Q., Bourdeix, J., Dutto, G., *et al.,* (2019). Small pelagic fish dynamics: A review of mechanisms in the Gulf of Lions. Deep Sea Research Part II: Topical Studies in Oceanography, 159: 52-61.

109. Scheffer, M., Baveco, J. M., DeAngelis, D. L., Rose, K. A., and van Nes, E. H. 1995. Super-individuals: a simple solution for modelling large populations on an individual basis. EcologicalModelling 80: 161 – 170.

110. Schismenou E., Palmer M., Giannoulaki M., Alvarez I., Tsiaras K., Triantafyllou G., *et al.,* 2016. Seasonal changes in otolith increment width trajectories and the effect of temperature on the daily growth rate of young sardines. Fisheries Oceanography, 25: 362–372.

111. Schismenou, E., 2012. Modern approaches in biology and ecology of reproduction and growth of anchovy (Engraulis encrasicolus) in the North Aegean Sea. PhD thesis, University of Crete, Greece.

112. Schismenou E., Tsiaras K., Kourepini M.I., Lefkaditou E., Triantafyllou G., Somarakis S. (2013) Seasonal changes in growth and condition of anchovy late larvae explained with a hydrodynamic-biogeochemical model simulation. Marine Ecology Progress Series 478: 197–209

113. Sempere, R., Panagiotopoulos, C., Lafont, R., Marroni, B., Van Wambeke, F., 2002.Total organic carbon dynamics in the Aegean Sea. Journal of Marine Systems, 33-34, 355-364.

114. Shiganova T. (1998). Invasion of the Black Sea by the ctenophore Mnemiopsis leidyi and recent changes in pelagic community structure. Fisheries Oceanography 7: 305-310.

115. Siokou-Frangou, I., Bianchi, M., Christaki, U., Christou, E.D., Giannakourou, A., Gotsis, O., Ignatiades, L., Pagou, K., Pitta, P., Psarra, S., Souvermezoglou, E., Van Wambeke, F., Zervakis, V., 2002. Carbon flow in the planktonic food web along a gradient of oligotrophy in the Aegean Sea (Mediterranean Sea). J. Mar. Syst. 33-34, 335–353.

116. Skliris N.; Sofianos S.; Gkanasos A.; Mantziafou A.; Vervatis V.; Axaopoulos P., *et al.,* Decadal scale variability of sea surface temperature in the Mediterranean Sea in relation to atmospheric variability. Ocean Dynamics 2012, 62, 13–30.

117. Skliris, N., Sofianos, S., Gkanasos, A., Axaopoulos, P., Mantziafou, A., Vervatis, V., 2011. Long-term sea surface temperature variability in the Aegean Sea. Adv. Oceanogr. Limnol. 2 (2), 125–139. https://doi.org/10.1080/19475721.2011.601325.

118. Skoulikidis, N.Th., 2009. The environmental state of rivers in the Balkans-A review within the DPSIR framework. Science of the Total Environment, 407, 2501-2516.

119. Smagorinsky, J., 1963. General circulation experiments with the primitive equations, i, the basic experiment. Mon. Weather Rev. 91, 99–164

120. Smith, S.V., Swaney, D.P., Talaue-McManus, L., Bartley, J.D., Sandhei, P.T., McLaughlin, C., Dupra, V.C., Crossland, C.J., Buddemeier, R.W., Maxwell, B.A., Wulff, F., 2003. Humans, hydrology and the distribution of inorganic nutrient loading to the ocean. Bioscience 53, 235–245.

121. Somarakis, S., Tsoukali, S., Giannoulaki, M., Schismenou, E., Nikolioudakis, N. 2019. Spawning stock, egg production and larval survival in relation to small pelagic fish recruitment. Marine Ecology Progress Series 617-618: 113-136.

122. Somarakis, S., Schismenou, E., Siapatis, A., Giannoulaki, M., Kallianiotis, A. and Machias, A. (2012). High variability in the Daily Egg Production Method parameters of an eastern Mediterranean anchovy stock: Influence of environmental factors, fish condition and population density. Fisheries Research, 117-118: 12-21.

123. Somarakis, S., N. Nikolioudakis, 2007. Oceanographic habitat, growth and mortality of larval anchovy (Engraulis encrasicolus) in the northern Aegean Sea (eastern Mediterranean). Marine Biology 152: 1143–1158.

124. Somarakis, S., Tsianis D.E., Machias A., Stergiou K.I. 2006. An overview of biological data related to anchovy and sardine stocks in Greek waters. In Palomares, M.L.D., K.I. Stergiou & D. Pauly (eds), Fishes in Database and Ecosystems Fisheries Centre Research Reports 14: 56–64. Fisheries Centre, University of British Columbia.

125. Somarakis, S., 2005. Marked inter-annual differences in reproductive parameters and daily egg production of anchovy in the northern Aegean Sea. Belg. J. Zool. 135, 247-252.

126. Somarakis S. 1999. Ichthyoplankton of the NE Aegean with emphasis on anchovy, Engraulis encrasicolus (Linnaeus, 1758) (June 1993, 1994, 1995, 1996). PhD thesis, University of Crete

127. Soufan, O., Kleftogiannis, D., Kalnis, P. and Bajic, V. (2015). DWFS: A Wrapper Feature Selection Tool Based on a Parallel Genetic Algorithm. PLOS ONE 10(2), p.e0117988.

128. STECF 2017. Scientific, Technical and Economic Committee for Fisheries. Mediterranean Stock Assessments 2017 part I (STECF-17-15). Publications Office of the European Union, Luxembourg, 2017, ISBN 978-92-79-67487-7, doi: 10.2760/897559, JRC109350

129. Stergiou, K., Somarakis, S., Triantafyllou, G., Tsiaras, K., Giannoulaki, M., Petihakis, G., Machias, A. and Tsikliras, A., 2016. Trends in productivity and biomass yields in the

Mediterranean Sea Large Marine Ecosystem during climate change. Environmental Development, 17, pp.57-74.

130. Takasuka, A., Oozeki, Y. and Aoki, I. (2007). Optimal growth temperature hypothesis: Why do anchovy flourish and sardine collapse or vice versa under the same ocean regime? Canadian Journal of Fisheries and Aquatic Sciences, 64: 768-776.

131. Takasuka, A., Yoneda, M. and Oozeki, Y., 2018. Density dependence in total egg production per spawner for marine fish. Fish and Fisheries, 20(1), pp.125-137.

132. Travers, M. & Shin, Y., 2010. Spatio-temporal variability in fish-induced predation mortality on plankton: A simulation approach using a coupled trophic model of the Benguela ecosystem. PROGRESS IN OCEANOGRAPHY, 84(1-2), pp.118-120.

133. Travers, M. *et al.,* 2009. Two-way coupling versus one-way forcing of plankton and fish models to predict ecosystem changes in the Benguela. Ecological Modelling, 220(21), pp.3089–3099.

134. Travers, M., Shin, Y.-J., Jennings, S., Cury, P., 2007. Towards end-to-end models for investigating the effects of climate and fishing in marine ecosystems. Progress in Oceanography 75, 751–770.

135. Triantafyllou, G., 2000. Temporal variations in benthic communities and their response to physicochemical forcing: a numerical approach. ICES J. Mar. Sci. 57, 1507–1516. doi:10.1006/jmsc.2000.0923

136. Triantafyllou, G., Hoteit, I., Petihakis, G., 2003. A singular evolutive interpolated Kalman filter for efficient data assimilation in a 3-D complex physical–biogeochemical model of the Cretan Sea. J. Mar. Syst. 40–41, 213–231. doi:10.1016/S0924-7963(03)00019-8

137. Triantafyllou, G., Yao, F., Petihakis, G., Tsiaras, K.P., Raitsos, D.E., Hoteit, I., 2014. Exploring the Red Sea seasonal ecosystem functioning using a three-dimensional biophysical model. J. Geophys. Res. Ocean. 119, 1791–1811. http://dx.doi.org/10.1002/2013JC009641.

138. Triantafyllou, G., Tsiaras, K., Petihakis, G., Politikos , D., Somarakis, S., Ito, S.-I., Megrey, B. and Pollani, A. 2010. Implementation and data assimilation on the 3D IBM for the European anchovy (Engraulis encrasicolus) in the north Aegean Sea (eastern Mediterranean). ICES CM 2010/L:14

139. Tsagarakis, K., Giannoulaki, M., Somarakis, S. and Machias, A. (2012). Variability in positional, energetic and morphometric descriptors of European anchovy Engraulis encrasicolus schools related to patterns of diurnal vertical migration. Marine Ecology Progress Series 446: 243-258.

140. Tsiaras, K., Kourafalou, V.H., Raitsos, D., Triantafyllou, G., Petihakis, G., Korres, G., 2012. Inter-annual productivity variability in the North Aegean Sea: influence of thermohaline circulation during the Eastern Mediterranean Transient. J. Mar. Syst. 96–97: 72–81.

141. Tsiaras, K., Petihakis G., Kourafalou, V., Triantafyllou G., 2014. Impact of the river nutrient load variability on the N. Aegean ecosystem functioning over the last decades. J. Sea Res. 86: 97-109.

142. Tsikliras A.C. 2007. Thermal threshold of the onset of maturation in clupeid fishes using quotient analysis. Rapport du Congrès de la Commission Internationale pour l'Exploration Scientifique de la Mer Méditerranée 38: 623.

143. Tsikliras, A., Dinouli, A., Tsiros, V. and Tsalkou, E. (2015). The Mediterranean and Black Sea Fisheries at Risk from Overexploitation. PLOS ONE, 10(3), p.e0121188.

144. Tsuruta, Y., Hirose, K., 1989. Internal regulation of reproduction in the Japanese anchovy (Engraulis japonica) as related to population fluctuation. In: Beamish, R.J., McFarlane, G.A. (Eds.), Effects of ocean variability on recruitment and an evaluation of parameters used in stock assessment models. Can. Spec. Publ. Fish. Aquat. Sci., NRC Research Press, vol. 108, pp. 111–119.

145. Tudela, S., Palomera, I. & Quilez, G., 2002. Feeding of anchovy Engraulis encrasicolus larvae in the north-west Mediterranean. JOURNAL OF THE MARINE BIOLOGICAL ASSOCIATION OF THE UNITED KINGDOM, 82(2), pp.349-350.

146. Tudela S, Palomera I, 1999. Potential e®ect of an anchovy-mediated pump on the vertical availability of nitrogen for primary production in the Catalan Sea (northwest Mediterranean). J. Sea Res. (42), 83-92.

147. Tudela, S. & Palomera, I., 1995. Diel feeding intensity and daily ration in the anchovy Engraulis encrasicolus in the northwest Mediterranean Sea during the spawning period. MARINE ECOLOGY-PROGRESS SERIES, 129(1-3), pp.55-61.

148. Tugrul, S., Besiktepe, S.T., Salihoglou, I., 2002. Nutrient exchange fluxes between the Aegean and Black seas through the marmara sea. Mediterr. Mar. Sci. 3, 33–42.

149. Tzanatos, E., Raitsos, D.E., Triantafyllou, G., Somarakis, S., Tsonis, A.A., 2014. Indications of a climate effect on Mediterranean fisheries. Clim. Change 122, 41-54.

150. Vasilakopoulos P, Maravelias CD, Tserpes G (2014) The alarming decline of Mediterranean fish stocks. Curr Biol 24: 1643−1648

151. VILIBIĆ, I., ČIKEŠ KEČ, V., ZORICA, B., ŠEPIĆ, J., MATIJEVIĆ, S. and DŽOIĆ, T., 2016. Hydrographic conditions driving sardine and anchovy populations in a land-locked sea. Mediterranean Marine Science, 17(1), p.1.

152. VOULGARIDOU, P. & STERGIOU, K.I., 2003 Trends in various biological parameters of the European sardine, Sardina pilchardus (Walbaum, 1792), in the Eastern Mediterranean Sea. Scientia Marina, 67: 269-280.

153. Zavatarelli, M., Mellor, G.L., Zavatarielli, M., Mellor, G.L., 1995. A numerical study of the Mediterranean Sea circulation. J. Phys. Oceanogr. 25, 1384–1414. doi:10.1175/1520-0485(1995)025<1384:ANSOTM>2.0.CO;2

154. Zervakis, V., Georgopoulos, D., 2002. Hydrology and circulation in the North Aegean (eastern Mediterranean) throughout 1997 and 1998. Medit. Mar. Sci. 3, 5–19.

155. Watkings, K. and Rose, K. (In press). Evaluating the performance of individual-based animal movement models in novel environments. Ecological Modelling.